Fabio Blaschke, BSc

Dual/Bi- Stage Curing of Nanocomposites from Renewable Resources upon Volumetric Expansion

MASTERARBEIT

Zur Erlangung des akademischen Grades

Diplom-Ingenieur

Masterprogramm Technical Chemistry

Eingereicht an der

Technischen Universität Graz

Betreuer

Priv.-Doz. Dipl.-Chem.Univ. Dr.rer.nat. Frank Wiesbrock

Institute for Chemistry and Technology of Materials

Graz, May 2020

Eidesstattliche Erklärung / Statuatory Declaration

Ich erkläre an Eides statt, dass ich die vorliegende Arbeit selbstständig verfasst, andere als die angegebenen Quellen/Hilfsmittel nicht benutzt und die den benutzten Quellen wörtlich und inhaltlich entnommenen Stellen als solche kenntlich gemacht habe.

Graz, am …………………………   ………………………………………………..

(Unterschrift)

I declare that I have authored this thesis independently, that I have not used other than the declared sources / resources, and that I have explicitly marked all material which has been quoted either literally or by content from the used sources.

……………………………   ………………………………………………..

date   (signature)

"Live, Love, Laugh, Leave a Legacy"

-Stephen R. Covey

Acknowledgement

First of all, I would like to express my very great appreciation to Priv.-Doz. Dipl.-Chem.Univ. Dr.rer.nat. Frank Wiesbrock for giving me the opportunity to complete this interesting project work as my master thesis and in particular for his enthusiastic encouragement and useful comments on this research work. I am very grateful for the excellent support and guidance for my thesis during the coronavirus crisis, although he had busy schedule to successfully handle other projects. It was a great privilege and honour to work and study under his guidance.

Secondly, I cordially thank laboratory technicians and scientific staff of the Institute for Chemistry and Technology of Materials at the Graz University of Technology and the PCCL, in particular: Birgit Ehmann for her continuous general support, Petra Kaschnitz for her support concerning the NMR measurements, Josephine Hobisch for her support concerning thermal analyses and gel permeation chromatography and Inge Mühlbacher for the excellent support in the course of the zeta potential measurements and the quantification of the surface energy.

Thirdly, I want to give big thanks to my working colleagues Matthias Windberger, Philipp Marx and Stefan Hirner for the great team spirit and, in addition, for the great scientific support and solution-oriented approaches in the laboratory. Special thanks are addressed to Philipp Marx for his great help in the course of the synthesis of spiroorthoesters.

Finally, I thank all my friends and companions for their consistent support throughout the whole study and life. Meta Ambrožič, Laura, Magdalena Buchinger, Katharina Dirnbauer, Sandro Letter, Johannes Schlaffer, Simon Pressler, Fabian Planitzer and the IAESTE Graz: Without you, life would be only half as beautiful.

And finally, I thank my whole family. Thank you for your support in every situation of my life. This journey would not have been possible without the support of my family. Especially to my parents, I am deeply committed. I feel so grateful and blessed to have parents like you in my life. In addition, thank you so much for your support, both emotionally and financially, over the years.

Table of Content

1 Introduction

Electrification is an important part of our modern live and is significantly involved in many achievements of our times, comprising products such as computers, cell phones, and power systems. Various forms of power generation, distribution, transmission, and conversion have been invented, which are primarily based on the interplay of two types of materials: electrical conductors and wide-energy-bandgap insulators. Concomitantly, non-conductive materials are highly relevant for electrification. These insulating materials are the key component for storing large electric energy and are therefore essential for the function of electronic devices and to ensure a stable operation.[1][2] Tuning of the energy bandgap of these non-conductive materials leads to a further enrichment of the storage capacity of electrical energy and was highly important for the construction of electrical devices like transformers, capacitors, resistors, diodes etc.[3][4][5]

Nevertheless, the rising needs for electrical power and electrification during the 21st century put dielectric materials on the world stage as a focal point for the development of new technology. The various DC-AC and AC-AC converters require new innovations in this area, in order to realize the projects / goals of the future, such as solar- and wind-farms, electric cars, primary and secondary electrochemical devices, military equipment and telecommunication applications,[6] all of them aiming to evolve society to the next level.

A major challenge and the key point in the future will be the increasing heat development, which mainly originates from the increasing processing speed and the on-going demand in miniaturization in microelectronics and high-voltage engineering in order to obtain a higher power-to-volume ratio. Ceramic capacitors are good heat conductors. Nonetheless, their comparably high pricing and the high temperatures involved in their processing are serious drawbacks in various applications fields; their counterpart, polymer-based dielectric materials, on the contrary, are not suitable for use at higher operating temperature in applications[7] and are superior to the ceramic materials in lightweight, scalability and shaping into intricate configurations.[8] The combination of organic and inorganic materials yields the so-called nanocomposites,

which (ideally) combine the positive properties of the organic and inorganic parts, offering the opportunity to fine-tune the material properties in diverse applications.[8]

The list of polymers used in the electric industry comprises polyolefins such as polyethylene PE, polypropylene PP, polyisoprene and polystyrene PS, hetero-atom bearing polyolefines like poly(tetrafluoro ethylene) PTFE, poly(vinyl chloride) and poly(acrylonitrile) PAN, polyamides like Kevlar and Nylon 6.6, polyesters and pseudo-polyesters such as poly(ethylene terephthalate), poly(methyl methacrylate) PMMA and polyvinyl acetate PVAc, and polycarbonates; commonly applied resins are alkyd resins, phenol-formaldehyde resins, and epoxy resins.[9]

Epoxy resins are the most commonly used polymer-based insulating adhesives in high-voltage engineering.[10] Most of the manufactured epoxides are based on Bisphenol A (BPA), which can have fatal impact on mammalian health, because it is an endocrine disruptor. BPA has been shown to be harmful in laboratory animal studies and in epidemiological studies examining the effect of BPA on the health of humans.[11] In the polymer matrix, BPA is linked by an ester bond to the polymeric material; however, in the course of material degradation, when it is exposed to high temperatures or to acidic or alkaline substances, BPA might be released.[12] In consequence, this harmful substance can be released in the environment. In December 2016, the European Commission decided to restrict the use of BPA in thermal paper in the EU. This ban is already in force (valid from 2020).[13] It is likely that the restrictions of BPA will continue and, hence, alternatives need to be sought.

Consequently, the second challenge in the course of insulator/material development (besides meeting the required technical parameters) are environmental aspects, which cannot be neglected any longer. A large part of the polymers used in microelectronics and high-voltage engineering are obtained from petrochemicals: In society, a more critical view has evolved considering aspects of sustainability and environmental challenges.[14] Oil is a raw material, on which the industry is heavily dependent on. Therefore, it is highly recommendable to replace the organic part of composites with polymers made from renewable resources in order to contribute to the environmental protection and lay the foundation for the future generations of non-fossil-based materials.

A promising alternative is offered by poly(2-oxazolines), which can be regarded as 'pseudo'-polyamides. 2-Oxazoline monomers with long aliphatic chains can be derived from fatty acids; in general, (co-)poly(2-oxazoline)s are known for their high temperature stability.[15] Precedent studies have already shown that the values of permittivity, loss factor and conductivity of this class of material are in the same range as for polyamides, classifying these materials as medium insulators.[16] These 'green' alternatives are very interesting for investigation as composite material. The influence on the electronic properties due to filling poly(2-oxazoline)s with inorganic particles, hence, is worth of detailed investigations.

2 Scope and Motivation

The challenges that will be placed on the dielectric materials of the future will be manifold. An important point for material development will be the increasing development of heat in electronic devices, connected to the increasing power density in the future. An additional challenge is the volumetric shrinkage during cross-linking, which leads to the formation of micro-cracks, micro voids and delamination, deteriorating the insulation properties.[17] This results in two important strategical aspects, which constitute the motivation for this Master Thesis.

Strategy 1: Thermal conductivity. The first aim for this Master thesis is to develop a composite material from renewable resources, which is to be competitive with materials currently used in microelectronics and high-voltage engineering such as polyamides (PA). As 'conventional' (fossil-based) PA, commercially available Nylon 12 with a maximum particle size of 50 µm is used. The 'green' counterpart material is a self-synthesized poly(2-oxazoline) copolymer. One important aspect is the thermal conductivity of the material in order to ensure an efficient heat flow through the material. A sufficiently high thermal conductivity is necessary to ensure that the material does not overheat and a constant electrical performance can be guaranteed. Hence, both polymer matrices are filled with particle contents of 40 wt.-%, aiming to yield composite materials that show higher thermal conductivity in comparison with the unfilled polymers. In the best-case, the percolation threshold should be achieved/exceeded. Particles with different sizes in the nano- and micrometer range are to be combined in order to determine their influence on the thermal behaviour. The dielectric performance is also a main criterion of this Master Thesis, and the impact of the particle size on the electric properties of the composites is to be investigated. The renewable material should, of course, also perform well in terms of dielectric strength and loss factor in comparison to Nylon 12.

Strategy 2: Volumetric shrinkage. In addition, the second aim is to suppress the volumetric shrinkage during the crosslinking of the polymers. This is a particularly valuable point of this work, because micro-cracks are the origin of a lot of disadvantageous properties and can heavily deteriorate the performance of a material. Therefore, a spiroorthoester (SOE) should be incorporated in different contents to the

two polyamide materials. Thereby, the volumetric shrinkage should be minimized or in the best case completely counter-balanced, yielding networks that are volume-neutral during curing. The effect should be examined, which special focus on the influences on the thermal, electrical and physical properties of the material. Therefore, the goal is to develop a dual curing system, in which the SOE is polymerized by cationic double ring-opening in the course of the crosslinking of the polymers, yielding a hybrid network system, in which the spiroorthoesters form part of the polymer matrix. One of the challenges is to develop a system that exclusively can be triggered by thermal stimuli.

As fillers, micro-scaled (hexagonal) boron nitride (BN), nano- and micro-scaled aluminium nitride (AlN) particles, as well as mixtures of the types of particles are to be added to the polymer networks. The focus will be put on composites with a particle content of no particles, 40 wt.-% BN, 20/20 wt.-% of the two types of AlN, and 20/10/10 wt.-% of BN and the two types of AlN. Additionally, composites with particles and SOE contents of 0, 15, and 30 wt.-% should also prepared.

Crosslinking of the polyamides will be initiated according to a thermal radical mechanism. In the materials that additionally contain SOEs, a dual-curing reaction needs to be carried out. Hence, a novel method for the cationic ring-opening of the SOE with a thermal initiator must be developed, for manufacturing test specimen in a platen press.

In summary, this experimental set-up yields two 4 (filling types; see hereinabove) x 3 (SOE contents; see hereinabove) = 12-membered libraries. These two material libraries (one for the Nylon 12- and one for the copoly(2-oxazoline)-based matrices) are to be fundamentally characterized by physico-chemical and dielectric properties in order to establish the correlations between the structure and the resulting properties.

3 State of the Art

3.1 Dielectric Materials

3.1.1 Dielectric Characteristics of Dielectric Materials

In general, dielectric materials are poor conductors, but show the remarkable property that these polarizable insulating mediums are able to store electrical charges.[18][19] These materials are an integral part for the construction of devices in microelectronics and high-voltage engineering and enable our modern lifestyle, ranging in products such as computers, cell phones, and power systems. [20] However, currently used polymer-based dielectric materials are not competitive for the electronic devices of the future. This can be explained by the example of the biaxially oriented polypropylene (BOPP). The maximum operation temperature of BOPP, which is a commonly used polymer in capacitors, is 105 °C.[21] This poses a major challenge for the electrical industry, because polymer materials are very poor thermal conductors. So, if dielectric polymers like BOPP reach their glass-transition temperature (T_g), they lose their shape and electromechanical stability, and, therefore, no stable operation of the electronic devices can be ensured any longer.[8] Because of the increasing heat development, which is connected to the increasing processing speed and the ongoing demand in minimization in microelectronics and in high-voltage (HV) engineering, a new strategy has to be chosen.

In general, two types of dielectric materials exist, which are divided into organic polymers and inorganic ceramics. Because of the scope of this Master Thesis, the organic dielectrics will be focussed on in this chapter. Nevertheless, it should be mentioned that ceramic-based capacitors demonstrate a high dielectric constant and permittivity.[3] They are the most widely used components for capacitors in modern electronics (~90 %) [22] and are well-suited for the application in high-temperature technology connected with a long-live performance.[18] Particularly interesting are the new multilayer ceramic capacitors (MLCCs), which exhibited production capacitance and voltage scalability higher than 100 µF.[23] However, they have also some disadvantages, compared to their organic counterparts. The organic polymer-based

dielectrics possess many advantages like lower dielectric loss, mechanical flexibility, higher breakdown strengths, scalability, and lightweight, and can be moulded into geometrically challenging configurations. [6][8]

3.1.2 Dielectric Characteristics of Nano-Dielectrics

A new and promising type of materials are the so-called nano-dielectrics, which are able to overcome the challenges discussed hereinabove and combine the advantages of organic and inorganic materials. The term nanodielectric refers to polymer nanocomposites, in which nanofillers are incorporated into the polymer matrix (

Figure 1). This concept was introduced by Lewis with the title 'Nanometric Dielectrics'.[24] He also developed the concept of the interface within his pioneer work, which is essential to understand the influence of the particles on the properties of the polymer composite.[25] Another breakthrough was achieved by the work of Nelson and Fothergill in 2002. They showed that the dielectric properties of an epoxy resin can be influenced by the reinforcement of TiO_2 nanoparticles.[26] On-going works in this research field of various working groups have shown that the use of nanocomposites for dielectric material can result in many additional advantageous properties. For example, the breakdown strength can be enhanced, and an increase of resistivity to partial discharges is also possible, both in comparison to the respective micro-composites and the unfilled polymers.[27]
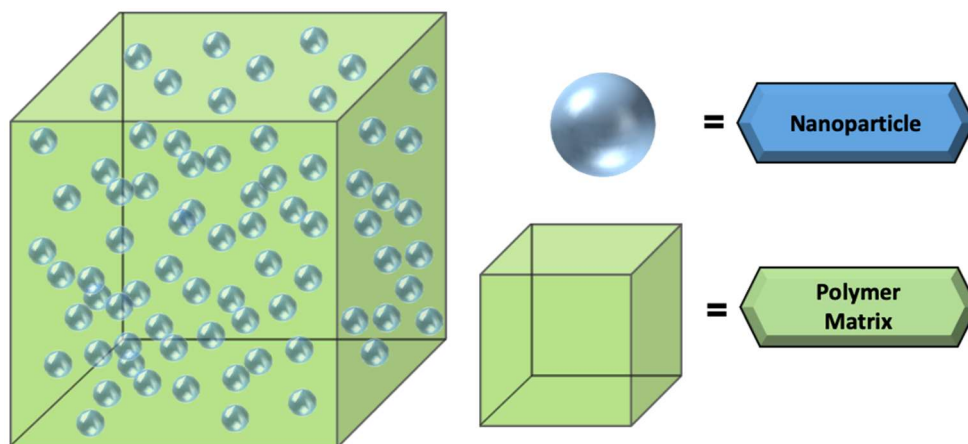

Figure 1: Schematic representation of a nanocomposite.

The famous Nobel laureate physicist Richard Feynman once said: 'There's plenty of room at the bottom.'[28] The key for success lies in this statement. Therefore, it is necessary to discuss the nanofiller/polymer interface phenomena to understand why the 'room' or scientifically expressed the interface, is the basis of the fundamental properties and various phenomena that polymer nanocomposites exhibit as dielectrics. Several interface models exist; in this thesis, selectively the multi-core model of Tanaka is discussed, because the electrochemical features developed within this hypothetic model have been experimentally verified.[27]

3.1.3 Influence of Particle Properties Connected to the Volume Fraction of the Interface

An important point that must be explained at first are the associated interface properties due to the size of the particles: Let us assume a system with two phases, in which A are nanoparticles and B is the polymer matrix. Of course, in this system, interfaces exist, because the particles and the polymer in the two-phase system will interact according to sets of short and long-range forces in the two-phase system. The particles of phase A have a finite size in the nanometer range and are surrounded by the polymer matrix B with the AB interface between them.[25] In detail, a particle with a finite thickness, an interface with a thickness t and the particle plus interface-thickness d must be considered (Figure 2).
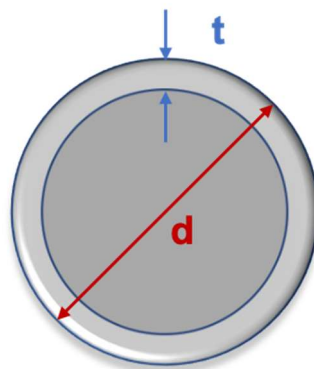

Figure 2: Schematic presentation of a spherical filler particle. D is the diameter of the particle plus the interface with the height t.

The volume fraction of the interface for a nanoparticle can be calculated with equation (1), in which the fraction of the interfacial volume (f) can be calculated from 2t/d < 1:[29]

8

$$f = 3 \cdot \frac{2t}{d} \cdot \left[1 - \left(\frac{2t}{d} \right) + \frac{1}{3} \cdot \left(\frac{2t}{d} \right)^2 \right] \qquad (1)$$

Correspondingly, in a particle with a diameter of d = 40 nm and an interface thickness of t = 4 nm, the volume fraction of the interfacial area accounts for approx. 50%, while the interfacial thickness to diameter ratio is d/t = 0.1.

From such calculations, it can be concluded that decreased particle sizes (concomitant with increasing d/t ratios) result in increased volume fractions of the interface, from which, in final consequence, alternative properties (in comparison to typical bulk properties) evolve as the interface properties become more dominant, and the interface forces differ from bulk forces.

Therefore, it is clearly demonstrated that the interface plays a significant role in this mesoscopic region. Obviously, the properties of the interface can greatly affect the overall dielectric properties of the composite.[25][30]

3.1.4 The Multi-Core Model of Tanaka

Several interface models exist that explain the 'interaction zone' between particles and polymer matrices. The electrochemical features of the multi-core model by Tanaka (Figure 3) have been proven experimentally.[27] In the multi-layered core model of the interface, proposed for a spherical inorganic filler particle embedded in a polymer matrix, it is assumed that the multi-layer consists out of four layers:

    (1) A bonded layer (the first layer)

    (2) A bound layer (the second layer)

    (3) A loose layer (the third layer)

    (4) An electric double layer overlapping the above three layers.

The first layer is a transitional layer and is tightly bound to both, the inorganic particle and to the organic polymer matrix. An example for this type of layer is present in nanocomposites in which the particle and the polymer are covalently bound, e.g. by a coupling agent such as silanes.

The second layer corresponds to an interfacial region consisting of a layer of polymer chains that are strongly interacting with the first layer and the surface of the particle.

The third layer interacts with the second layer and is only loosely coupled, because of the different chain conformation. This layer (still) has a different chain mobility, crystallinity, chain conformation and free volume compared to rest of the polymer matrix.

In addition, the Gouy-Chapman layer, which is the fourth layer, corresponds to the far field-effects. As such, the fourth layer superimposes the other three layers: In consequence, if the interaction zones of one nanoparticle overlap with those of a neighbouring nanoparticle, cooperative effects evolve between the nanoparticles.
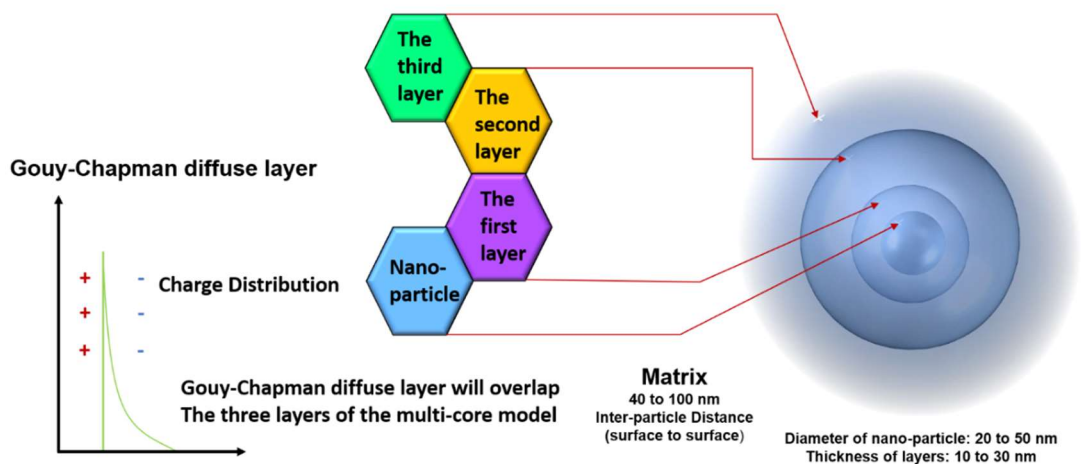
Figure 3: The multi-core model for polymer-nanocomposites proposed by Tanaka et al.[29]

This Tanaka model is an important concept to understand how electrical properties of particles affect the properties of the dielectric composite. Due to the size and shape of the particle, the free volume changes and as a result, the dielectric behaviour of the composite changes. Also, the nature, crystallinity and mobility of the polymer chains have an enormous impact. In addition, the triboelectricity of the polymer and particles influences the thickness of the interface and changes the properties of the nanocomposite dramatically. For example, if the polymer is tightly bound to the particle surface (like in case of a bonded layer), the T_g will increase, while the permittivity and conductivity will decrease due to the highly immobile polymer chain.

In addition, the electrical losses can be influenced by the addition of particles to a dielectric material. The loss factor tanδ is lower in epoxy-organically modified layered silicate nanocomposites than in unfilled epoxy resins. It is also remarkable that the addition of silicates enables to suppress an increase of permittivity and tanδ at elevated temperatures.[31] Nevertheless, it must be kept in mind that also impurities can influence the electronic properties. At low frequency, the loss tangent and low field DC conductivity are also sensitive to the existence of mobile ionic impurities and polar radicals with a dipole moment.[28]

3.1.5 Influence of the Electrical- and Thermal-Properties due to Affinity of Polymers with Inorganic Particles

Another interesting aspect is the (homogeneity of the) distribution of the particles in the polymer matrix. In a perfect nanocomposite, the particles are separated by the polymer matrix; if charge injection takes place, the Gouy-Chapman diffuse layer is formed.[29] However, due to different affinities or different triboelectricity effects of particles to/in the polymer matrix, inhomogeneous dispersion and agglomeration of nanoparticles can occur during the production of nanocomposites. This can result in the deterioration of the material properties: Not only are the electrical properties affected,[28] but also the mechanical and thermal properties changes.[27]

This is an important factor to be considered, as advances in microelectronics and HV engineering have led to miniaturization of the devices and machinery, which enables higher processing speeds (more transistors can be integrated in a single device).[32] The demand of secure heat dissipation in microelectronics, hence, has become increasingly important.[33] If the operating temperature of the connection points changes by a small value, in the order of magnitude of 10-15 K, it can lead to a two-fold reduction in the life of devices.[32] Consequently, an efficient heat transport is necessary to prevent unfavoured increase of temperature in the material.

The percolation threshold is a key parameter of materials in order to guarantee an excellent thermal conductivity within the material, which was already been mentioned hereinabove (Figure 4): As schematically shown in Figure 4a, no effective heat flow can occur due to agglomeration of the particles. In Figure 4b, the percolation threshold could not be reached, because the micro-scaled particles do not fit perfectly in the

interstices of the polymer matrix. However, a higher and sufficient heat conductivity can be reached: Figure 4c shows the optimum conditions for an efficient heat transport. A thermal conductivity pathway through the material is formed, ensuring a high and perfect heat transport. Therefore, it can be concluded that increased amounts of particles (of various sizes) and their homogeneous distribution in the polymer is the best way to ensure a high heat conductivity. In particular, the fillers must reach a high fraction to reach the percolation threshold.
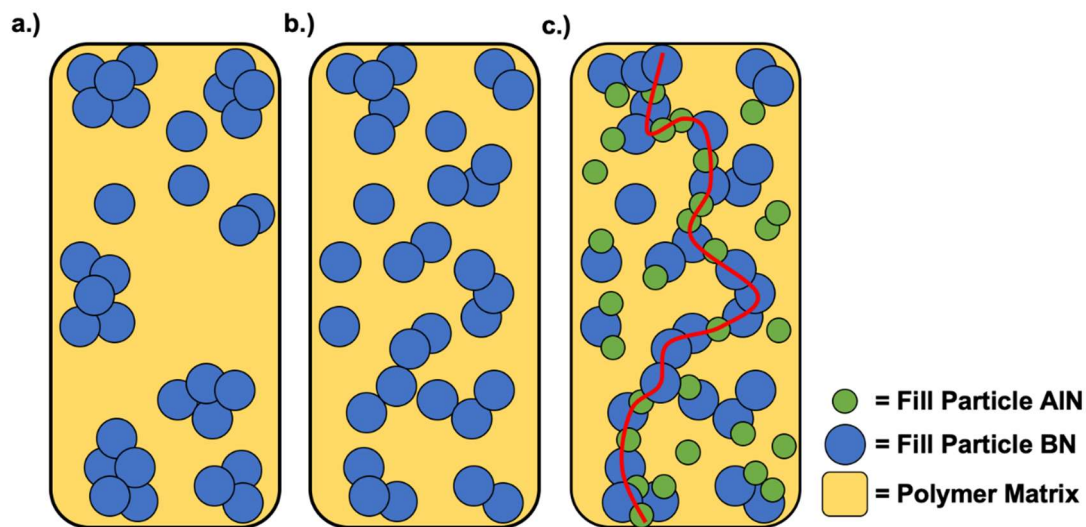

Figure 4 a.) Agglomeration of the particles in the polymer matrix leads to low heat conductivity. b.) Well-dispersed particles in the polymer matrix lead to higher heat conductivity. c.) Percolation threshold: Long-range connectivity is reached due mixing of particles with various sizes, resulting in high heat conductivity.

Ishida and Rimdusit reported a very high thermal conductivity of 32.5 $W \cdot m^{-1} \cdot K^{-1}$ in a BN-filled poly(benzoxazine)-based composite at a filler loading of 78.5 vol.-%.[33] If the particle content is increased further, negative effects occur such as a decrease of the mechanical flexibility, difficulties in manufacturing like scaling-up the film production process and lower breakdown strength.[6] Oxide fillers such as alumina (Al_2O_3) and silica (SiO_2) have been used as suitable candidates in industry because of their low costs and processability in mixing procedures. However, compared to the ceramic nitrides such as BN, AlN, and silicon nitride (Si_3N_4), their intrinsic thermal conductivity is 1 to 2 orders of magnitude lower than the nitride-based fillers.[34] Hence, ceramic fillers should be used in order to ensure an efficient heat transport.

It was shown by transmission electron microscopy (TEM) that BN tends to agglomerate in the polymer matrix.[10] An interesting report shows that the usage of a hybrid-filler system of Al_2O_3 and AlN with different particle sizes can overcome the problems of forming inflexible voids.[35] Hence it is interesting to see, if it is possible to reach the percolation threshold by the usage of different size of particles in categories of ceramic nitride, to ensure a higher heat conductivity at a constant particle content low enough to prevent the negative effects due to high filler content (Figure 4c).

3.1.6 Dielectric Characteristics of Dielectric Materials

It is important to characterize materials with regard to their electrical properties in order to evaluate whether they are suitable for a certain application or for which area they can be used and of course to compare them with each another.

Dielectric materials are electrical insulators and are able to store electrical charges. If a dielectric material is placed between a plate or an electrode with the positive pole of a DC voltage source on one side and the negative pole on the other, an electric field E is built up between the electrode pads, and the material is polarized to different degrees at different frequencies.[36] The polarisation P of a dielectric material can be represented by the following formula: [37]

$$P = (1 - \varepsilon_r) \cdot \varepsilon_0 \cdot E \tag{2}$$

The relative complex permittivity is expressed as ε_r and is a dimensionless number; ε_0 is the vacuum permittivity, which is a physical constant (ε_0 = 8.854.10-12 F/m). ε_r quantifies the polarization ability of a material in the electric field.

In a parallel plate capacitor, an electrical field E is built up between the electrode pads Figure 5). The plate capacitor can be described by the following equation:[38]

$$C = \frac{\varepsilon_0 \cdot \varepsilon_r \cdot A}{d} \tag{3}$$

C is the capacity of the capacitor, which indicates the storage capacity. Equation 3 shows that C is directly proportional to the permittivity ε_r.
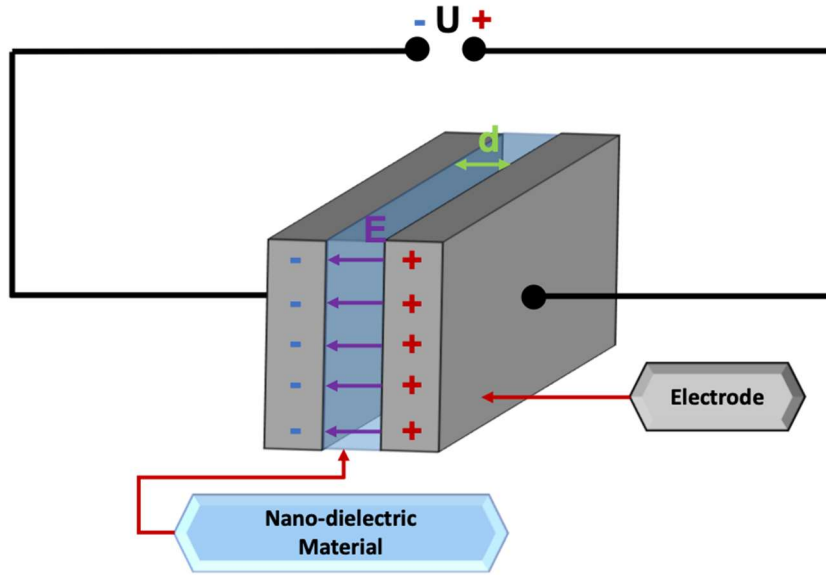
Figure 5: Model of a parallel plate capacitor, with two conducting plates separated by a gap filled with a dielectric with the thickness d.

The storage capacity depends on the permittivity ε_r and shows the ability to store electrical energy.[36] It should be noted that the value of ε_r depends on the frequency; it is particularly challenging to produce a capacitor that operates at very high frequencies. The value of ε_r for a given material also changes with temperature.[38] This is an important point that additionally reveals why the thermal conductivity of the material must be guaranteed to ensure a stable operation performance in electronic devices.

There are further important parameters for the description of a dielectric material. Perfect homogeneity of the particle distribution in a nanocomposite cannot be ensured. This inhomogeneity can occur in the case of high filler contents and/or different attracting forces among the particles and to the polymer matrix (see chapter 3.1.5). Also the presence of impurities and incomplete contact of the dielectric with the electrode lead to regions of accumulated trap charges in the dielectric medium and reduces the performance of the capacitor.[39] These phenomena can be represented by equation 4: The relative complex permittivity ε_r^* of a material consists of two parts: the real part $\varepsilon_r^{'}$ and the imaginary part $\varepsilon_r^{''}$. [5][36]

$$\varepsilon_r^* = \varepsilon_r^{'} - i \cdot \varepsilon_r^{''} \tag{4}$$

The real part ε_r' represents the storage ability, and the imaginary part ε_r'' represents the energy loss. The real part of the relative permittivity ε_r', is therefore a measure of how much energy from an external electric field can be stored by the dielectric material. It is frequently referred as the 'dielectric constant'. For most solids and liquids, ε_r' is larger than 1. The imaginary part of the relative permittivity ε_r'' is indicative of the loss of electrical energy. An important identification number for dielectric materials is the so-called loss factor tanδ, calculated by the ratio of ε_r' and ε_r'' (Equation 5):[36][39]

$$\tan \delta = \frac{\varepsilon_r''}{\varepsilon_r'}$$ (5)

As said, tanδ is also referred to as loss tangent or dissipation factor; as it is the ratio of the energy lost to the energy stored, it quantifies the relative 'lossiness' of a material.[36][39]

For an ideal capacitor, tanδ should have value of zero. This would be perfect, because electrical energy is not lost (transferred to adjacent areas). The production of a perfect capacitor is not possible as no ideal dielectric exists.

tanδ is also an important parameter to characterize dielectrics in AC operations. The field forces in AC operations also act on the dielectric when the capacitor coatings are reloaded. The electron shells of the solid-state molecules are deformed; if they form dipole structures, they are reoriented according to the field direction. The shifting in the dielectric is partly converted into heat. With increasing frequency, the heat development increases until the reorientation of the molecular dipoles can no longer follow the excitation frequency.[39] tanδ is therefore an excellent parameter for the quality of a dielectric material. Notably, in nanocomposites lower tanδ values than in unfilled polymers can be achieved.[28]

3.2   Crosslinking of Polymers

3.2.1   Properties of Crosslinked Polymers

Crosslinking refers to a chemical reaction, in which a bond is formed from one polymer chain to other; as such, it is a polymer analogous reaction.[40] Three-dimensional networks are often used as organic dielectrics as they have properties different to those of the non-crosslinked polymers.[40]

Solubility: By crosslinking, a 3D-network is created. In comparison to the non-crosslinked polymer, the 3D polymer network cannot be solved any longer (if high degrees of crosslinking have been achieved). This is beneficial (among others) if polymer films come into contact with solvents during application, but supposedly do not dissolve (solvent resistance).[41] These insoluble polymers can still absorb solvents and start to swell.[42] This means that small molecules can get into the network structure of the polymers and corresponding nanocomposites and change their properties. One prominent example is water, which plays an essential role in microelectronics and HV engineering due to its pronounced dipole character: Hence, it can change the dielectric properties of the material.[43] This can lead to decreased dielectric performance, metal corrosion and/or mechanical failure at interfaces of the devices.[44] Therefore, polymers that show low water/moisture uptake are preferred.

Glass-transition temperature (T_g): Crosslinking increases the glass-transition temperature T_g of a polymer. A low degree of crosslinking leads to a small shift of the T_g; at high crosslinking degrees, the shift is large due to the resulting decrease of the free volume.[40][45] Hence, the mechanical properties such as elasticity and stress-strain behaviour are influenced.[45] Large degrees of crosslinking render thermoplastic polymers into thermosets that can no longer be deformed under the influence of heat and maintain their shape.[40] This is important for developing nanocomposites to ensure form stability even at temperatures above the T_g. Better contact with the nanoparticles due to the reduction of the free space can be achieved, which was already discussed by the Tanaka model.

3.2.2 Volumetric Shrinkage during the Crosslinking of Polymers

The effect of volumetric shrinkage during crosslinking is the molecular origin for a lot of negative impacts of a material and can lead to a decrease of the material performance. The reason for shrinkage lies in the chemical reaction: During crosslinking, a covalent bond is formed, which is shorter than the sum of the van-der-Waals radii.[46][47] As a result, micro-cracks and micro-voids as well as delamination can occur and induce material failure.[48] Consequently, the suppression or control of the volume shrinkage is of great importance in the design of nanocomposites in order to guarantee good performance in electronic devices.

A suitable method to prevent shrinkage during polymerization is the usage of expanding monomers, which show volumetric expansion during polymerization. Commonly, the volumetric expansion is due to ring-opening in the course of the reaction. Several classes of expanding monomers are known, such as spiroorthoesters (SOEs), bicycloorthoesters (BOEs), and spiroorthocarbonates (SOCs), which can be polymerized via a cationic mechanism involving double ring-opening.[49]

SOEs can be synthesized in a one-step reaction from glycidyl ether and γ-butyrolactone (Scheme 1a). Four different stereoisomers are formed, the ratio (A+B) / (C+D) (Scheme 1b) of which can be calculated from ^{1}H-NMR spectroscopy.[50] γ-butyrolactone is as reactant and solvent at the same time. Moreover, it is a renewable monomer and is ranked first in the DOEs top 12 biomass derived.[51]
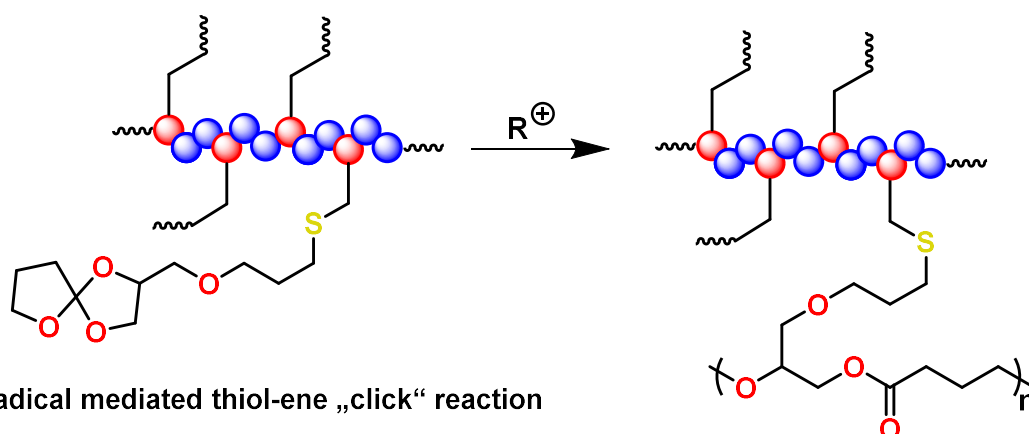
a.) Synthesis of the spiroorthoesters
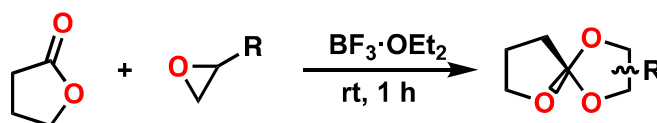

b.) Stereoisomers of SOE

| A | B | C | D |
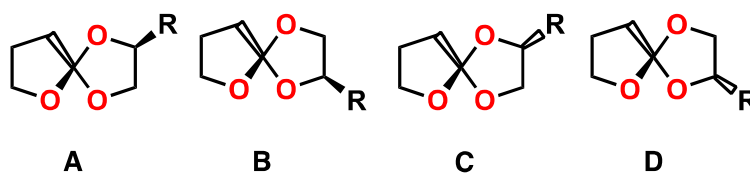
Scheme 1: a.) Synthesis of a SOEs from glycidyl ether, γ-butyrolactone, catalysed by BF$_3$·OEt$_2$ b.) Possible stereoisomers of SOEs, which can be formed during the synthesis.

In a recent publication, the authors have reported a dual-curing system involving SOEs and a bifunctional allyl-bisphenol.[52] The two monomers were copolymerized and crosslinked by thiol-ene click reactions (Scheme 2). In order to initiate the crosslinking reaction, the radical initiator phenylbis(2,4,6-trimethylbenzoyl) phosphine oxide (BAPO) (R_1 in Scheme 2b) was used. The ring-opening polymerisation of the SOE was initiated by the Crivello salt p-(octyloxyphenyl) phenyliodonium hexafluoro antimonate $\{[(R)\Phi_2I]^+[SbF6]^-\}$ (R^+ in Scheme 2a). The reaction was triggered by visible light using sensitizers. It was possible to control the volume shrinkage during the copolymerisation in wider rage by changing the content of the SOE: It was possible to form a network, which is volume-neutral during curing, by combination of the allyl-bisphenol in content of 90 wt.-% and the SOE with 10 wt.-%.

a.) Cationic double ring-opening polymerisation of SOEs

**b.) Radical mediated thiol-ene „click" reaction**
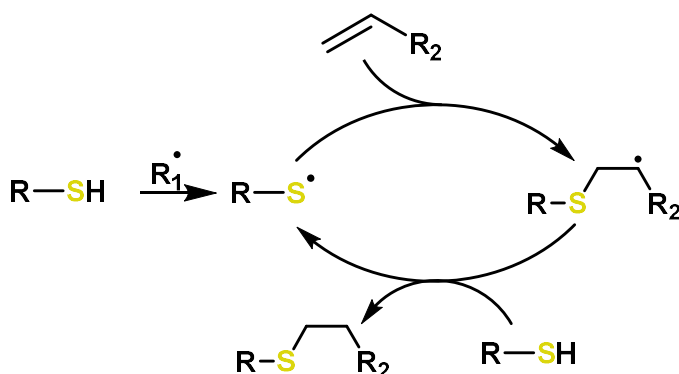
Scheme 2: a.) Structural representation of the spiroorthoester ring-opening polymerization during cross-linking. b.) Mechanism of the thiol-ene reaction for the formation of the three-dimensional network.

3.3 Poly(2-oxazoline)s

3.3.1 The Living Cationic Ring-Opening Polymerization of 2-Oxazolines

In the middle of the 1960s, four research groups independently reported a new synthetic class of polymers known as poly(2-oxazoline)s.[53][54][55][56] These were synthesized by the cationic ring-opening polymerization (CROP) of 2-oxazolines (Scheme 3).[57] In the first step, an electrophilic initiator, such as methyl tosylate initiates the (pseudo-living) polymerization by a nucleophilic attack of the nitrogen lone pair, forming an oxazolinium cation. This cationic species propagates in the polymerization, yielding the respective homopolymer. The polymerization can be terminated by quenching the reaction mixtures with water.

It should be mentioned that a great number of initiators exists and that the chemical structure of the initiator also influences the control of the molecular weight. The list of initiators is very diverse, comprising Lewis acids such as boron trifluoride diethyl etherate ($BF_3 \cdot OEt_2$), zirconium tris(pentafluorophenyl)borate, and alkyl esters such as tosylates, triflates and also halide initiators, which range from chloride to iodide and as well acetyl halide, and many more. [58]
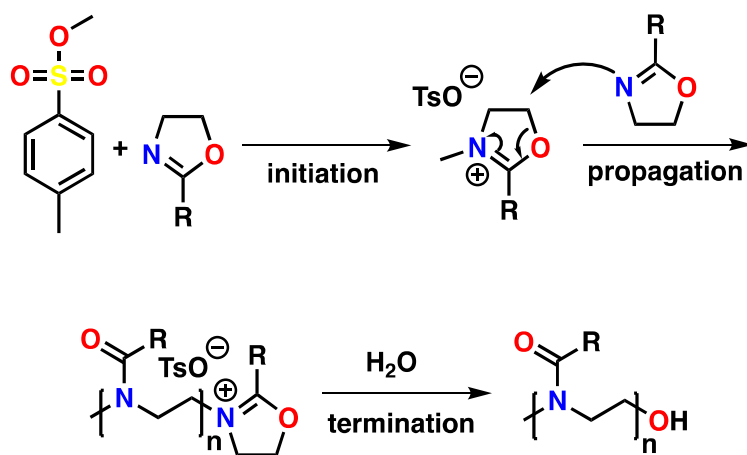
Scheme 3: Schematic representation of the cationic ring-opening polymerization of 2-oxazoline monomers with methyl tosylate as initiator.

3.3.2 Microwave-Assisted Polymerization of 2-Oxazolines

The cationic ring-opening polymerization of 2-oxazolines is a very slow polymerization process, with reaction times in the order of 1-3 day(s) under standard reflux conditions.[59] However, the emergence of microwave-assisted synthesis technology in organic chemistry, has pushed the synthesis of poly(2-oxazoline)s to the next level. In general, a microwave-heated reaction paves the way to performance of chemical reactions under autoclave conditions, and leads to higher yield and selectivity.[60]

In sealed vessels, solvents can be easily heated fast above their boiling temperature. This so called superheating effect allows for an increase of the pressure and the reaction rate.[61] Investigations of the microwave-assisted CROP of 2-oxazolines in superheated acetonitrile at 200° C have shown that the reaction is completed in less than 1 min, while under reflux conditions 6 h are required for completion.[57]

Nevertheless, at higher reaction temperatures, also the number and amount of by-products increases due to side reactions. If the polymerization is performed at 140 °C, an optimum of fast reaction time with simultaneously low amount of side-products can be achieved.[62][63] Hence, a microwave system has proven to be a powerful device to carry out the living polymerization of 2-oxazoline in a short time, yielding polymers with a narrow molecular weight distribution.[57]
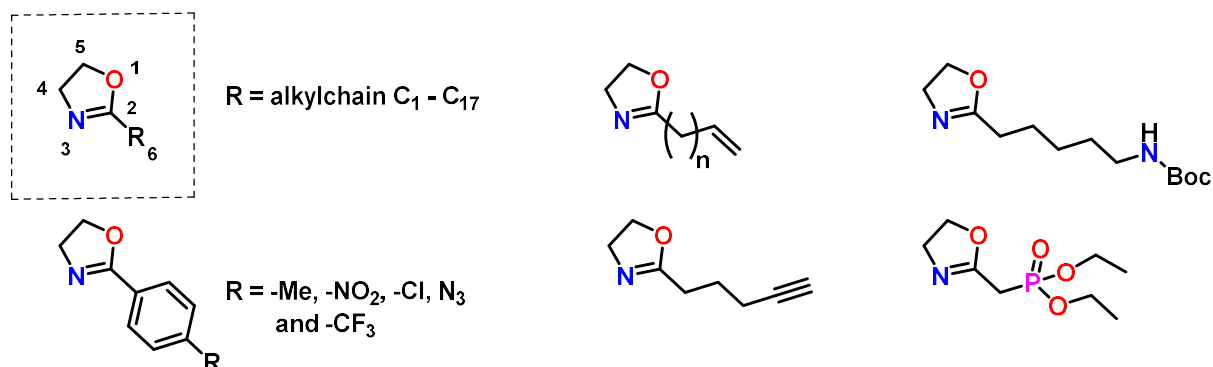
3.4 2-Oxazolines

3.4.1 Introduction

The molecule 2-oxazoline, which is the monomer for the synthesis of the poly(2-oxazoline)s, is a five membered heterocyclic compound with an oxygen atom at position 1, a double bond at position 2, and a nitrogen atom at position 3 (
Scheme 4).

Scheme 4 displays a short summarized overview of various 2-oxazolines.[64] An overview of the enormous diversity of poly(2-oxazoline)s (POx) with varying side-chain structures can be found in the review of Hoogenboom et al.[15]

By the usage of 2-oxazolines with different substituents R, a wide range of polymers with tuneable properties can be synthesized. This can be achieved by using different amounts of various 2-oxazolines in a one-pot synthetic procedure, in combination with a microwave assisted CROP reaction. Hence, a huge variety of different homopolymers or copolymers can be synthesized. This offers the great opportunity to develop polymers with tailor-made properties for diverse applications.

Hydrophilic, hydrophobic, fluorophilic materials can be synthesized as well as different architectures such as star-shaped, block- or graft-copoly(2-oxazoline)s.[65] Further crosslinking or functionalisation by the thiol-ene click reaction can be carried out easily, for example if double bonds are present in the side-chains of the (co-)poly(2-oxazoline)s.[66]


Scheme 4: Overview of 2-oxazoline monomers with various functional side-groups. The molecule at the top left shows the structure of a 2-oxazoline with atomic numbering.

3.4.2 Synthesis of 2-Oxazoline Monomers

A huge number of different synthetic strategies for the production of 2-oxazoline monomers exists.[67] Historically, the first 2-oxazoline derivative was synthesized in 1889 (

Scheme 5).[68] However, this first reported 2-oxazoline is not a suitable candidate for the CROP reaction, as the nucleophilic amine group terminates the polymerization at a premature stage or even completely due to the interference with the initiation process.[64] Hence, synthetic routes for the preparation of 2-oxazolines, which have been most frequently employed in CROP, will be focussed on hereinafter. The following chapters show the different synthesis strategies for 2-oxazolines.
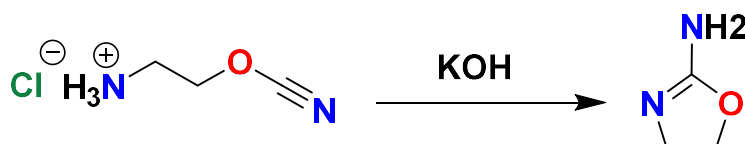
**Scheme 5:** Synthesis route of the first 2-oxazoline in 1889.

3.4.3 Synthesis according to Witte and Seeliger

In 1974, Witte and Seeliger reported a simple one-pot reaction, in which 2-oxazolines are obtained from the conversion of a nitrile with an 1,2-amino alcohol in the presence of a metal salt catalyst under nitrogen atmosphere (

Scheme 6).[69]

In general, the reaction is performed at a temperature of 130 °C with a catalyst load of 0.025 eq. per nitrile group. The products are recovered by distillation and recrystallization. In most of these reactions, the educts themselves act as solvent. The few exceptions (requiring solvents) are a couple of 2-oxazolines with long-chain residues at position 2. In order to solubilize the cadmium catalyst, *n*-butanol was added as solvent.

The following catalysts are used for the reaction: zinc chloride, cadmium acetate dihydrate, zinc acetate dehydrate and copper(II) sulfate. Unfortunately, the use of this environmentally harmful salts is essential for a high yield. In addition, highly toxic HCN

or metal cyanides are used to produce nitriles.[70] Nevertheless, the Witte and Seeliger reaction is an ideal method for access to a large number of 2-oxazolines, benefiting from the wide range of commercially available nitriles on the market.[64][71]
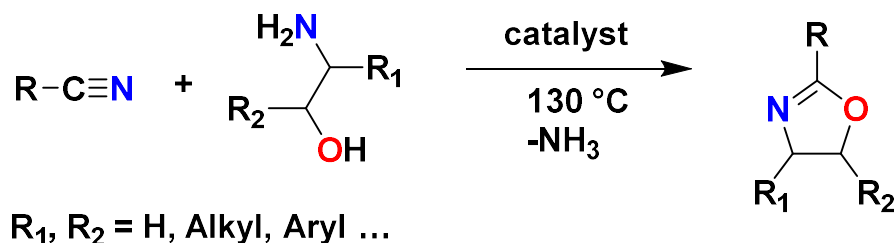
Scheme 6: Schematic representation of the one-pot reaction for the synthesis of 2-oxazolines from nitriles according to Witte and Seeliger.[69]
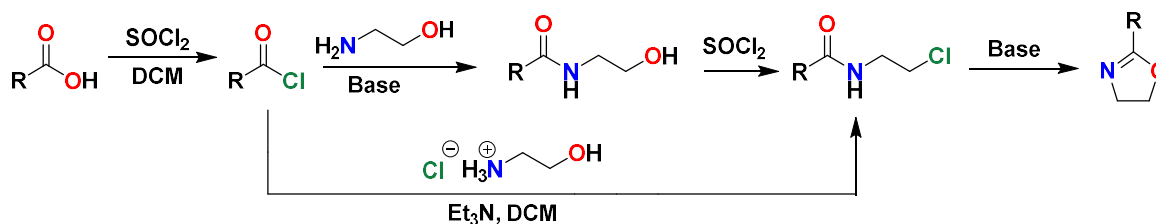
3.4.4 Synthesis according to Wenker

In addition to the Witte-Seeliger synthesis for 2-oxazolines, a synthetic strategy for short side-chain 2-oxazolines is the modified Wenker method. The starting material is an activated carboxylic acid in form of an acyl chloride.[64] Compared to the conventional Wenker process,[72][73] the modified route can be done in a 2-step synthesis instead of a 3-step synthesis, by the choice of a 2-chloroethyl amine hydrochloride via cyclization of β-halo amide (Scheme 7a).[15][64]
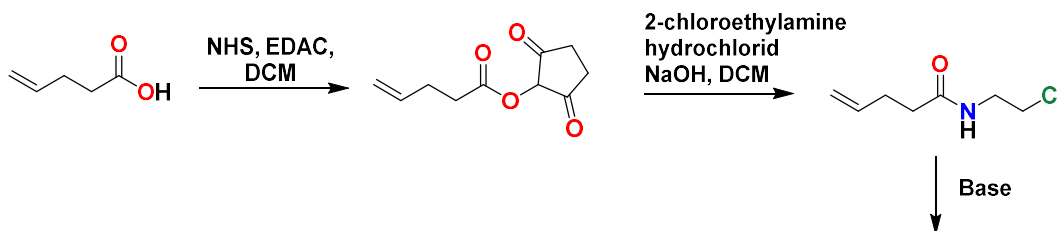
A variation of the Modified Wenker Method is the 3-step synthesis reported by Gress et al.[74] In the first step, pent-4-enoic acid reacts with 1-(3-dimethylpropyl)-3-ethylcarbodiimide hydrochloride (EDAC) and *N*-hydroxy succinimide (NHS) in dichloromethane (DCM) at room temperature, yielding *N*-succinimidyl-4-pentenate (Scheme 7b). The active ester is subsequently reacted with 2-chloroethane-1-amine, yielding the amide *N*-(2-chloroethyl)-pent-4-enamide. In the last reaction step, the amide is reacted with potassium hydroxide, yielding the targeted 2-oxazoline.[74] This is a suitable way to replace the thionyl chloride (Wenker method), which reacts with moisture yielding toxic gases.[75][76]

A new and simple allylation method to synthesize short chain 2-oxazolines via α-deprotonation 2-methyl-2-oxazoline has been reported by Hoogenboom for a cost-effective preparation in laboratory scale (Scheme 7c).[76]
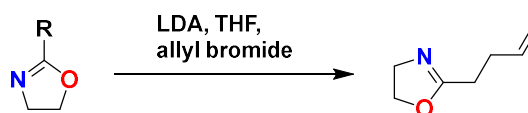
a.) Wenker method and modified Wenker method:

b.) Modified Wenker method:

c.) Synthesis according to Hoogenboom:

Scheme 7: a.) Synthesis of 2-oxazolines by cyclization of β-hydroxy amides (Wenker method) or shortened synthesis way of 2-oxazolines by avoiding β-hydroxy amides (modified Wenker method). b.) The modified Wenker Method according to Gress et al. c.) α-Deprotonation method according to Hoogenboom et al.

3.4.5 Synthesis according to the Henkel Patent

The Henkel patent describes an industrially relevant method to synthesize 2-oxazolines from renewable raw materials.[77] The process is a one-pot reaction involving the direct synthesis of 2-oxazolines from non-activated carboxylic acids in the presence of a catalyst at 120-230 °C for 24 h (Scheme 8). The fatty acid is converted to the corresponding ester amide by the reaction with ethanolamine. The subsequent ring-closing reaction yields the corresponding 2-oxazoline by the help of homogenous catalyst. Suitable catalysts are titanium compounds such as titanium(IV) *tert*-butoxide and titanium acetylacetonate. Zirconium compounds are also effective catalysts.

The water and the 2-oxazoline monomer formed in the course of the reaction are continuously distilled from the reaction mixture under vacuum over a fractionation column. The reactive distillation shifts the equilibrium to the right site. The synthesis is

suitable to produce 2-oxazolines with long-chained substituents R, in the range of 7-21 carbon atoms. Also, unsaturated fatty acids can be used.

The numerous advantages are therefore evident for Henkel patent method, compared to the previously mentioned synthetic processes. The method is environmentally friendly, because no dangerous substances are used such as highly toxic HCN, metal cyanides, or environmentally harmful salts. Moreover, with this solvent-free reaction, 2-oxazolines can be produced from (cheap) renewable materials like fatty acids in industrial scale.
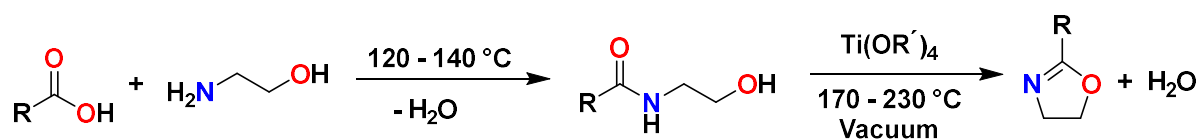
R = C_7 - C_{21}

Scheme 8: Synthetic route for the preparation of 2-oxazolines from fatty acids.

4 Results and Discussion

Two (pseudo-)polyamides and the corresponding composites were evaluated as dielectrics in this Master Thesis based on structure-property relationships. As (pseudo-)polyamides, commercially available Nylon 12 and a self-synthesized copoly(2-oxazoline) from renewable resources were chosen. The experimental set-up, which considered a variation of the content of the expanding monomer SOE (0, 15, and 30 wt.-%; 3 variations) and the type of fillers (no filler, 40 wt.-% micro-scaled BN, 20/20 wt.-% of nano-/micro-scaled AlN, and 20/10/10 wt.-% of micro-scaled BN and nano-/micro-scaled AlN), yielded a 3 x 4 = 12-membered matrix library for each of the two polymers (
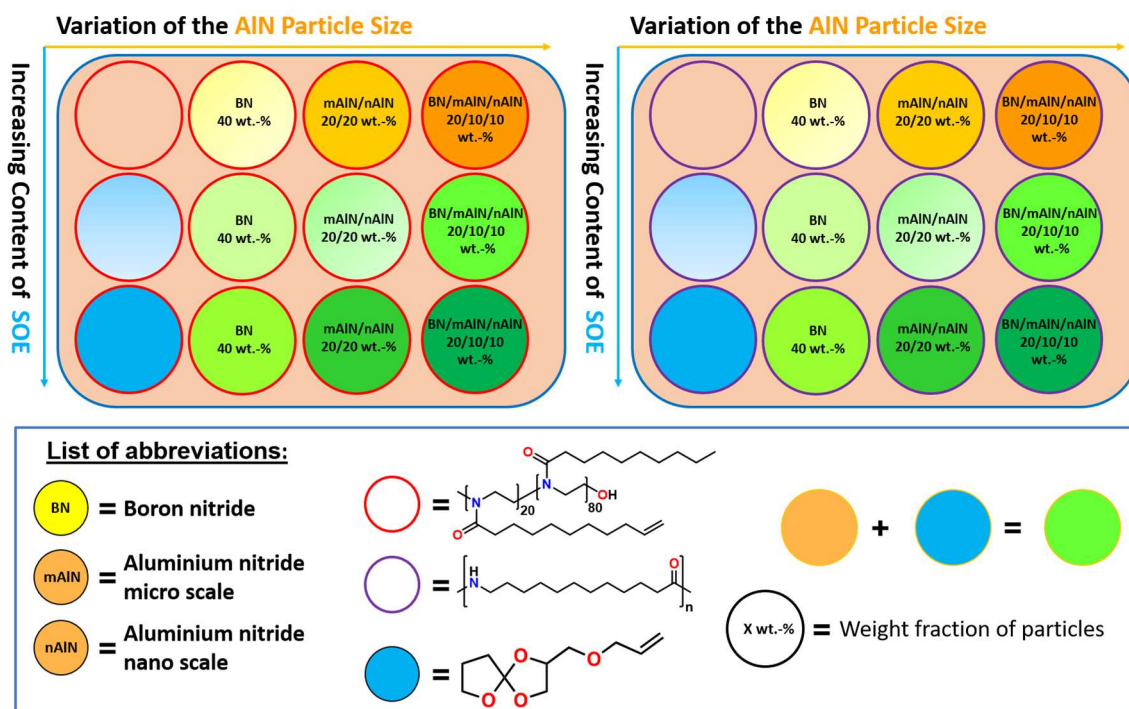Figure 6:).

Figure 6: Overview and schematic representation of the material library of the unfilled polymers and composite materials.

The aim was to prepare 12 different samples per polymer; all samples contained a crosslinked polymer. The polymer blends and composites were characterized (among others) by the following measurements techniques to establish structure-property relationships:

- IR spectroscopy,

- dielectric spectroscopy (permittivity measurements),

- light-flash analysis (thermal conductivity),

- density measurements (volumetric expansion),

- contact angle measurements (surface energy), and

- elektrokinetic potential (zeta potential; isoelectric points).

In this study, two different polymers of the polyamide class were to be investigated. The renewable polymer was represented by a copoly(2-oxazoline), and the commercially available polyamide was represented by Nylon 12. These polymers were tested as unfilled bulk material and as composites, the latter containing submicron-scaled BN, nano- and micro-scaled AlN particles, as well as mixtures of the two types of particles in a content of 40 wt.-%.

The polymer shrinkage during crosslinking was influenced by addition of the SOE 2-((allyloxy)methyl)-1,4,6-trioxaspiro[4.4] nonane to the corresponding polyamide or pseudo-polyamide in a content of 0, 15, and 30 wt.-%, respectively.

The crosslinking of the polymer matrix was carried out by using the thermal initiator dicumyl peroxide. If SOE was present in the mixture, a dual-curing reaction was done by (additionally) adding the thermal initiator 1-butylpyridin-1-ium hexafluoro phosphate(V) for the cationic double ring-opening of the spiroorthoester.

4.1 Synthesis of the Monomers Dec$^=$Ox and NonOx

The synthesis of both 2-oxazoline monomers was set up according to the Henkel Patent.[77] As starting material, renewable resources were used. For the synthesis of 2-nonyl-2-oxazoline (NonOx) and 2-dec-9'-enyl-2-oxazoline (Dec$^=$Ox), coconut oil and castor oil were used, respectively. The fatty acid was reacted with ethanolamine in the presence of the catalyst Ti(OBu)$_4$ (Scheme 9). The ethanolamine also acted as solvent. The synthesis was performed on the 200 g scale. Both reactions mixtures were stirred under reflux conditions for 40 h before the product was obtained from vacuum distillation and subsequent column chromatography with CHCl$_3$ as eluent. The yield was 53.3 % for NonOx and 68.4 % for Dec$^=$Ox.

a.)

b.)
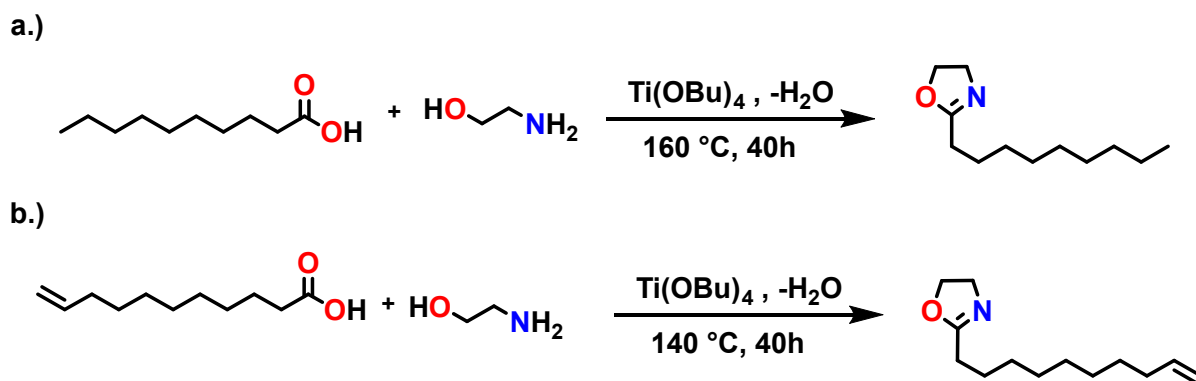
Scheme 9: Schematic representation of the synthesis of a.) 2-nonyl-2-oxazoline and b.) 2-dec-9'-enyl-2-oxazoline according to the Henkel patent.

In the ^{1}H-NMR spectra of NonOx (Figure 7), the signals at δ = 0.88, 1.27, 1.63 and 2.26 ppm (grey, green, blue and purple framed peak) represent the hydrogen atoms of the saturated side-chain. The four hydrogen atoms of the 2-oxazoline ring can be identified at δ = 3.81 and 4.21 ppm (red and orange framed peak). Also, the signals of the ^{13}C-NMR spectrum have been labelled accordingly.

In the ^{1}H-NMR spectra of Dec$^=$Ox (Figure 8), the signals at δ = 1,23, 1.55, 1.97 and 2.19 ppm (green, blue, black and purple framed peak) represent the hydrogen atoms of the saturated part of the side-chain. Furthermore, the signals of the hydrogen atoms of the double bond are identified at δ = 4.88 and 5.72 ppm (grey and yellow framed peak). The four hydrogen atoms of the 2-oxazoline pentacycle can be identified at the peaks at δ = 3.74 and 4.14 ppm (orange and red framed peak). Also, the signals of the ^{13}C-NMR spectrum have been labelled accordingly.
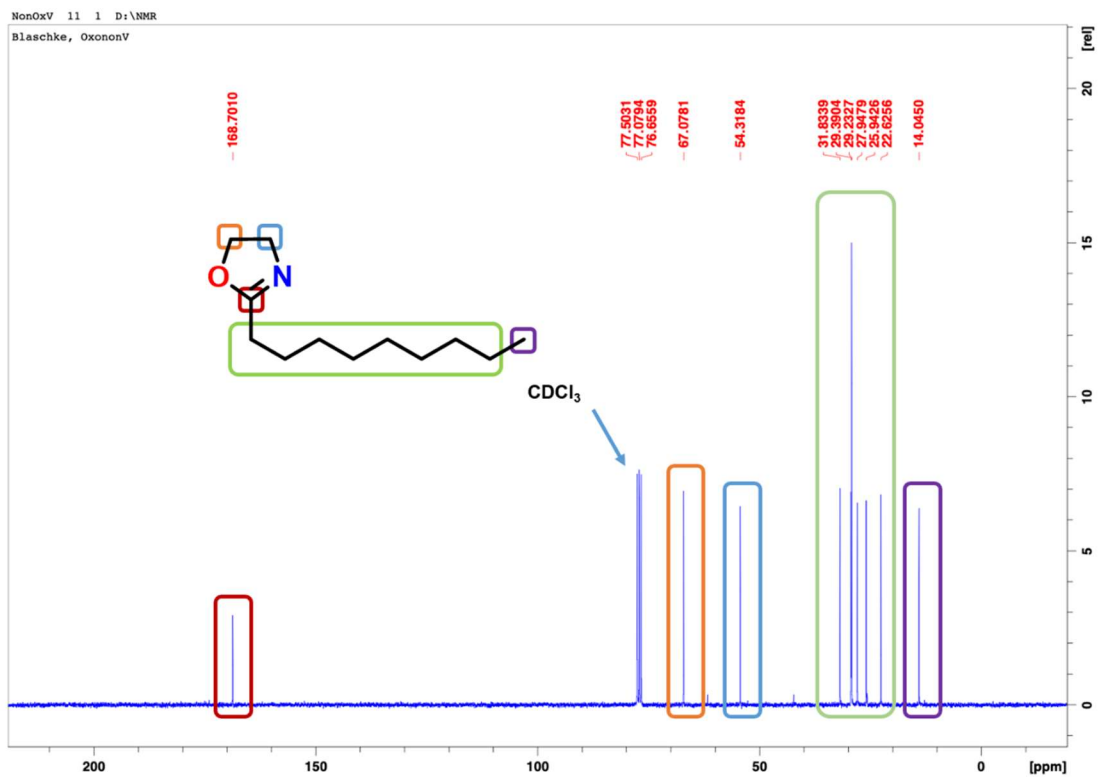
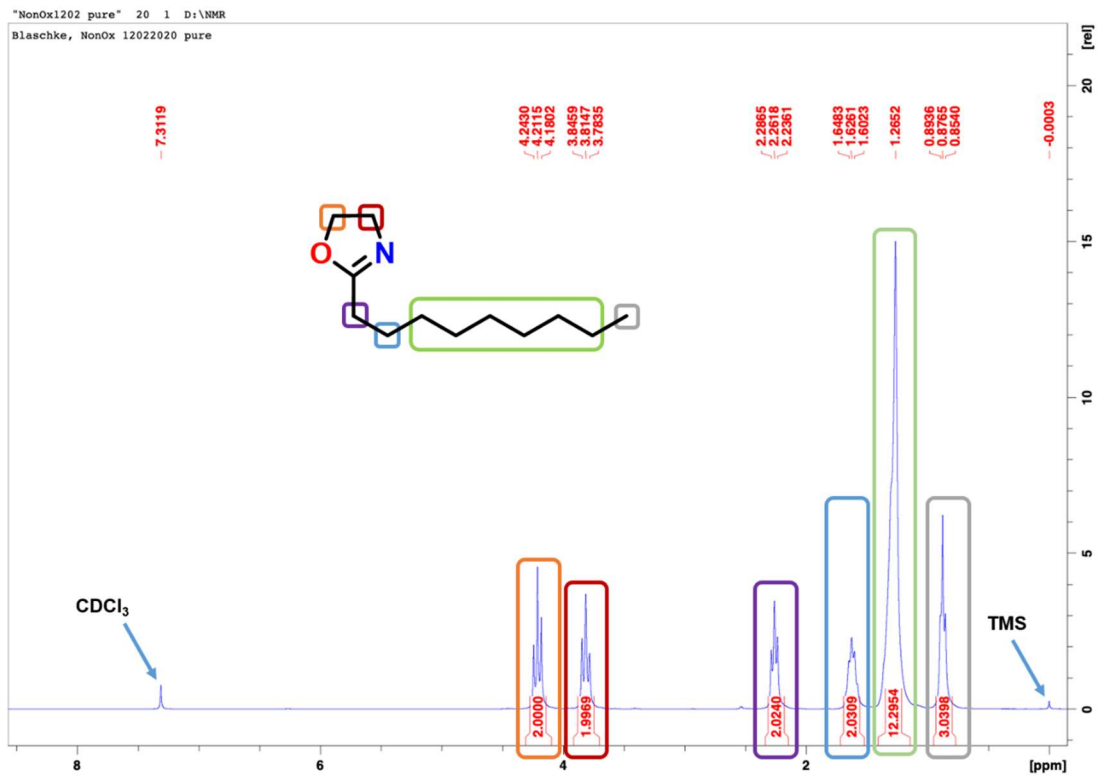**Figure 7:** Top: ^{1}H-NMR spectrum of NonOx in CDCl$_3$ with TMS 0.03 % (v/v) as internal standard, with signals assigned to the chemical structure. Bottom: ^{13}C-NMR spectrum of NonOx in CDCl$_3$.
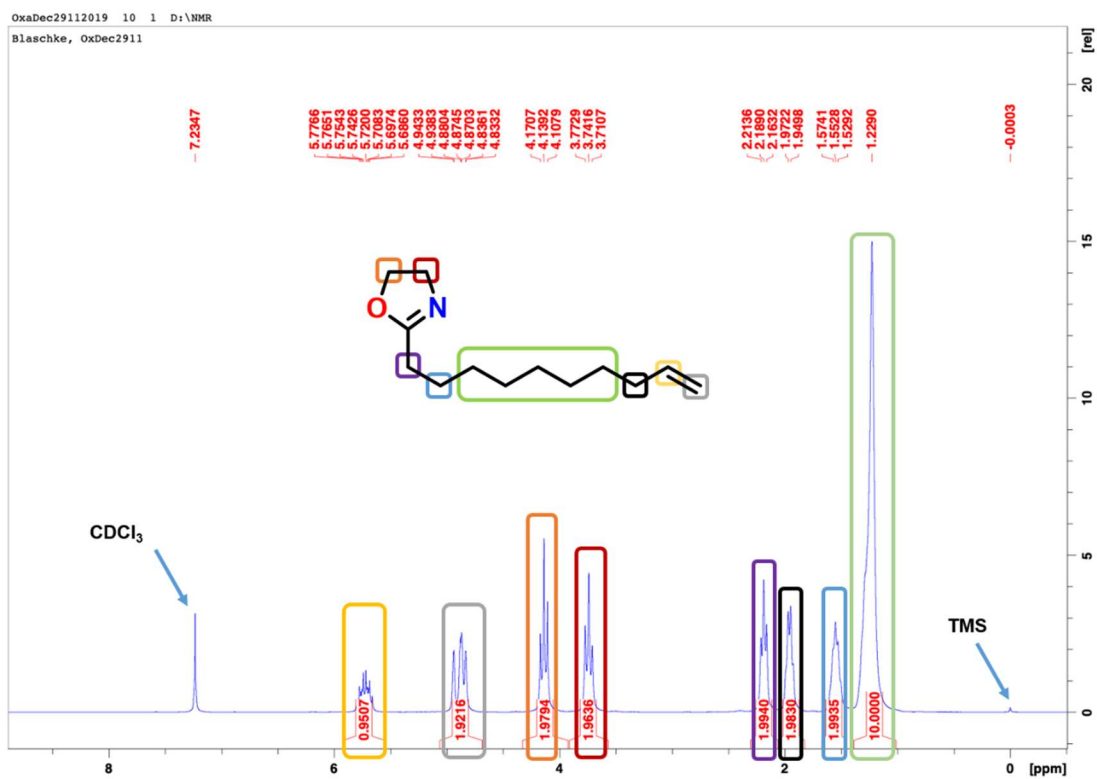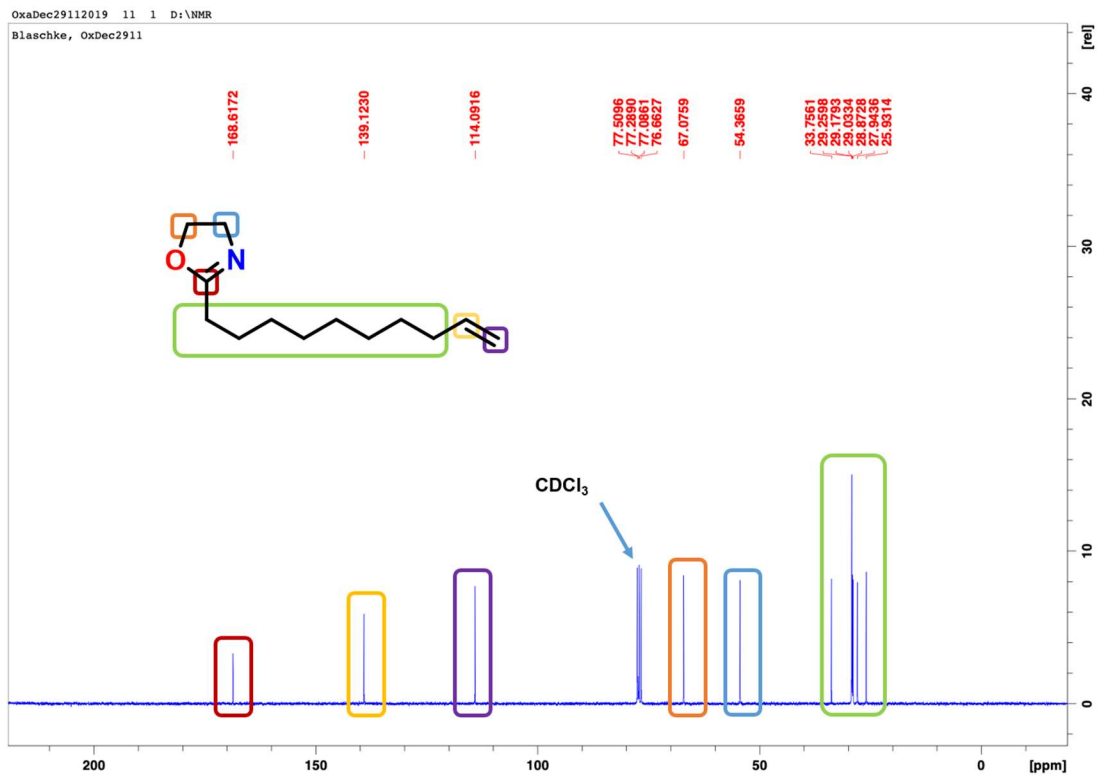
Figure 8: Top: ^{1}H-NMR spectrum of Dec$^=$Ox in CDCl$_3$ with TMS 0.03 % (v/v) as internal standard, with signals assigned to the chemical structure. Bottom: ^{13}C-NMR spectrum of Dec$^=$Ox in CDCl$_3$.

4.2 Synthesis of the Copolymer Poly(2-nonyl-2-oxazoline)-*stat*-Poly(2-dec-9'-enyl-2-oxazoline)

The 'green' copoly(2-oxazoline) was synthesised from the monomers Dec$^=$Ox and NonOx (see hereinabove). The copolymerization of Dec$^=$Ox and NonOx was performed via the microwave-assisted synthesis technique in a reaction scale of 25 g. The following stoichiometric ratio was chosen: 20 equiv. of Dec$^=$Ox and 80 equiv. of NonOx were mixed. As initiator, 1 equiv. of methyl tosylate (MeOTs) was added; as solvent, acetonitrile (ACN) was used. Under autoclave conditions at 140 °C in sealed reaction vials, the copolymer pNonOx$_{80}$-*stat*-pDec$^=$Ox$_{20}$ was synthesized according to a microwave-assisted CROP reaction for 2 h (Scheme 10). A white powder was obtained after solvent evaporation, grinding of the product in a mortar and further drying on the Schlenk line (Figure 9).
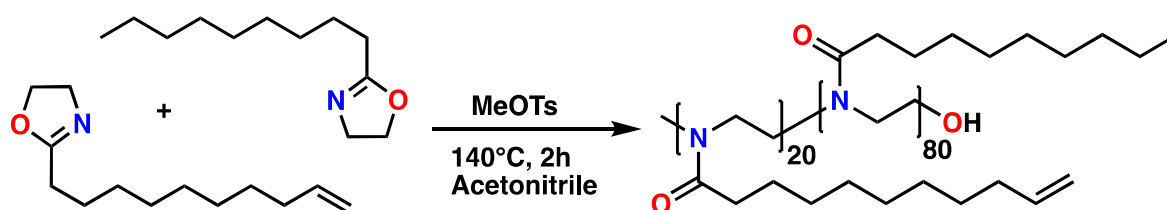
Scheme 10: Synthesis of poly(2-nonyl-2-oxazoline)-*stat*-poly(2-dec-9'-enyl-2-oxazoline) from Dec$^=$Ox and NonOx via a microwave-assisted CROP reaction in acetonitrile, using methyl tosylate as initiator.
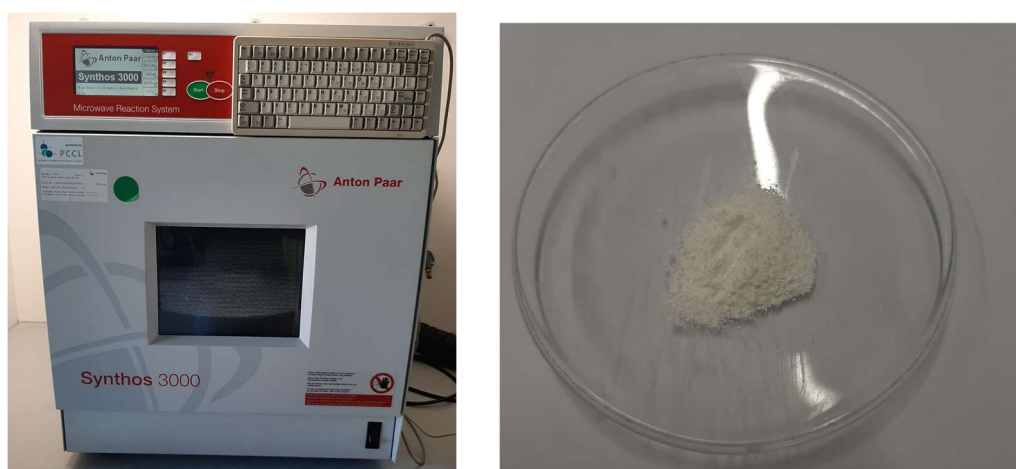
Figure 9: Left: Photography of the microwave reactor Synthos 3000 by Anton Paar, in which the CROP reaction of the 2-oxazolines was carried out. Right: Recovered and dried pNonOx$_{80}$-*stat*-pDec$^=$Ox$_{20}$.

The copoly(2-oxazoline) was characterized by NMR-spectroscopy. The ^{1}H-NMR und ^{13}C-NMR measurements of pNonOx$_{80}$-*stat*-pDec$^=$Ox$_{20}$ were performed in CDCl$_3$ with tetramethylsilane (TMS) 0.03 % (v/v) as internal standard (Figure 10).
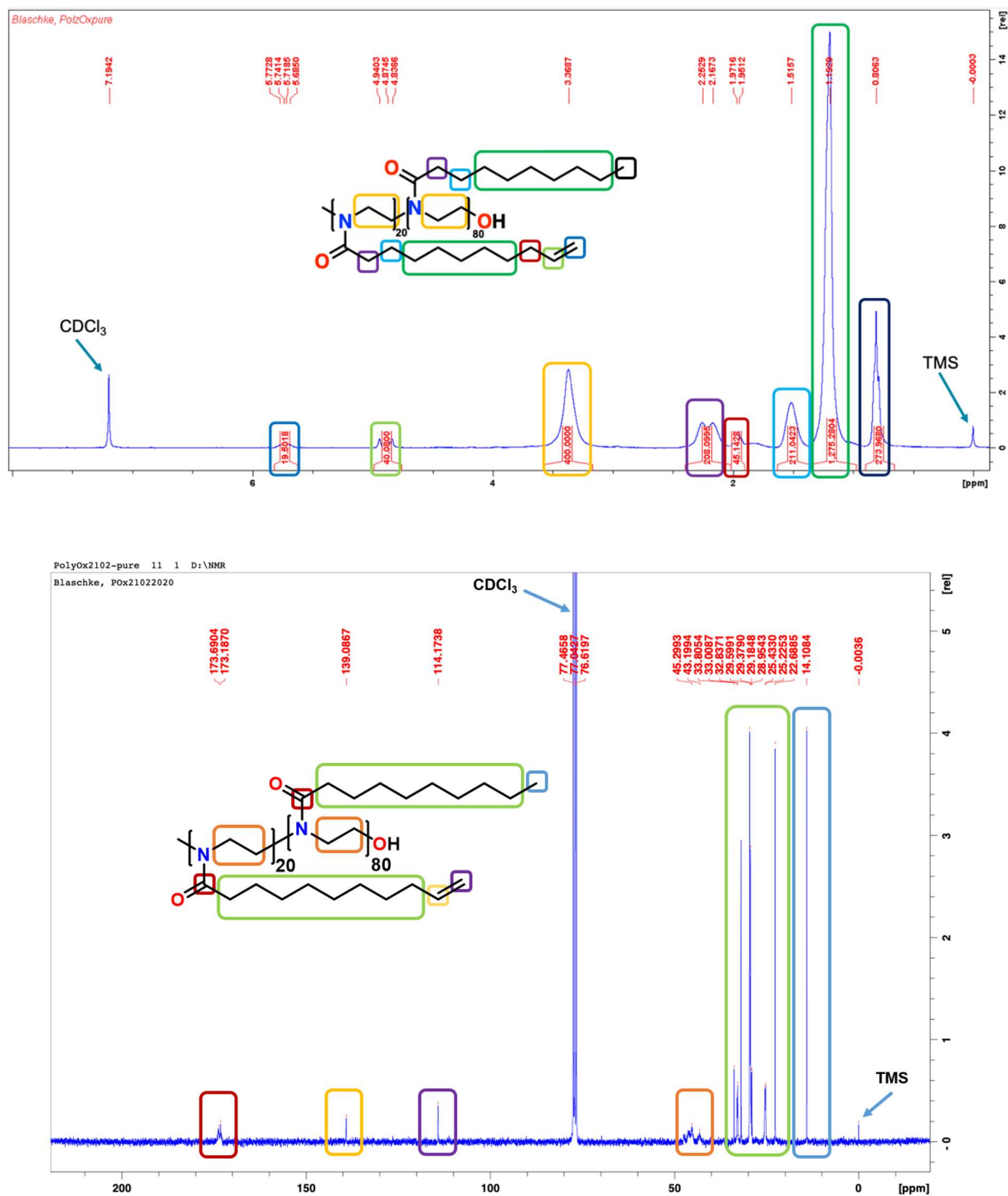
Figure 10: ^{1}H-NMR spectrum of pNonOx$_{80}$-*stat*-pDec$^=$Ox$_{20}$ in CDCl$_3$ with TMS 0.03 % (v/v) as internal standard, with signals assigned to the chemical structure. ^{13}C-NMR spectrum of pNonOx$_{80}$-*stat*-pDec$^=$Ox$_{20}$ in CDCl$_3$ with TMS 0.03 % (v/v).

In the ^{1}H-NMR spectrum, the signals at δ = 0.81, 1.19, 1.52, 1.95-1.97 and 2.17-2.25 ppm (Figure 10) represent the saturated parts of the two different side-chains. The signals at δ = 4.83-4.94 and 5.69-5.77 ppm are identified as the hydrogens atoms of the double bond of the side-chain in Dec$^=$Ox. The hydrogen atoms of the polymer main chain are identified at the chemical shift of δ = 3.37 ppm (marked in yellow). The integral of the ^{1}H-Spectra was calibrated to the backbone of the copolymer. Assuming hundred repetition units, the integral in the yellow square was set to 400.

The copolymer was additionally characterized by gel permeation chromatography (GPC), and IR spectroscopy. The values have been summarized in the Experimental Part. Also, thermogravimetric analysis (TGA) and differential scanning calorimetry (DSC) were performed (see hereinafter).

The TGA analysis (Figure 11) shows the mass decrease from 20 to 550 °C with a heating rate of 10 K·min^{-1} under helium atmosphere. Up to a temperature of 200 °C, no mass losses can be determined. The weight losses (m < 95%) start at a temperature as high as 350 °C; the polymer is degraded in one step. At a temperature of 500 °C, the polymer is fully decomposed, and no solid material is left.
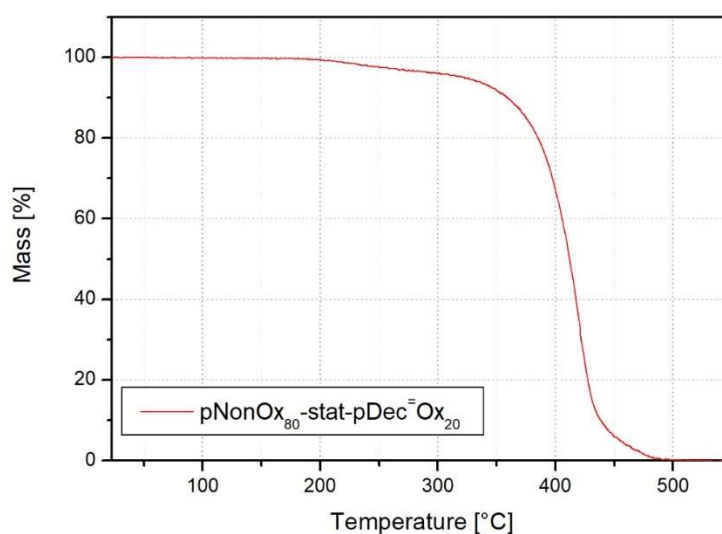
Figure 11: Thermogravimetric analysis of pNonOx$_{80}$-*stat*-pDec$^=$Ox$_{20}$.

The DSC measurement was performed in a range from 20 to 550 °C with a heating rate of 10 K·min^{-1} under helium atmosphere (Figure 12). Three endothermic reactions are represented in the diagram. The first peak at the temperature of 41 °C represents the glass-transition point, and the peak at 138 °C the melting point of the copolymer. The third peak is the decomposition peak of the copolymer.
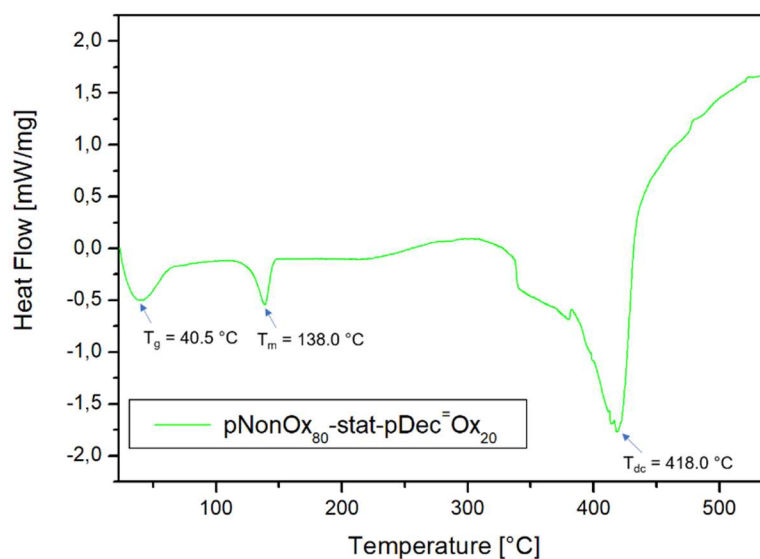
Figure 12: DSC analysis of pNonOx$_{80}$-*stat*-pDec$^=$Ox$_{20}$. T_g is the glass-transition point, T_m is the melting point, and T_{dc} is the (peak of the) decomposition temperature.

4.3 Synthesis of the Spiroorthoester 2-((Allyloxy)methyl)-1,4,6-trioxaspiro[4.4] nonane

The synthesis of the spiroorthoester was performed according to the procedure described by Marx et al.[52] Under nitrogen atmosphere, a mixture of the Lewis acid $BF_3 \cdot OEt_2$ and γ-butyrolactone was dropped into the allyl glycidyl ether. The reaction was cooled under stirring (Scheme 11).[78] The γ-butyrolactone also acts as sol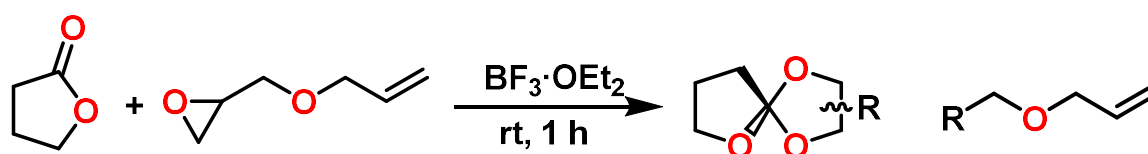vent. The reaction was quenched with NEt_3, and reaction mixture was worked up with H_2O and CH_2Cl_2. Purification was done via vacuum distillation.

Scheme 11: Schematic representation of the synthesis of 2-((allyloxy)methyl)-1,4,6-trioxaspiro[4.4]nonane.

The purified spiroorthoester was characterized via ^{1}H-NMR and ^{13}C-NMR NMR-spectroscopy in $CDCl_3$ (Figure 13) and IR-spectroscopy (Experimental Part).

From ^{1}H-NMR spectroscopy, the enantiomers are (pair-wise) indistinguishable (e.g., the structures A and B cannot be distinguished by ^{1}H-NMR measurements, neither can C and D; cp. Scheme 1), but the ratio of the two pairs of enantiomers may be calculated from the ^{1}H-NMR spectra [e.g., the ratio (A+B):(C+D)]. Due to the lack of steric hindrance during the synthesis, the two pairs of enantiomers of SOE were formed in almost identical amount [(A+B):(C+D) $\approx$ 5:5]. Additionally, the peaks of the NMR-spectroscopy and the IR analysis were in best alignment with those reported in the literature.[52]
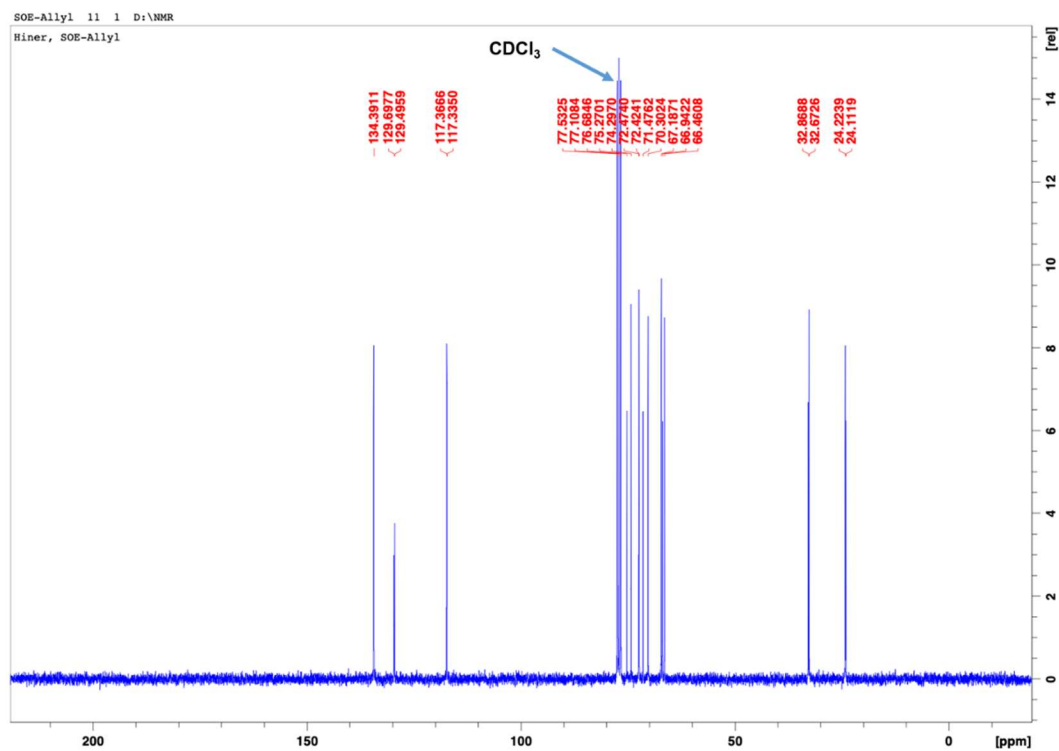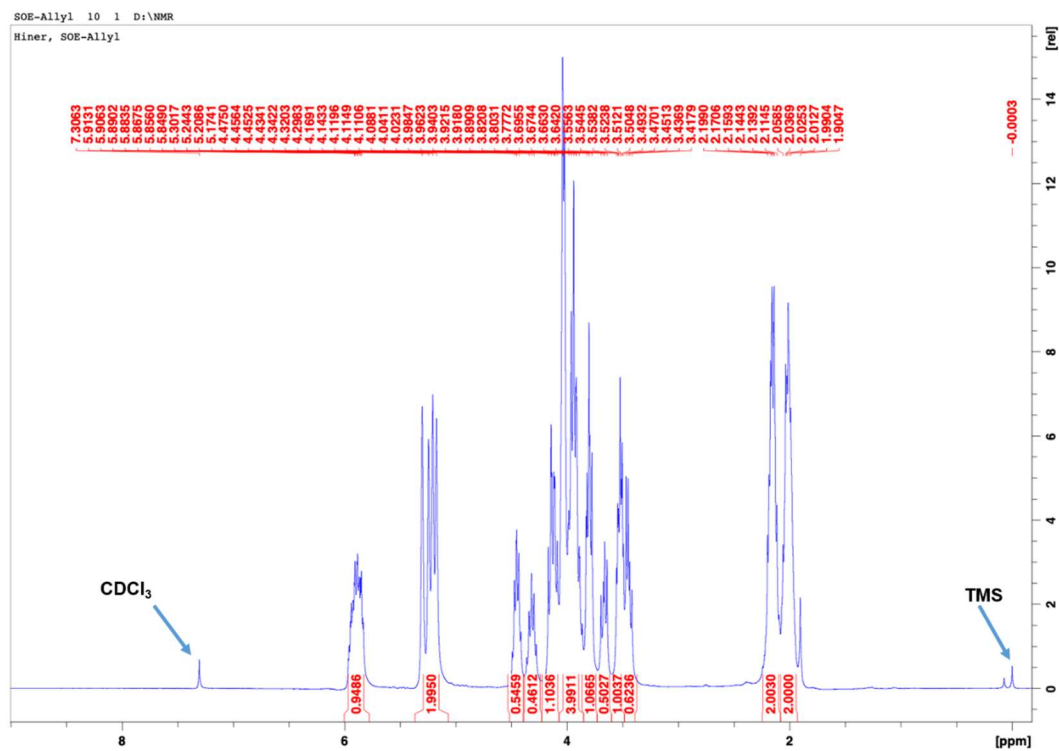
Figure 13: Top: ^{1}H-NMR spectrum of 2-((allyloxy)methyl)-1,4,6-trioxaspiro[4.4] nonane in CDCl$_3$ with TMS 0.03 % as internal standard. **Bottom:** ^{13}C-NMR spectrum of 2-((Allyloxy)methyl)-1,4,6-trioxaspiro[4.4] nonane in CDCl$_3$.

4.4 Development of the Dual/Bi-Stage Curing System and Preparation of Specimens of the Unfilled Polymer and the Polymer Nanocomposites

Twelve types of test specimens were prepared by crosslinking for both of the two different polymer matrixes pNonOx$_{80}$-*stat*-pDec$^=$Ox$_{20}$ and Nylon 12.

With special respect to the processing procedure, the polymerisation was to be triggered by thermal initiation. pNonOx$_{80}$-*stat*-pDec$^=$Ox$_{20}$ bears a double bond in the aliphatic side-chain of the Dec$^=$Ox repetition unit (Scheme 10). This side-chain functionality offers an excellent opportunity for the crosslinking of the polymer and the embedding of the particles in the network. By contrast, Nylon 12 has no double bonds in the polymer structure. As a recently published patent revealed, saturated polyamides can be crosslinked as well by the usage of a radical organic peroxide initiator.[79]

Therefore, dicumyl peroxide (DCP) was used as thermal initiator for the crosslinking reaction. DCP is solid at room temperature and can be mixed with the polymer and the nanoparticles. This ensures the preparation of homogeneous starting mixtures. DCP homolytically splits into to two radical species at elevated temperatures,[32] which initiate the crosslinking reaction (
Scheme 12, 2b).[80] Optimum crosslinking conditions were achieved for the POx samples using a content of 5 mol-% of DCP (related to the number of double bonds) in the copoly(2-oxazoline), and 2 wt.-% of DCP for the Nylon 12 samples.

The unfilled POx sample was subjected to sol:gel analysis in CHCl$_3$ to quantify the degree of crosslinking. The sol:gel ratio was found to be 99:1 for the crosslinked POx. The Nylon 12 sample could not be tested analogously, because Nylon 12 is almost insoluble in any common solvent already prior to crosslinking. Therefore, the crosslinking of Nylon 12 was tested by heating of the corresponding samples: A crosslinked and a non-crosslinked Nylon 12 sample were heated at 240 °C for 1 h. The non-crosslinked polymer changed the form, because it was heated above the melting point. The crosslinked polymer did not show this behaviour; the shape remained unchanged. This indicates that the crosslinking was performed successfully.

In case of the formulations containing SOE, an additional cationic thermal initiator for the double ring-opening of SOE had to be found in order to ensure dual-curing, in the course of which a crosslinked polymer with reduced shrinking at the same time was prepared. For the crosslinking of SOE, the same initiator DCP (Scheme 12) was used.

It was shown in a patent that quaternary ammonium salt of an aromatic heterocyclic compound containing 1 or 2 nitrogen atoms and a complex halide anion are able to polymerize epoxides at a temperature of 160 °C.[81] Hence, as cationic initiator 1-butylpyridin-1-ium hexafluoro phosphate(V) was chosen, because of following properties:

- It is a white solid compound and therefore a homogenous starting mixture can be easily produced with the polymer powder, the nanoparticles and the thermal initiator DCP.
- It is a metal free catalyst.
- The cationic initiator melts at a temperature of 75 °C.[82]

While the thermal decomposition of this cationic initiator has not yet been supported with sufficient experimental data in the literature, the formation of a super acid (with hexafluoro phosphate as anion) is a likely assumption.
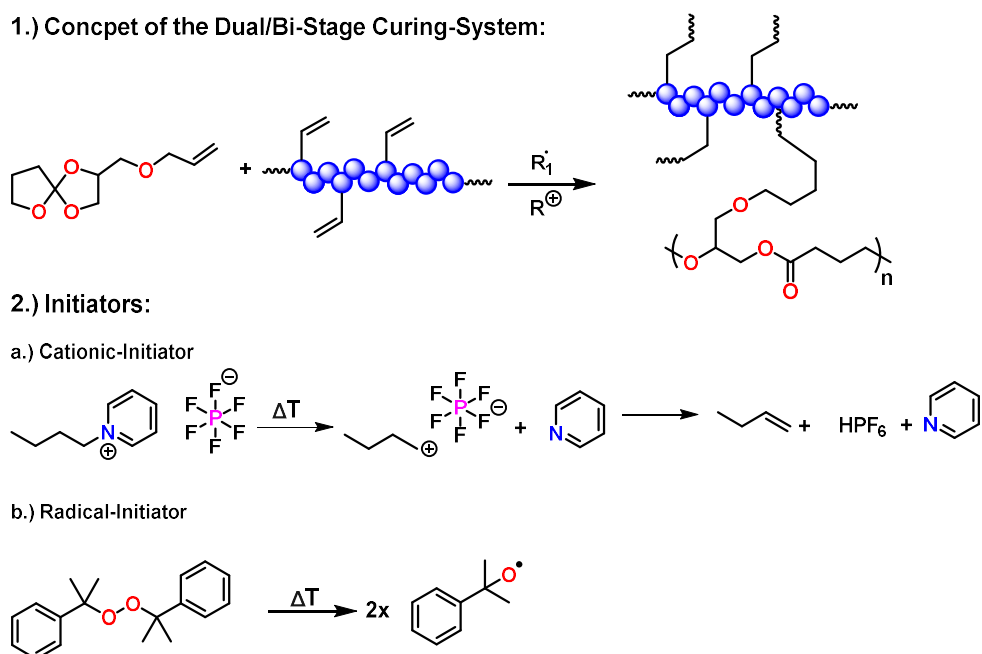
Scheme 12: 1.) Schematic concept of the dual/bi-stage curing system involving radical crosslinking and cationic (double) ring-opening at the same time, the latter in order to reduce/prevent volume shrinkage. 2.) a.) Cationic initiator 1-butylpyridin-1-ium hexafluorophosphate(V) b.) Radical initiator dicumyl peroxide.

Three types of differently sized test specimen were successfully prepared in the platen press of the copoly(2-oxazoline) and the Nylon 12 polymer (Figure 14):

- squares with an area of 8 x 8 cm and a height of 300 µm for dielectric spectroscopy,
- circles with a diameter of 4 cm and a height of 300 µm for light flash analyses, and
- rectangles with an area of 1 x 2 cm and a height of 300 µm for the zeta potential and the contact angle measurements.
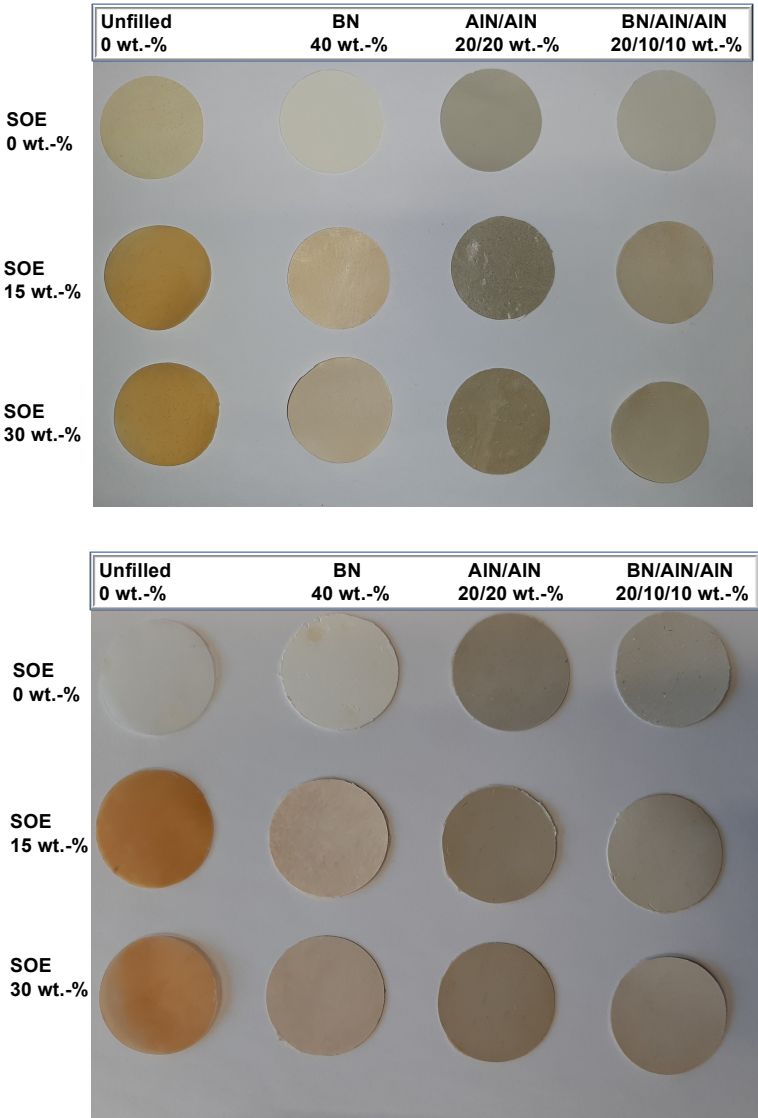

Figure 14: Photography of the circular-shaped test specimen. The diameter of the specimen is d = 40 mm. TOP: POx; bottom: Nylon 12.

4.5 Determination of the Volumetric Expansion

In order to determine the influence of the SOE on the volumetric change during the crosslinking of the polymer, the mass (m) and the dimensions of each sample were measured. The thickness and length of the test specimens were determined with a caliper at 8 different measuring points. The volume (V) of the test specimens was calculated from the mean values of the thickness and the length. The density (ρ) was calculated by the following formula:

$$\rho = \frac{m}{V} \qquad\qquad (6)$$

The volume expansions were calculated relative to the density of the specimen without SOE (Table 1 and Table 2). The addition of SOE induces a volume expansion compared to the sample without the spiroorthoester. The relative volume expansion of the POx samples due to the addition of SOE in a content of 15 wt.-% is in the range of 1.23-1.54%, and for a SOE content of 30 wt.-% in the range of 4.29-7.69%. The relative volume expansion of the Nylon 12 samples due to the addition of SOE in a content of 15 wt.-% is smaller than 1%, and for a SOE content of 30 wt.-% in the range of 1.41-2.48%.

Hence, the POx samples show higher volume expansion than the Nylon 12 samples. A possible explanation can be the steric hindrance in the condensed phase due to the hydrophobic (nonyl and decenyl) side-chains in the POx system, which, in final consequence, induces different separation among the polyamide and polyester/polyether phases than in the Nylon 12. This phenomenon needs to be subjected to further investigation.

Nevertheless, volume shrinkage could be reduced in both polymer systems. A thermally triggered dual/bi-stage curing system could be developed by using a combination of the thermal radical initiator dicumyl peroxide and the thermal cationic initiator 1-butylpyridin-1-ium hexafluorophosphate(V). This is an important step towards the delivery of a new synthetic protocol to reduce the formation of micro-cracks, micro-voids or delamination.

Table 1: Density in g·cm^{-3} of the POx samples and the relative calculated volumetric expansion.

POx								
SOE wt.-%	Particles 0 wt.-% [g/cm^3]	Volume Expansion [%]	BN 40 wt.-% [g/cm^3]	Volume Expansion [%]	AlN/AlN 20/20 wt.-% [g/cm^3]	Volume Expansion [%]	BN/AlN/AlN 20/10/10 wt.-% [g/cm^3]	Volume Expansion [%]
0	1.05	-	1.23	-	1.29	-	1.29	-
15	1.04	1.54	1.21	1.39	1.24	3.70	1.23	4.97
30	1.01	4.39	1.17	4.84	1.19	7.69	1.19	7.50

Table 2: Density in g·cm^{-3} of the Nylon 12 samples and the relative calculated volumetric expansion.

Nylon 12								
SOE wt.-%	Particles 0 wt.-% [g/cm^3]	Volume Expansion [%]	BN 40 wt.-% [g/cm^3]	Volume Expansion [%]	AlN/AlN 20/20 wt.-% [g/cm^3]	Volume Expansion [%]	BN/AlN/AlN 20/10/10 wt.-% [g/cm^3]	Volume Expansion [%]
0	1.02	-	1.21	-	1.26	-	1.28	-
15	1.01	0.98	1.20	0.84	1.25	0.46	1.27	0.84
30	0.99	2.48	1.19	1.41	1.24	1.92	1.26	1.60

4.6 Contact Angle and Surface Energy Measurement

Polymer networks and nanocomposites, which show a high static contact angle to water, exhibit a nonwetting surface. This behaviour improves the performance of outdoor insulators in polluted and wet environments and also the life time.[83] In addition, the surface energy is an important value for the wetting behaviour of a surface, in order to form a stable film on the material surface. This is interesting for example in coating or printing processes.[84] It also an important parameter for the electronic performance in thin-film transistors.[85]

In order to determine the surface properties of the Nylon 12 and POx samples, contact angle measurements were performed. Each sample was measured with the test liquids distilled water and diiodomethane. At least 5 individual points on the surface (drop volume 3 µL) were measured with each test liquid. The surface energies were calculated according to Owens-Wendt-Rabel-Kaelble.

Table 3: Overview of the values of the contact angles and the calculated surface energy of the POx and Nylon 12 samples. SD is the abbreviation for the standard deviation.

POx	Contact angle measurement with water [°]							
SOE wt.-%	Particle 0 wt.-%	SD	BN 40 wt.-%	SD	AlN/AlN 20/20 wt.-%	SD	BN/AlN/AlN 20/10/10 wt.-%	SD
0	98.48	0.97	136.70	1.18	104.38	1.12	119.55	1.57
15	114.15	5.69	125.25	3.47	102.46	3.20	104.43	2.31
30	74.22	5.24	99.11	3.70	92.82	2.87	109.00	1.71

POx	Contact angle measurement with diiodomethane [°]							
SOE wt.-%	Particle 0 wt.-%	SD	BN 40 wt.-%	SD	AlN/AlN 20/20 wt.-%	SD	BN/AlN/AlN 20/10/10 wt.-%	SD
0	74.49	3.51	87.34	3.27	80.86	1.36	71.36	6.15
15	64.99	4.43	89.34	2.77	74.63	3.58	71.15	1.68
30	57.80	1.11	75.38	3.18	63.85	1.80	77.64	1.75

POx	Surface Energy [mN/m]							
SOE wt.-%	Particle 0 wt.-%	SD	BN 40 wt.-%	SD	AlN/AlN 20/20 wt.-%	SD	BN/AlN/AlN 20/10/10 wt.-%	SD
0	22.34	2.35	15.01	1.83	18.34	0.94	22.36	3.67
15	25.80	2.83	13.03	1.35	21.43	2.59	22.79	1.25
30	38.32	3.26	21.80	2.66	28.58	1.81	19.09	1.12

Nylon 12	Contact angle measurement with water [°]							
SOE wt.-%	Particle 0 wt.-%	SD	BN 40 wt.-%	SD	AlN/AlN 20/20 wt.-%	SD	BN/AlN/AlN 20/10/10 wt.-%	SD
0	101.82	5.49	109.83	4.97	116.97	4.83	118.84	2.56
15	89.05	3.10	101.23	3.51	101.91	1.73	127.07	1.81
30	107.36	1.22	100.95	2.08	84.79	3.93	95.58	6.24

Nylon 12	Contact angle measurement with diiodomethane [°]							
SOE wt.-%	Particle 0 wt.-%	SD	BN 40 wt.-%	SD	AlN/AlN 20/20 wt.-%	SD	BN/AlN/AlN 20/10/10 wt.-%	SD
0	67.14	4.26	67.08	3.28	67.91	3.57	74.90	0.90
15	61.04	2.22	62.10	2.45	67.94	1.65	80.43	2.34
30	58.88	1.09	53.83	2.15	60.09	1.61	57.90	3.02

Nylon 12	Surface Energy [mN/m]							
SOE wt.-%	Particle 0 wt.-%	SD	BN 40 wt.-%	SD	AlN/AlN 20/20 wt.-%	SD	BN/AlN/AlN 20/10/10 wt.-%	SD
0	25.15	3.24	24.53	1.97	24.22	2.36	20.27	0.60
15	30.95	2.26	27.83	1.85	24.74	1.21	17.76	1.41
30	29.22	0.64	32.29	1.39	32.80	2.38	30.85	2.90

The Nylon 12 samples with 0-30 wt.-% SOE show values in the range of 23-30 mN·m^{-1}, which are hardly altered upon the addition of fillers (Figure 15). The lowest surface energy of 18 mN·m^{-1} is found at the Nylon 12 sample with 15 wt.-% of SOE and BN/AlN/AlN filling.

The influences on the surface energies are more clearly pronounced in the case of the POx samples. Two general trends are discernible: increased values for increased contents of SOE vs. decreased values for increased contents of inorganic fillers. The BN fillers show a more pronounced effect on decreasing the surface energy than the AlN fillers; correspondingly, the lowest surface energy of 13 mN·m^{-1} is found for the POx/15 wt.-% SOE composite with 40 wt.-% BN. Notably, this value is as low as that of Teflon, a poly(tetrafluoro ethylene) and indicative of pronouncedly hydrophobic surfaces.

The different influence of blending and compounding of the Nylon 12 and POx samples on the surface energy will be subjected to further investigations (see also chapter 4.7. hereinafter); different degrees of phase separation (see hereinabove) are a likely origin on the molecular level for this macroscopic property.
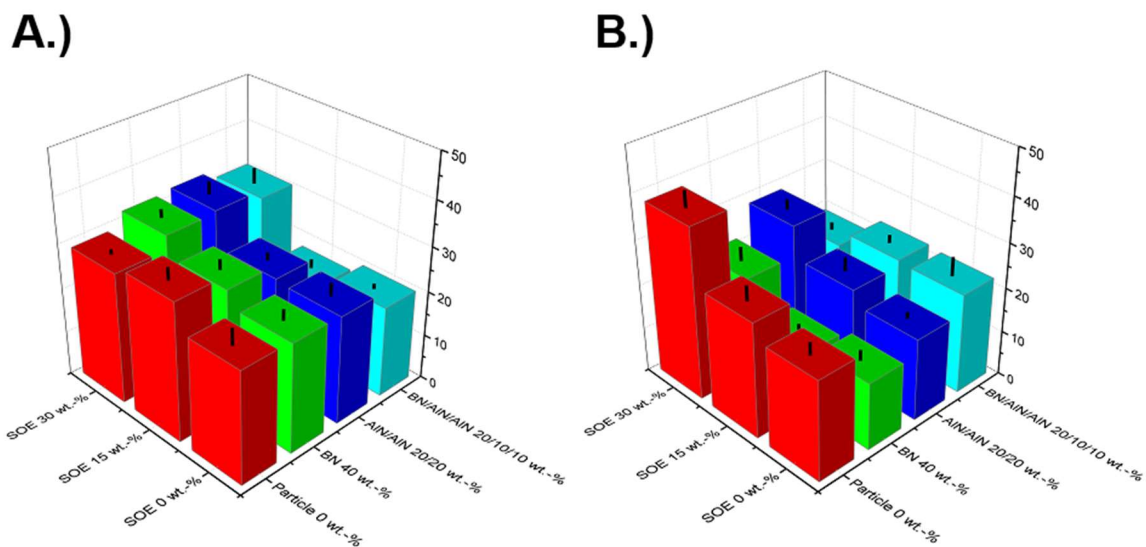

Figure 15: Surface energy calculated according to Owens-Wendt-Rabel-Kaelble. A.) Nylon 12 samples; B.) POx samples. The black line represents the standard deviation.

4.7 Zetapotential Measurements

In order to further investigate the surface properties of the POx and Nylon 12 samples, their zetapotentials were measured in a cell with a 1mM KCl solution. The isoelectric points (IEPs) were determined by titration with 50 mM HCl and 50 mM NaOH.

Table 4: Isoelectric points of the different POx samples from zetapotential measurements.

POx	IEP of the Zetapotential Measurements			
SOE wt.-%	Particle 0 %	BN 40 wt.-%	AIN/AIN 20/20 wt.-%	BN/AIN/AIN 20/10/10 wt.-%
0	5.93	6.78	8.64	6.38
15	7.92	7.20	7.49	7.91
30	8.25	8.15	7.42	7.21

Table 5: Isoelectric points of the different POx samples from zetapotential measurements.

Nylon 12	IEP of the Zetapotential Measurements			
SOE wt.-%	Particle 0 %	BN 40 wt.-%	AIN/AIN 20/20 wt.-%	BN/AIN/AIN 20/10/10 wt.-%
0	4.05	3.90	4.47	3.95
15	4.81	4.60	5.63	5.23
30	4.61	4.54	5.19	5.34

The IEPs of the POx and Nylon 12 samples (Figure 16) span two different ranges: While the IEPs of the Nylon 12 samples are in the range pH = 3.9-5.6 (neutral to slightly acidic range of zetapotential measurements), the IEPs of the POx samples are in the range pH = 5.9-8.6 (slightly alkaline to alkaline range of zetapotential measurements). This trend can be retraced to the amide structural motif in the two types of polyamides: In Nylon 12, the motif R-NH-CO-R is present, which can form the tautomer R-N=C(OH)-R tautomer (that can be deprotonated); in POx, the motif R_2-N-CO-R is present, which can (only) be protonated.[86]

As a general trend, the incorporation of SOE in the polymer network (introduction of polyester structural motifs) shifts the IEP to higher values. Minor deviations from this trend can only be observed in the composites that contain AlN particles, which can be protonated/deprotonated to minor extent.

In summary, for an estimation of the IEP, (at least) three points have to be considered:

- tautomer formation of the amides
- (de-)protonability of esters (and their tautomers)
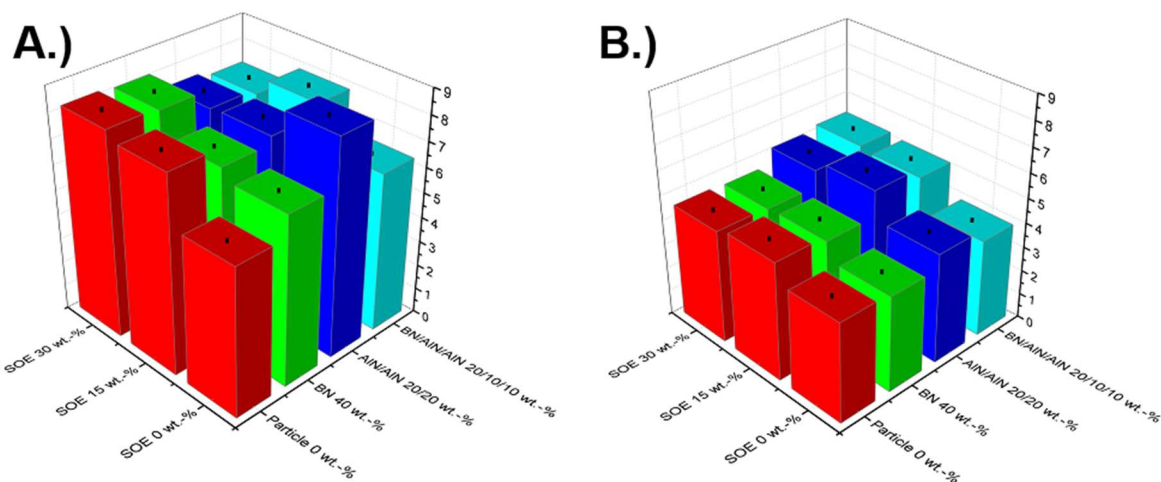- (de-)protonability of particle surfaces.

Figure 16: Isoelectric point of zetapotential measurements of the different test specimen: A.) POx samples; B.) Nylon 12 samples. The black line represents the standard deviation of the glass electrode.

4.8 Thermal Conductivity of the Polymers and the Nanocomposites

The different test specimens were also investigated for their thermal behaviour. Therefore, the thermal diffusivity was determined by LFA measurements at seven different temperatures: −20, 20, 60, 100, 140, 180, and 220 °C. Test specimen with a diameter of 4 cm and a height of 300 µm were used.

The thermal diffusivity follows the general trends summarized hereinafter in straightforward fashion: The thermal diffusivity

- decreases with increasing temperature and reaches a constant value at high temperatures (which has been reported for numerous other materials as well, in particular for polymers)
- decreases with increasing content of SOE (which can be retraced to the higher thermal conductivity of polyamides in comparison to polyesters/polyethers AND the lowered density upon the addition of SOE as expanding monomer)
- increases with the filler content in the order no filler < AlN/AlN < BN/AlN/AlN < BN (perfectly reproducing the different thermal conductivity of the polymer, AlN, and BN)

By adding different particle sizes of AlN, no higher heat transport could be achieved. Thus, the thermal behaviour in this test series, depends purely on the thermal conductivity of the material, and the particle size does not show any influence on the thermal diffusivity (cp. chapter 3.1.5). Hence, the use of different particle sizes of AlN, cannot exceed the thermal conductivity properties of BN at a filler content of 40 wt.-%.

At higher temperatures, the values for the thermal diffusivity of the two polymer systems converge. For BN = 40 wt.-% (T = 180 and 220 °C) and AlN/AlN = 20/20 wt.-% (T = 220 °C), the POx composites show higher values than the Nylon 12 composites.

Table 6: Thermal diffusivity values of the LFA measurement of the POx and Nylon 12 samples.

POx — Thermal Diffusivity [mm²/s]

T [°C]	SOE wt.-%	Particles 0 wt.-%	BN 40 wt.-%	AlN/AlN 20/20 wt.-%	BN/AlN/AlN 20/10/10 wt.-%
-20	0	0.106	0.234	0.171	0.185
-20	15	0.099	0.200	0.160	0.193
-20	30	0.096	0.208	0.136	0.181
20	0	0.090	0.197	0.140	0.154
20	15	0.081	0.157	0.129	0.156
20	30	0.076	0.161	0.110	0.147
60	0	0.077	0.172	0.122	0.132
60	15	0.070	0.140	0.116	0.132
60	30	0.068	0.145	0.098	0.126
100	0	0.073	0.164	0.117	0.126
100	15	0.066	0.133	0.111	0.121
100	30	0.062	0.133	0.094	0.115
140	0	0.071	0.158	0.113	0.122
140	15	0.063	0.127	0.105	0.112
140	30	0.058	0.125	0.091	0.106
180	0	0.068	0.151	0.107	0.116
180	15	0.061	0.122	0.099	0.109
180	30	0.056	0.124	0.087	0.101
220	0	0.065	0.144	0.104	0.111
220	15	0.059	0.117	0.094	0.105
220	30	0.055	0.121	0.083	0.097

Nylon 12 — Thermal Diffusivity [mm²/s]

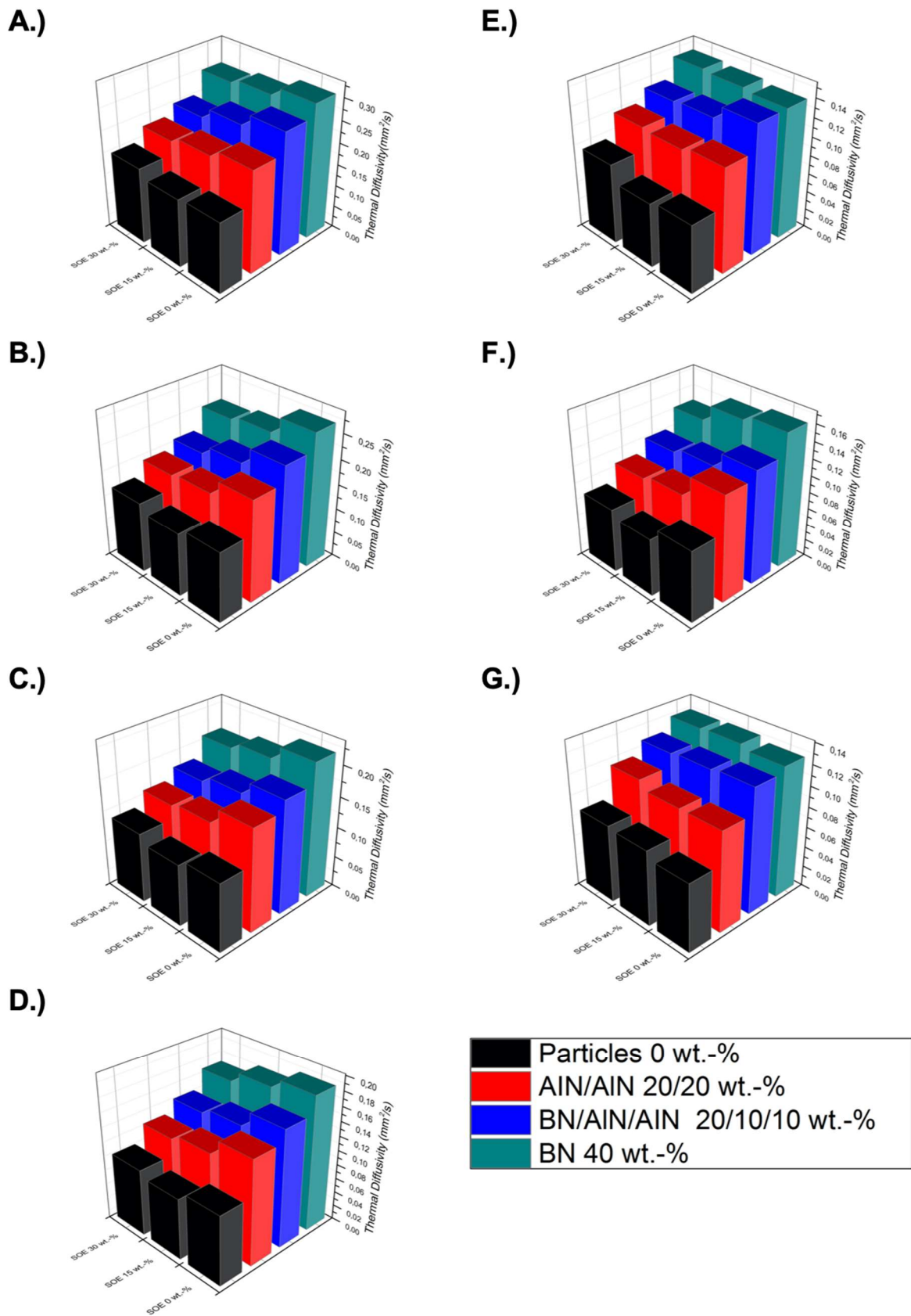| T [°C]	SOE wt.-%	Particles 0 wt.-%	BN 40 wt.-%	AlN/AlN 20/20 wt.-%	BN/AlN/AlN 20/10/10 wt.-%
-20	0	0.162	0.308	0.234	0.280
-20	15	0.157	0.288	0.217	0.252
-20	30	0.175	0.278	0.204	0.227
20	0	0.000	0.000	0.204	0.237
20	15	0.000	0.000	0.174	0.203
20	30	0.000	0.000	0.169	0.185
60	0	0.112	0.219	0.168	0.185
60	15	0.101	0.197	0.142	0.164
60	30	0.114	0.186	0.136	0.153
100	0	0.097	0.187	0.146	0.163
100	15	0.085	0.174	0.124	0.141
100	30	0.093	0.159	0.116	0.133
140	0	0.085	0.161	0.127	0.136
140	15	0.069	0.155	0.102	0.118
140	30	0.077	0.135	0.097	0.112
180	0	0.073	0.139	0.112	0.139
180	15	0.069	0.142	0.108	0.125
180	30	0.086	0.144	0.110	0.123
220	0	0.067	0.127	0.098	0.122
220	15	0.074	0.131	0.098	0.120
220	30	0.076	0.130	0.106	0.118

Figure 17: LFA measurements of the Nylon 12 samples. A.) −20 °C, B.) 20 °C, C.) 60 °C, D.) 100 °C, E.) 140 °C, F.) 180 °C, and G.) 220 °C.
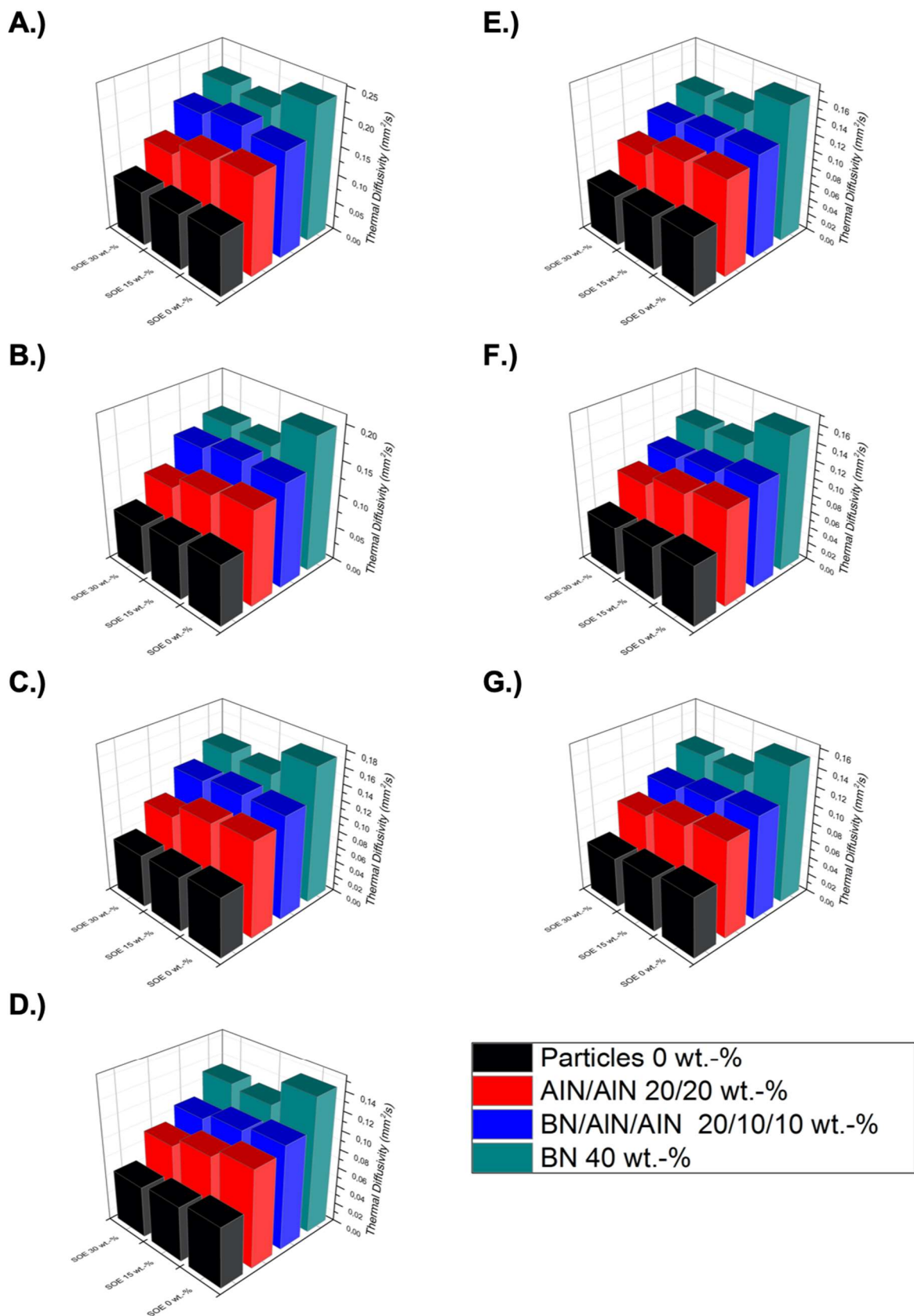
Figure 18: LFA measurements of the POx samples. A.) –20 °C, B.) 20 °C, C.) 60 °C, D.) 100 °C, E.) 140 °C, F.) 180 °C, and G.) 220 °C.

4.9 Dielectric Characterization of the Polymers and the Composites

4.9.1 Dielectric Characterization of the Nylon 12 Specimens

The Nylon 12 samples were characterized for their real part and the imaginary part of the permittivity as well as the loss factor tanδ. The real part of the permittivity increases with decreasing frequencies for all Nylon 12 samples in a frequency range from 0.1 Hz to 5 kHz.

If no SOE was added to the formulations, the unfilled samples have approximately the same permittivity as the composites filled with particles. Conversely, the permittivity increases for the samples that contain SOE. This observation can be referred to the volume expansion by adding SOE to the polymer matrix, which means that the free volume increases.

According to the Tanaka Modell, a change of the interfacial region changes the distance of the multi-layers, and, hence, the electronic properties must change adequately. This is also the reason why the imaginary part of the permittivity increases due to the incorporation of SOE to the polymer matrix. The loose layer (the third layer of the Tanaka model) increases and can be correlated with the increase of the loss of the stored energy.

A significant increase of both, the real and the imaginary part of the permittivity, can be observed for the lower range of frequencies. The influence on the polarizability by the network density requires a detailed inspection: electronic polarization, atomic polarization, and orientation polarization can be excluded to cause these phenomena. At the lower range of frequencies in the range of 10 Hz and lower, interfacial polarization with typical frequencies of 10^{-5} to 10^2 Hz can be held responsible to cause the polarization effects.[16][87] Hence, this observation can be perfectly aligned with the predictions according to the Tanaka model described hereinabove.
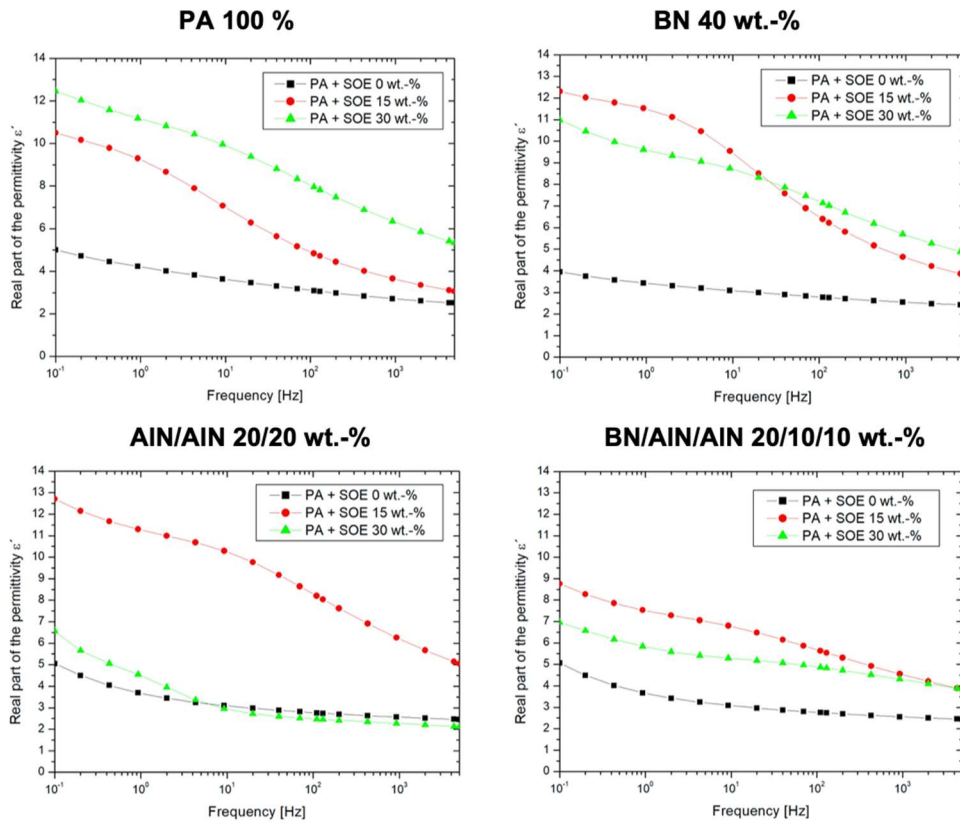
Figure 19: Real part of the permittivity of the Nylon 12 samples in a frequency range of 0.1 Hz to 5 kHz.
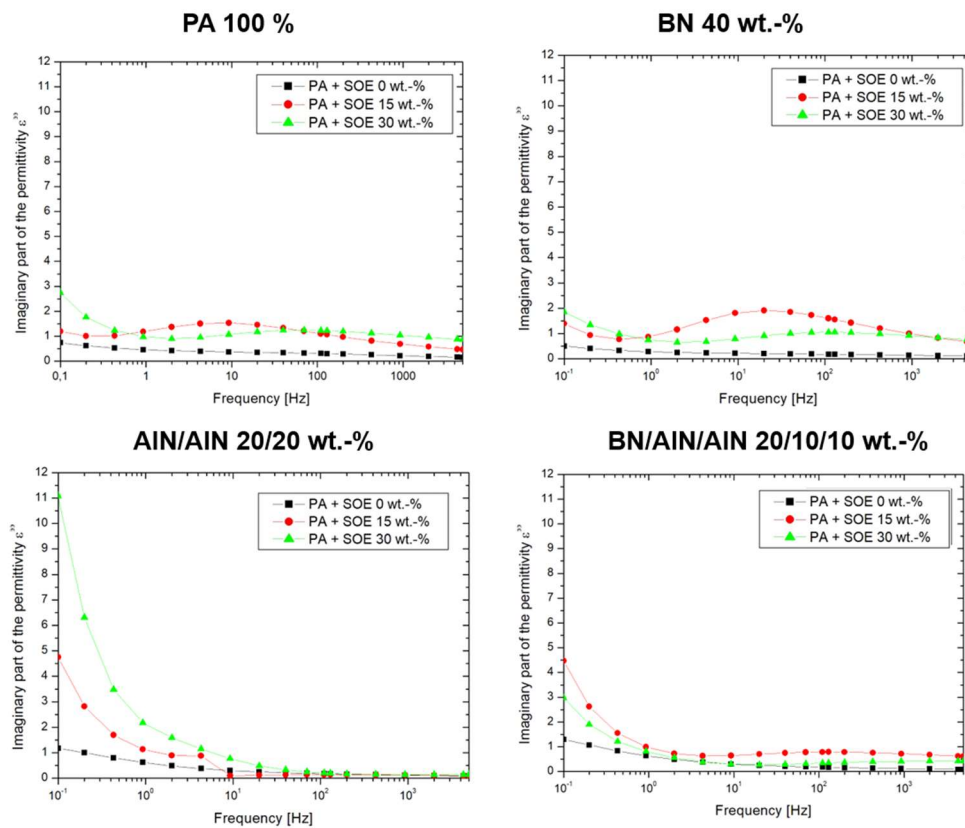

Figure 20: Imaginary part of the permittivity of the Nylon 12 samples in a frequency range of 0.1 Hz to 5 kHz.

At a standardized frequency of approx. 50 Hz, all composites have a tanδ equal to or lower than the unfilled samples (Figure 21), which renders them superior as dielectrics, as less electric charges are lost during operation. The addition of SOE (15 or 30 wt.-%) increases tanδ of the filled and unfilled polymer samples. This is due to the increase of the free volume, the decrease of the material density, and the increased extent of interfacial polarization (see hereinabove).

The composites with the two types of AlN particles show the smallest tanδ values. If no SOE is added, tanδ is as low as 0.07 (at 40 Hz), which is a remarkably low value for non-polyolefinic dielectrics. Moreover, the tanδ values are quasi-constant over a wide range of frequencies and increase only at frequencies lower than of 1 Hz. Hence, it may be argued that the AlN/AlN/Nylon 12 hybrid system is the best-suited dielectric of the Nylon 12 series.
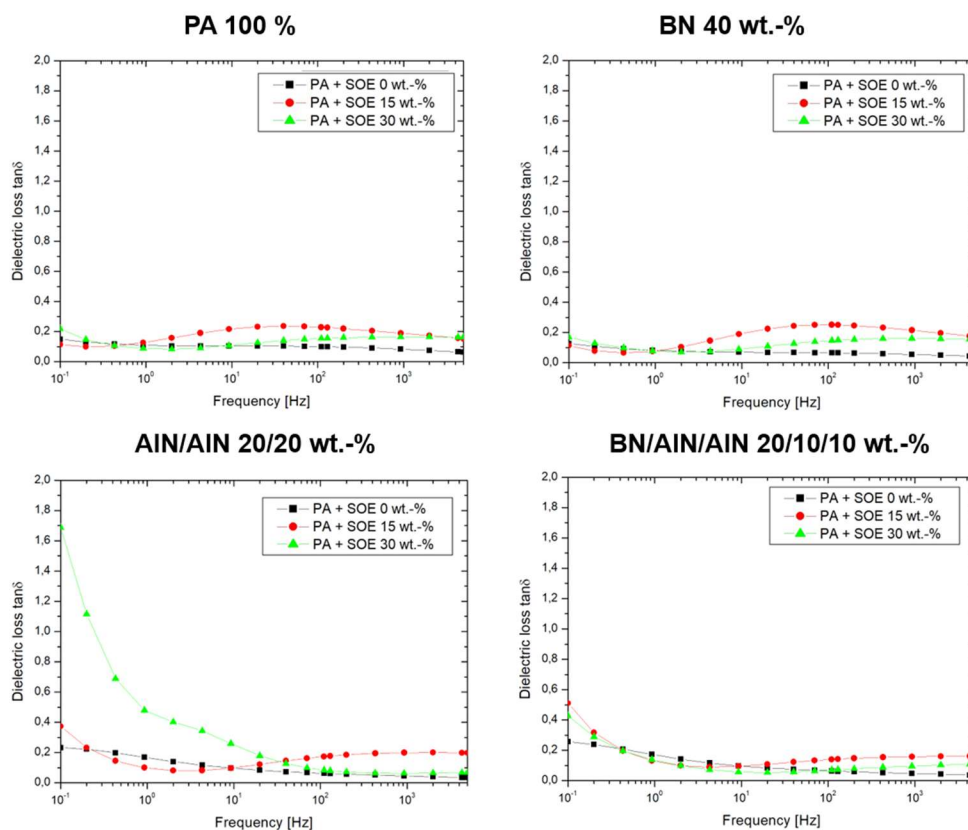
Figure 21: The dielectric loss tanδ of the Nylon 12 samples in a frequency range of 0.1 Hz to 5 kHz.

4.9.2 Dielectric Characterization of the POx Specimens

The real part as well as the imaginary part of the permittivity increase with decreasing frequencies for all POx samples. The real part of the permittivity increases with decreasing frequencies for all POx samples in a frequency range from 0.1 Hz to 5 kHz.

The real part of the permittivity increases with increasing content of SOE (in all of the four sub-series with identical filler content), yet to significantly lesser extent than in the Nylon 12 sub-series. While the density changes upon the addition of SOE were more pronounced in the POx series than in the Nylon 12 series (Table 1 and Table 2), it is tempting to refer this observation to a different extent of phase separation in the two types of polyamides (cp. with the comments/assumptions of phase separation hereinabove). The POx samples have a (relative) volume expansion of 4-7% at 30 wt.-% of SOE, while Nylon 12 shows (relative) volume expansion of only 1-2%.

The real part of the permittivity of the unfilled polymer and the composite with AlN/AlN = 20/20 wt.-% are very comparable over the whole range of frequencies; the addition of SOE (15 or 30 wt.-%) only has a minor influence. On the contrary, the increase of the real part of the permittivity in the lower range of frequencies is very pronounced in the resins containing 30 wt.-% of SOE and BN particles (40 wt.-% BN as well as 20/10/10 wt.-% BN/AlN/AlN).

On the contrary, the imaginary part of the permittivity increases tremendously in all samples containing 30 wt.-% of SOE (in all of the four sub-series with identical filler content) in the lower range of frequencies, while the imaginary part of the permittivity of the SOE-free polymer and composites is very comparable to those containing 15 wt.-% of SOE.

In summary, it may be argued that the interfacial polarization (in the lower range of frequencies) in the POx series is most significantly increased upon the addition of SOE in 30 wt.-% quantities and/or BN in 20 or 40 wt.-% quantities.
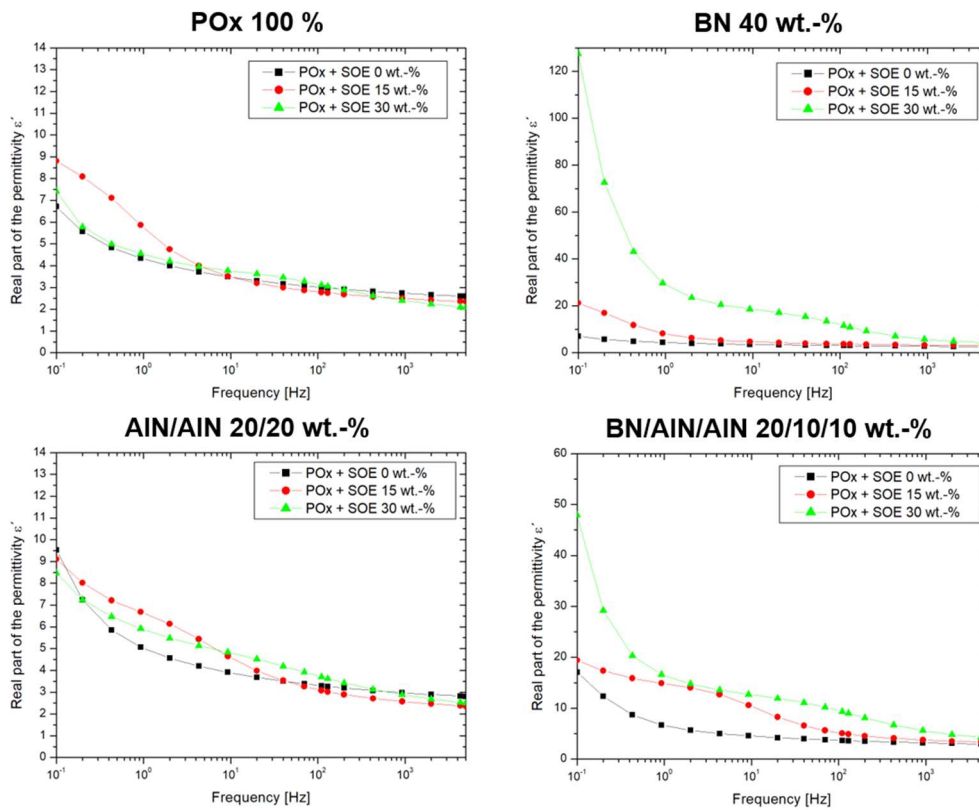
Figure 22: Real part of the permittivity of the POx samples in a frequency range of 0.1 Hz to 5 kHz.
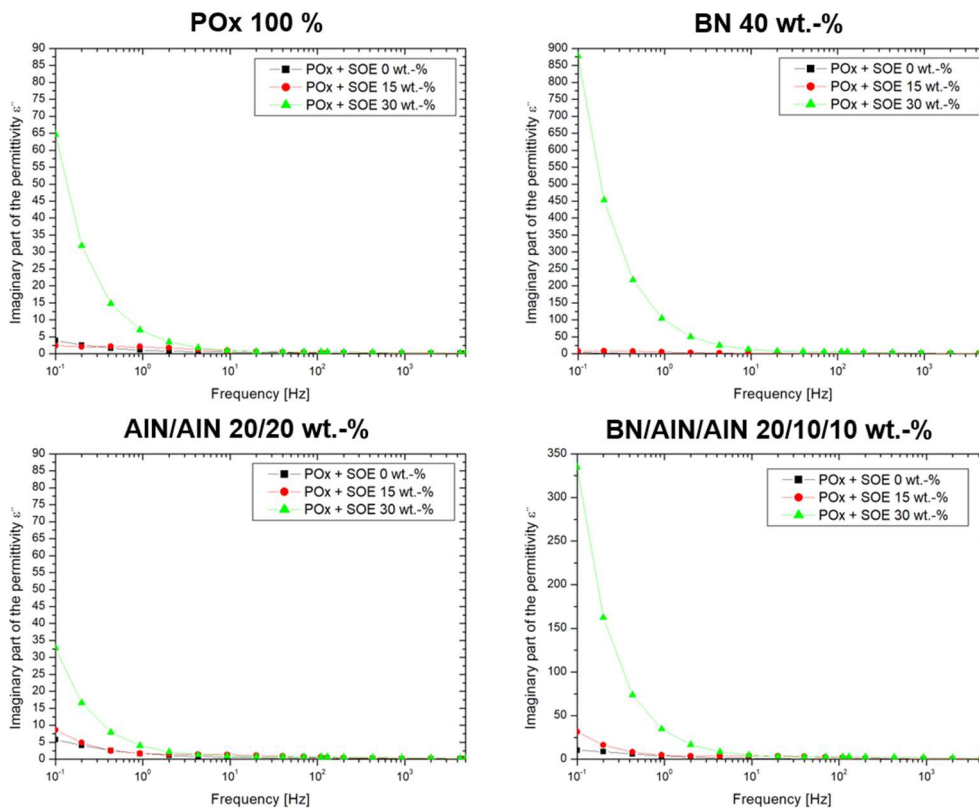

Figure 23: Imaginary part of the permittivity of the POx samples in a frequency range of 0.1 Hz to 5 kHz.

In particular the trends of the imaginary part of the frequency of the POx series are reproduced in the tanδ values, and may be summarized as follows:

- All samples containing SOE in a content of 30 wt.-% show very high loss factors in the lower range of frequencies.
- The loss factors of the (sub-)series containing no SOE or 15 wt.-% SOE are very comparable.
- In case of the samples containing 15 or 30 wt.-% of SOE, the loss factors are highest if BN is additionally present.

Notably, while the lowest values of the loss factor are reached within the Nylon 12 series (at the low range of frequencies), low values of tanδ can be reached in the POx series even if SOE is present in 15 wt.-% quantities, which offers advantages during the processing of these formulations due to reduced shrinkage during curing.
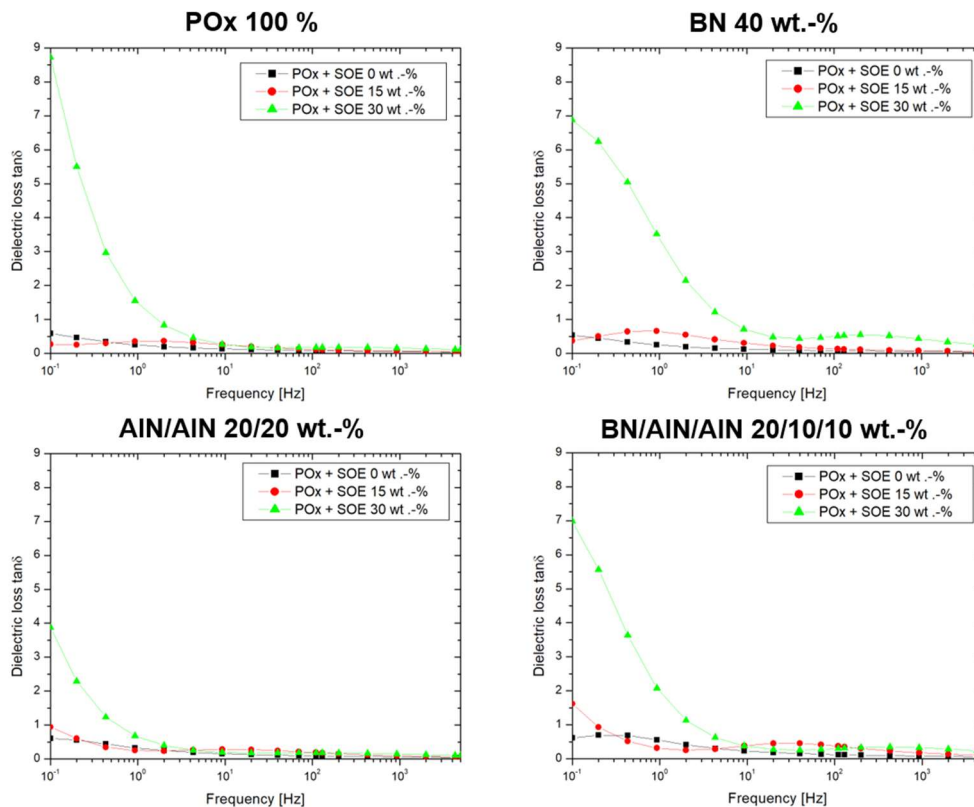

Figure 24: The dielectric loss tanδ of the POx samples in a frequency range of 0.1 Hz to 5 kHz.

4.9.3 Comparison of the POx Samples with the Nylon 12 Samples

For a comparison of the dielectric properties of the Nylon 12 and POx samples, the respective dielectric losses were summarized at a frequency of 40 Hz, which is the frequency range of standard table works in literature.

The unfilled POx samples show nearly the same values of tanδ as the Nylon 12 samples; as the POx was synthesized from renewable resources, it can be argued that this 'green' alternative shows competitive dielectric behaviour in comparison with fossil-based Nylon 12.

At the 'medium' range frequency of 40 Hz, the addition of 15 wt.-% of SOE to POx is less deteriorating for the dielectric properties than to Nylon 12 if no BN particles are present. At 40 Hz, the addition of 30 wt.-% of SOE can be only argued for the production of Nylon12-based dielectrics.

In summary, the interfacial polarization in the lower range of frequencies needs to be subjected to further studies. In particular the influence of covalent attachment of the particles to the polymer matrix is worth of further investigations.

Table 7: The dielectric loss tanδ of the POx and Nylon 12 samples at a frequency of 40 Hz.

POx	tanδ of the Dielectric Measurements			
SOE wt.-%	**Particle 0 %**	**BN 40 wt.-%**	**AlN/AlN 20/20 wt.-%**	**BN/AlN/AlN 20/10/10 wt.-%**
0	0.10	0.09	0.11	0.16
15	0.16	0.18	0.25	0.46
30	0.17	0.44	0.18	0.26
Nylon12	tanδ of the Dielectric Measurements			
SOE wt.-%	**Particle 0 %**	**BN 40 wt.-%**	**AlN/AlN 20/20 wt.-%**	**BN/AlN/AlN 20/10/10 wt.-%**
0	0.10	0.07	0.07	0.07
15	0.24	0.24	0.15	0.12
30	0.14	0.13	0.13	0.06

5 Conclusions and Outlook

Dielectric materials are important for the electronic industry. Due to the on-going miniaturization, novel material concepts have to be developed in order to fulfil the targets of the future: The increasing heat development is connected with the increasing processing speed in microelectronics and in high voltage engineering, aiming to obtain a higher power to volume ratio.

The efficient heat transport through (polymer-based) dielectric materials is an important challenge to ensure stable performance. Additionally, the volumetric shrinkage in the course of material processing (e.g., curing) plays an essential role on the lifetime and the performance of electric materials.

A large part of polymer-based dielectrics is obtained from petrochemicals and have been reviewed more critical by society due to the aspects of using fossil fuels for their production and the resulting environmental problems.

Considering this background, the aim of the present work was to develop dielectric materials, which are produced from renewable resources, show minimized volume shrinkage during crosslinking, and exhibit increased thermal conductivity.

The investigated systems consisted of a polyamide matrix, spiroorthoesters (SOEs) as expanding monomers, and nanoparticles. Commercially available Nylon 12 was to be compared with a self-synthesized copoly(2-oxazoline) from renewable resources. For the curing of the polymers, blends, and composites, a dual/bi-stage curing mechanism needed to be developed. Twelve different polymer samples for each polymer matrix were produced for this study (Figure 25).

The first part of this work focussed on the polymer synthesis from renewable resources. The Henkel patent was chosen as synthetic protocol to obtain the two monomers 2-nonyl-2-oxazoline (NonOx) and 2-dec-9'-enyl-2-oxazoline (Dec=Ox) from fatty acids. Via a microwave-assisted synthesis, poly(2-nonyl-2-oxazoline)-*stat*-poly(2-dec-9'-enyl-2-oxazoline) (POx) was obtained and subjected to detailed physico-chemical characterization. Notably, the pseudo-polyamide POx shows high temperature stability of up to 380 °C.

Figure 25: Overview and schematic representation of the material library investigated.

In order to simultaneously crosslink the polymers according to a radical mechanism (showing volumetric shrinkage) and to (double) ring-open the SOE (showing volumetric expansion), a thermally-initiated dual/bi-stage curing system needed to be developed. 1-Butylpyridin-1-ium hexafluoro phosphate(V) was found to be a well-suited thermal initiator for the polymerization of the SOE. As radical initiator, dicumyl peroxide was used.

The SOE increases the volume of the polymer matrix and decreases the density of the blends/composites (Table 8). Hence, the formation micro-cracks or micro-voids during curing is significantly reduced. The relative volume expansion of the Nylon 12 samples is in the range of 0.46-2.48%, and in the range of 1.39-7.69% for the POx samples. Hence, the POx samples exhibit much higher volumetric expansion than the Nylon 12 samples, which potentially originates from different extents phase separation in the two polyamide series.

Table 8: Density in g·cm^{-3} of the Nylon 12 and the POx samples as well as the calculated volumetric expansion in %.

	POx							
SOE wt.-%	**Particles 0 wt.-% [g/cm³]**	**Volume Expansion [%]**	**BN 40 wt.-% [g/cm³]**	**Volume Expansion [%]**	**AlN/AlN 20/20 wt.-% [g/cm³]**	**Volume Expansion [%]**	**BN/AlN/AlN 20/10/10 wt.-% [g/cm³]**	**Volume Expansion [%]**
0	1.05	-	1.23	-	1.29	-	1.29	-
15	1.04	1.54	1.21	1.39	1.24	3.70	1.23	4.97
30	1.01	4.39	1.17	4.84	1.19	7.69	1.19	7.50
	Nylon 12							
SOE wt.-%	**Particles 0 wt.-% [g/cm³]**	**Volume Expansion [%]**	**BN 40 wt.-% [g/cm³]**	**Volume Expansion [%]**	**AlN/AlN 20/20 wt.-% [g/cm³]**	**Volume Expansion [%]**	**BN/AlN/AlN 20/10/10 wt.-% [g/cm³]**	**Volume Expansion [%]**
0	1.02	-	1.21	-	1.26	-	1.28	-
15	1.01	0.98	1.20	0.84	1.25	0.46	1.27	0.84
30	0.99	2.48	1.19	1.41	1.24	1.92	1.26	1.60

The Nylon 12 samples with 0-30 wt.-% SOE show surface energies in the range of 23-30 mN·m^{-1}, which are hardly altered upon the addition of fillers. The lowest surface energy of 18 mN·m^{-1} is found at the Nylon 12 sample with 15 wt.-% of SOE and BN/AlN/AlN filling. The influences on the surface energies are more clearly pronounced in the case of the POx samples. Two general trends are discernible: increased values for increased contents of SOE vs. decreased values for increased contents of inorganic fillers. The BN fillers show a more pronounced effect on decreasing the surface energy than the AlN fillers; correspondingly, the lowest surface energy of 13 mN·m^{-1} is found for the POx/15 wt.-% SOE composite with 40 wt.-% BN. An interesting future investigation is to examine the water absorption of the Nylon 12 and POx samples.

The incorporation of SOE in the polymer network (introduction of polyester structural motifs) shifts the isoelectric point (IEP) to higher values. Minor deviations from this trend can only be observed in the composites that contain AlN particles, which can be protonated/deprotonated to minor extent. In summary, for an estimation of the IEP, the tautomer formation of the amides (polyamides with the R-NH-CO-R motif vs. pseudo-polyamides with the R_2-N-CO-R motif), the (de-)protonability of esters (and their tautomers), and the (de-)protonability of particle surfaces have to be considered.

As parameter for the thermal conductivity, the thermal diffusivity was measured by light flash analyses. It follows the general trends that it (i) decreases with increasing temperature and reaches a constant value at high temperatures (which has been reported for numerous other materials as well, in particular for polymers), (ii) decreases with increasing content of SOE (which can be retraced to the higher thermal conductivity of polyamides in comparison to polyesters/polyethers AND the lowered density upon the addition of SOE as expanding monomer), and (iii) increases with the filler content in the order no filler < AlN/AlN < BN/AlN/AlN < BN (perfectly reproducing the different thermal conductivity of the polymer, AlN, and BN).

The thermal behaviour in this test series depends purely on the thermal conductivity of the material, and the particle size does not show any influence on the thermal diffusivity. Hence, the use of different particle sizes of AlN, cannot exceed the thermal conductivity properties of BN at a filler content of 40 wt.-%. The Nylon 12 samples show higher thermal diffusivity at lower temperatures, and the POx materials have better performance at high temperatures.

In order to quantify the dielectric properties, the real and imaginary part of the permittivity were measured, and the loss factor $\tan\delta$ was calculated.

If no SOE was added to the Nylon 12 formulations, the unfilled samples have approximately the same permittivity as the composites filled with particles. Conversely, the permittivity increases for the samples that contain SOE. This observation can be referred to the volume expansion by adding SOE to the polymer matrix, which means that the free volume increases. According to the Tanaka Modell, a change of the interfacial region changes the distance of the multi-layers, and, hence, the electronic properties must change adequately. This is also the reason why the imaginary part of the permittivity increases due to the incorporation of SOE to the polymer matrix. The loose layer (the third layer of the Tanaka model) increases and can be correlated with the increase of the loss of the stored energy.

A significant increase of both, the real and the imaginary part of the permittivity, can be observed for the lower range of frequencies in the Nylon 12 series. The influence on the polarizability by the network density requires a detailed inspection: electronic polarization, atomic polarization, and orientation polarization can be excluded to cause these phenomena. At the lower range of frequencies in the range of 10 Hz and lower,

interfacial polarization with typical frequencies of 10^{-5} to 10^2 Hz can be held responsible to cause the polarization effects. Hence, this observation can be perfectly aligned with the predictions according to the Tanaka model described hereinabove.

In the POx series, the real part of the permittivity increases with increasing content of SOE (in all of the four sub-series with identical filler content), yet to significantly lesser extent than in the Nylon 12 sub-series. While the density changes upon the addition of SOE were more pronounced in the POx series than in the Nylon 12 series, it is tempting to refer this observation to a different extent of phase separation in the two types of polyamides.

The real part of the permittivity of the unfilled POx and the composite with AlN/AlN = 20/20 wt.-% are very comparable over the whole range of frequencies; the addition of SOE (15 or 30 wt.-%) only has a minor influence. On the contrary, the increase of the real part of the permittivity in the lower range of frequencies is very pronounced in the resins containing 30 wt.-% of SOE and BN particles (40 wt.-% BN as well as 20/10/10 wt.-% BN/AlN/AlN).

On the contrary, the imaginary part of the permittivity increases tremendously in all samples containing 30 wt.-% of SOE (in all of the four sub-series with identical filler content) in the lower range of frequencies, while the imaginary part of the permittivity of the SOE-free polymer and composites is very comparable to those containing 15 wt.-% of SOE.

For a comparison of the dielectric properties of the Nylon 12 and POx samples, the respective dielectric losses were summarized at a frequency of 40 Hz (Table 9), which is the frequency range of standard table works in literature.

The unfilled POx samples show nearly the same values of tanδ as the Nylon 12 samples; as the POx was synthesized from renewable resources, it can be argued that this 'green' alternative shows competitive dielectric behaviour in comparison with fossil-based Nylon 12.

At the 'medium' range frequency of 40 Hz, the addition of 15 wt.-% of SOE to POx is less deteriorating for the dielectric properties than to Nylon 12 if no BN particles are present. At 40 Hz, the addition of 30 wt.-% of SOE can be only argued for the production of Nylon12-based dielectrics.

In summary, the interfacial polarization in the lower range of frequencies needs to be subjected to further studies. In particular the influence of covalent attachment of the particles to the polymer matrix is worth of further investigations.

Table 9: Dielectric loss tan δ of the POx and Nylon 12 samples at frequency of 40 Hz.

POx	tan δ from the dielectric measurements			
SOE wt.-%	Particle 0 %	BN 40 wt.-%	AIN/AIN 20/20 wt.-%	BN/AIN/AIN 20/10/10 wt.-%
0	0.10	0.09	0.11	0.16
15	0.16	0.18	0.25	0.46
30	0.17	0.44	0.18	0.26
Nylon12	tan δ from the dielectric measurements			
SOE wt.-%	Particle 0 %	BN 40 wt.-%	AIN/AIN 20/20 wt.-%	BN/AIN/AIN 20/10/10 wt.-%
0	0.10	0.07	0.07	0.07
15	0.24	0.24	0.15	0.12
30	0.14	0.13	0.13	0.06

For future projects in this research area it is highly interesting to use functionalized particles, which can be covalently attached to the polymer matrix, to increase the thermal and electrical properties of the SOE containing materials.

A suitable method would be a thiol-ene click reaction to establish a bonded layer (the first layer of the Tanaka model). The dual/bi-stage curing system, which was developed in this Master Thesis, is as a suitable tool for this project. By using the radical initiator dicumyl peroxide, the functionalized particles could be covalently attached to the matrix via a thiol-ene mediated click reaction, whereas the volume shrinking can be prevented by double ring-opening of the SOE with the cationic initiator. Distribution of the particles, electronic properties, and the thermal conductivity could be improved due to the covalent attachment of the particles to the polymer matrix.

6 Abstract

The aim of the master thesis was to develop a dielectric material (nanodielectric) from renewable resources. 2-Oxazoline monomers were synthesised from renewable resources (fatty acids) according to the Henkel Patent, and copolymerized via a microwave-assisted cationic ring-opening polymerization reaction. The material properties of the self-synthesized pseudo-polyamide poly(2-nonyl-2-oxazoline)-*stat*-poly(2-dec-9'-enyl-2-oxazoline) POx, which was derived from fatty acids, were to be compared with commercially available Nylon 12.

These polymers with blended with expanding monomers, namely spiroorthoesters (SOEs), and compounded with inorganic fillers with high thermal conductivity, namely AlN and BN. The samples were crosslinked and expanded by a thermally triggered dual/bi-stage curing system, comprising the crosslinking of the polyamides and SOEs according to a radical mechanism (showing volumetric shrinkage) and the (double) ring-opening of the SOE according to a cationic mechanism (showing volumetric expansion). The experimental set-up yielded a 4 x 3 = 12 membered-library for POx and Nylon 12.

Due to the addition of SOE, the relative volume expansion of the Nylon 12 samples is in the range of 0.46-2.48%, and in the range of 1.39-7.69% for the POx samples. Hence, the formation micro-cracks or micro-voids during curing is significantly reduced.

The Nylon 12 samples with 0-30 wt.-% SOE show surface energies in the range of 23-30 $mN \cdot m^{-1}$, which are hardly altered upon the addition of fillers. In the POx samples, increased surface energies for increased contents of SOE vs. decreased surface energies for increased contents of inorganic fillers can be observed. The lowest surface energy as low as 13 $mN \cdot m^{-1}$ was found for the POx/15 wt.-% SOE composite with 40 wt.-% BN. The incorporation of SOE in the polymer network shifts the isoelectric point (IEP) to higher values. For an estimation of the IEP, it was found that the tautomer formation of the amides (polyamides with the R-NH-CO-R motif vs. pseudo-polyamides with the R_2-N-CO-R motif), the (de-)protonability of esters (and their tautomers), and the (de-)protonability of particle surfaces have to be considered.

The thermal diffusivity was measured by light flash analyses; it (i) decreases with increasing temperature and reaches a constant value at high temperatures, (ii) decreases with increasing content of SOE, and (iii) increases with the filler content in the order no filler < AlN/AlN < BN/AlN/AlN < BN. All these observations perfectly fitted well-supported structure-property relationships.

For a comparison of the dielectric properties of the Nylon 12 and POx samples, in particular the respective dielectric losses were investigated at a frequency of 40 Hz. The unfilled POx samples show nearly the same values of tanδ as the unfilled Nylon 12 samples; as the POx was synthesized from renewable resources, it can be argued that this 'green' alternative shows competitive dielectric behaviour in comparison with fossil-based Nylon 12. At the 'medium' range frequency of 40 Hz, the addition of 15 wt.-% of SOE to POx is less deteriorating for the dielectric properties than to Nylon 12 if no BN particles are present.

7 Kurzfassung

Ziel dieser Masterarbeit war es, aus nachwachsenden Rohstoffen ein dielektrisches Material (Nanodielektrikum) zu entwickeln. 2-Oxazolinmonomere wurden aus nachwachsenden Rohstoffen (Fettsäuren) gemäß dem Henkel-Patent synthetisiert und über eine mikrowellenunterstützte kationische Ringöffnungspolymerisation copolymerisiert. Die Materialeigenschaften des aus Fettsäuren selbstsynthetisierten Pseudo-Polyamids Poly(2-nonyl-2-oxazolin)-*stat*-poly(2-dec-9'-enyl-2-oxazolin) POx sollten mit handelsüblichem Nylon 12 verglichen werden.

Diese Polymere wurden mit expandierenden Monomeren, namentlich Spiroorthoestern (SOEs), und anorganischen Füllstoffen mit hoher Wärmeleitfähigkeit, namentlich AlN und BN, gemischt. Die Proben wurden durch ein thermisch ausgelöstes zweistufiges Härtungssystem vernetzt und expandiert, welches die Vernetzung der Polyamide und SOEs gemäß einem radikalischen Mechanismus (volumetrische Schrumpfung) und die (doppelte) Ringöffnung des SOE gemäß einem kationischen Mechanismus (zeigt volumetrische Expansion) umfasst. Der Versuchsaufbau ergab eine 4 × 3 = 12 Mitglieder umfassende Bibliothek für POx und Nylon 12.

Aufgrund der Zugabe von SOE liegt die relative Volumenexpansion der Nylon 12-Proben im Bereich von 0,46 bis 2,48% und im Bereich von 1,39 bis 7,69% für die POx-Proben. Daher wird die Bildung von Mikrorissen oder Mikrohohlräumen während des Aushärtens signifikant verringert.

Die Nylon 12-Proben mit 0-30 Gew.-% SOE zeigen Oberflächenenergien im Bereich von 23-30 mN·m^{-1}, die durch Zugabe von Füllstoffen kaum verändert werden. In den POx-Proben können erhöhte Oberflächenenergien bei erhöhten SOE-Gehalten gegenüber verringerten Oberflächenenergien für erhöhte Gehalte an anorganischen Füllstoffen beobachtet werden. Die niedrigste Oberflächenenergie von nur 13 mN·m^{-1} wurde für den POx / 15 Gew.-% SOE-Verbundstoff mit 40 Gew.-% BN gefunden.

Der Einbau von SOE in das Polymernetzwerk verschiebt den isoelektrischen Punkt (IEP) auf höhere Werte. Für eine Abschätzung des IEP wurde gefunden, dass die

Tautomerbildung der Amide (Polyamide mit dem R-NH-CO-R-Motiv vs. Pseudopolyamide mit dem R_2-N-CO-R-Motiv), die (De-)Protonierbarkeit von Estern (und ihren Tautomeren) und die (De-)Protonierbarkeit von Partikeloberflächen berücksichtigt werden müssen.

Das thermische Diffusionsvermögen wurde mit LFA gemessen; es (i) nimmt ab mit zunehmender Temperatur und erreicht bei hohen Temperaturen einen konstanten Wert, (ii) nimmt ab mit zunehmendem SOE-Gehalt und (iii) nimmt zu mit dem Füllstoffgehalt in der Reihenfolge: kein Füllstoff <AlN / AlN <BN / AlN / zu. AlN <BN. Alle diese Beobachtungen passen perfekt zu gut unterstützten Struktur-Eigenschafts-Beziehungen.

Zum Vergleich der dielektrischen Eigenschaften der Nylon 12- und POx-Proben wurden insbesondere die jeweiligen dielektrischen Verluste bei einer Frequenz von 40 Hz untersucht. Die ungefüllten POx-Proben zeigen nahezu die gleichen tanδ-Werte wie die ungefüllten Nylon 12-Proben. Da POx aus nachwachsenden Rohstoffen synthetisiert wurde, kann argumentiert werden, dass diese "grüne" Alternative im Vergleich zu fossilbasiertem Nylon 12 ein kompetitives dielektrisches Verhalten zeigt. Bei einer Frequenz im mittleren Bereich von 40 Hz verschlechtern sich durch die Zugabe von 15 Gew.-% % SOE zu POx dessen dielektrischen Eigenschaften weniger signifikant als die des Nylon 12, wenn nicht zusätzlich BN-Partikel vorhanden sind.

8 Experimental

8.1 Used Chemicals

All chemicals were used as received, except for methyl tosylate that was distilled prior to use.

Table 10: List of chemicals used.

Substance	Deliverer	Purity
Acetonitrile (≤10 ppm H_2O)	Carl Roth, Austria	≥99.9%
Allyl glycidyl ether	Sigma-Aldrich	≥99%
Aluminium(III)nitride, particle size 50 nm	IoLiTec	99%
Aluminum(III)nitride, particle size 1.0-15.0 μm	ABCR	high purity
Boron nitride, particle size 70 nm	MKNano	-
Boron trifluoride diethyl etherate	Sigma-Aldrich	-
1-Butylpyridin-1-ium hexafluorophosphate(V)	ABCR	-
γ-Butyrolactone	Sigma-Aldrich	≥99%
Chloroform (stabilized with 0.6 % ethanol)	VWR chemicals	99.0-99.4%
Chloroform- [D1]	VWR Chemicals	(99.8% D)
Chloroform- [D1] + 0.03%TMS	VWR Chemicals	(99.8% D)
Decanoic acid	SAFC	98%
Dichloromethane	Fisher Chemical	≥99%
Dicumyl peroxide	Sigma-Aldrich	98%
Ethanolamine	Sigma-Aldrich	≥99.0%
Methyl tosylate	Sigma-Aldrich	99 %
Nylon 12, particle size 25-30 μm	Goodfellow Limited	-
Sodium sulphate, anhydrous	VWR chemicals	≥99.0%
Titanium(IV) butoxide	Sigma-Aldrich	97%
Triethylamine	Sigma-Aldrich	≥99%
10-Undecenoic acid	Sigma-Aldrich	≥95%

8.2 Analytical Methods

NMR measurements. All NMR measurements were performed with a Bruker Advance III 300 MHz spectrometer. As solvent, $CDCl_3$ with an internal standard of 0.03 % TMS were used. All NMR spectra were processed using Bruker's TopSpin™ NMR software. All chemical shift values are reported in parts per million (ppm) relative to the TMS standrad $\delta(^1H)$ = 0.00 ppm with coupling constant (J) values reported in Hz. The ^{13}C-NMR spectra were calibrated to the signal of chloroform: $\delta(^{13}C)$ = 77.0 ppm. The notation of signals is: Proton: δ chemical shift in ppm (number of protons, multiplicity). Carbon: δ chemical shift in ppm. The following peak shapes are indicated: s (singlet), d (doublet), t (triplet), m (multiplet).

Microwave-assisted syntheses. The microwave-assisted polymerization was performed with the Synthos 3000 Microwave Synthesis Platform from Anton Paar GmbH in screwable Wheaton® glass vials (15x46 mm) with a Rotor 64.

IR-measurements. Infrared spectroscopy was performed with an Alpha Fourier-Transform Infrared Spectrometer with ATR support. The background was determined before every measurement. The scan area was from 400 to 4000 cm^{-1}, and 48 scans were performed for each measurement.

Zetapotential measurements. The zeta-potential measurements were performed with an EKA Electro Kinetic Analyzer and the SurPASS Electro kinetic Analyzer from Anton Paar. Titration medium: 0.05 M HCl and 0.05 M NaOH. Electrolyte: 1mM KCl. Measuring cell: gap measuring cell (AGC), sample size: 2 pieces of 1cm x 2cm each.

Gel Permeation Chromatography. For the determination of the average molar mass of the polymers, GPC analyses were performed with a Merck Hitachi L-6000A pump, a column from Polymer Standards Service column (8\300 mm STV linear XL 5 μm grade size), and a differential refractometer Waters 410 detector. As solvent, THF was used.

Thermogravimetry and DSC measurement. The thermogravimetry and DSC measurement was performed with the Netzsch STA 449C Jupiter device coupled with

quadrupole mass spectrometry. The temperature range was from 20 to 550 ° C with a heating rate of 10 K·min^{-1}. The measurement was performed under helium atmosphere.

LFA measurements. The thermal diffusivity was measured on a LFA 467 Hyper flash system (Netzsch, Selb, Germany) at temperatures of −20, 20, 60, 100, 140, 180, and 220 °C. The samples were coated with a thin graphite layer before the measurement in order to avoid reflection.

Contact angle measurements and surface energies. The contact angles were measured with the KRÜSS DSA 100 automatic goniometer using the sessile drop method. A drop of a test liquid (deionized water, diiodomethane) was applied to the surface to be measured using a microliter syringe. The drop profile was recorded using a CCD camera, and the contact angle was determined by adapting the drop profile to the surface in the area of the three-phase point using the DSA (Drop Shape Analysis) software. For each sample, at least 5 individual drops (drop volume 3 μL) were measured with each test liquid. The surface energies were calculated according to Owens-Wendt-Rabel-Kaelble (OWRK).

Platen press. For the preparation of the Nylon 12 and POx test specimens, a Collin P 200 Laboratory Platen Press was used. The press is equipped with a vacuum pump and a water-cooling system. A temperature of 180 °C and a pressure of 40 bar were applied for 20 min. A steel plate was covered with a 0.2 mm thick PTFE-foil from Haberkorn and a stainless-steel form was place on it. The respective amount of the powder mixture was added in the stainless-steel form (square, circle or rectangle). The top was again covered with a PTFE-foil and a steel plate. The composite samples were dried in a vacuum oven at 60 °C and 1 mbar, for 72 h.

Dielectric characterization. Dielectric characterization was performed with a Spectano 100 from Omicron Lab. All samples were characterized in a frequency range of 0.1 Hz to 5 kHz.

8.3 Synthesis of 2-Nonyl-2-oxazoline
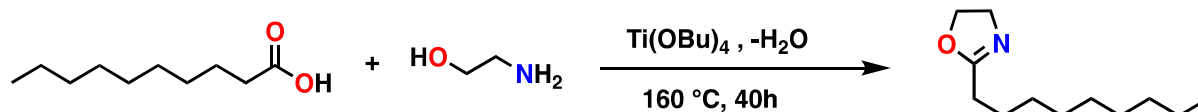
Figure 26: Synthesis of 2-nonyl-2-oxazoline according to the Henkel-Patent.

In a 500 mL three-neck round-bottom flask equipped with a magnetic stirring bar and a reflux condenser, 135 g of decanoic acid (0.78 mol, 1 equivalent), 71 mL of ethanol-2-amine (1.18 mol, 1.5 equivalents) and as well 1.4 mL of the catalyst titanium(IV) *n*-butoxide (3.92 mmol, 0.005 equivalent) were stirred under reflux at 160 °C for 24 h. Further amounts of 1.4 mL of the catalyst titanium(IV) *n*-butoxide (3.92 mmol, 0.005 equivalent) were added after 20 and 24 h. After that, the reflux condenser was removed, and the mixture was stirred for additional 12 h to remove the reaction water. The crude NonOx product was obtained via fractional distillation under vacuum (125 °C, 6 mbar), yielding a yellow liquid. Purification by column chromatography with chloroform yielded a colourless viscous liquid of pure NonOx. The yield was 53.3 % (82.36 g).

^{1}H-NMR (300 MHz, 298 K, CDCl$_3$): δ (ppm) = 0.88 (3H, t), 1.27 (12H, s), 1.63 (2H, t), 2.26 (2H, t), 3.82 (2, t), 4.21 (2H, t).

^{13}C-NMR (75 MHz, 298 K, CDCl$_3$): δ (ppm) = 14.1, 22.6, 25.9, 28.0, 29.2, 29.4, 31.8, 54.3, 67.1, 168.7.

IR (ATR): ν (cm^{-1}) = 2923, 2854, 1688, 1464, 1362, 1231, 1165, 986, 950, 908, 754, 722.

8.4 Synthesis of 2-Dec-9'-enyl-2-oxazoline
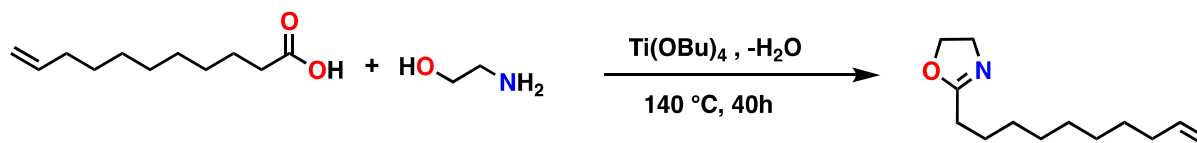
Figure 27: Synthesis of 2-dec-9'-enyl-2-oxazoline according to the Henkel-Patent.

In a 500 mL three-neck round-bottom flask equipped with a magnetic stirring bar and a reflux condenser, 135 g of 10-Undecenoic acid (0.73 mol, 1 equivalent), 70 mL of ethanol-2-amine (1.17 mol, 1.6 equivalents) and as well 1.3 mL of the catalyst titanium(IV) *n*-butoxide (3.66 mmol, 0.005 equivalent) were stirred under reflux at 140 °C for 24 h. Further amounts of 1.3 mL of the catalyst titanium(IV) *n*-butoxide (3.66 mmol, 0.005 equivalent) were added after 20 and 24 h. After that, the reflux condenser was removed, and the mixture was stirred for additional 12 h to remove the reaction water. The crude Dec$^=$Ox product was obtained via fractional distillation under vacuum (116°C, 6 mbar), yielding a yellow liquid. Purification by column chromatography with chloroform yielded a colourless viscous liquid of pure Dec$^=$Ox. The yield was 68.4 % (104.9 g).

^{1}H-NMR (300 MHz, 298 K, CDCl$_3$): δ (ppm) = 1.23 (10, s), 1.55 (2, t), 1,95 (2H, d), 2.19 (3H, t), 3,74 (2, t), 4,14 (2H, t), 4,88 (2H, m), 5,72 (1H, m).

^{13}C-NMR (75 MHz, 298 K, CDCl$_3$): δ (ppm) = 25.9, 27.9, 28.9, 29.0, 29.2, 29.3, 31.8, 54.3, 67.1, 114.1, 139.1, 168.6.

IR (ATR): ν (cm^{-1}) = 2924, 2853, 1668, 1640, 1461, 1432, 1385, 1361, 1227, 1167, 987, 952, 907, 723.

8.5 Synthesis of Poly(2-nonyl-2-oxazoline)-*stat*-poly(2-dec-9'-enyl-2-oxazoline)
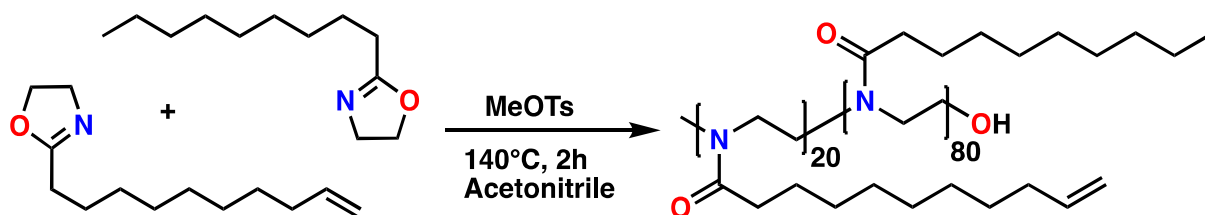
Figure 28: Microwave-assisted statistical copolymerization of Dec$^=$Ox and NonOx.

All glass vials and magnetic stirrers were dried at 120 °C for 12 h. 15.81 g of NonOx (80.1 mmol, 80 equiv.) and 4.19 g of Dec$^=$Ox (20.0 mmol, 20 equiv.), 186.5 mg of methyl tosylate (1.00 mmol, 1 equiv.) and 20.0 mL of acetonitrile were added to a 20 mL vial. The mixture was stirred for 5 min and divided into 2 mL portion in Wheaton® glass vials (15x46 mm) containing a stirring bar. The reaction mixture was heated under microwave irradiation at 140 °C for 2 h. After cooling, a white solid was obtained. The solvent was removed under reduced pressure. The material was mortared and further dried on the Schlenk line with a water bath at 40 °C for 4 h. A white solid powder of pNonOx$_{80}$-*stat*-pDec$^=$Ox$_{20}$ with a yield of ≥ 98 % (19.8 g) was obtained.

^{1}H-NMR (300 MHz, 298 K, CDCl$_3$): δ (ppm) = 0.81 (274 H), 1.19 (1275 H), 1.51 (211 H), 1.97 (45 H), 2.17 (208 H), 3.37 (400 H), 4.88 (40 H), 5.74 (20 H).

^{13}C NMR (75 MHz, 298 K, CDCl$_3$): δ (ppm) = 14.1, 22.7, 25.2, 25.4, 29.0, 29.2, 29.4, 29.6, 32.0, 33.0, 33.8, 43.3, 45.3, 114.2, 139.1, 173.2, 173.7.

IR (ATR): ν (cm^{-1}) = 2921, 2852, 1640, 1462, 1430, 1183, 1177, 907, 773, 722.

GPC: M$_w$ = 17.6 kDa; M$_n$ = 8.87 kDa; Đ= 1.81.

8.6 Synthesis of the Spiroorthoester 2-((Allyloxy)methyl)-1,4,6-trioxaspiro[4.4] nonane
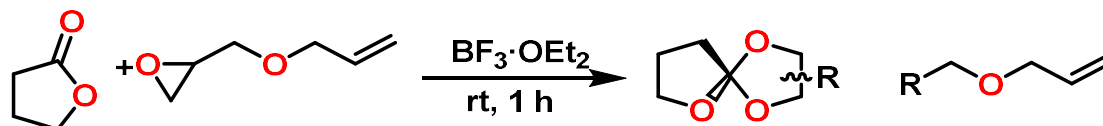
Figure 29: Synthesis of the spiroorthoester 2-((allyloxy)methyl)-1,4,6-trioxaspiro[4.4] nonane.

11.41 g (0.1 mmol, 1.0 eq.) of allyl glycidyl ether were added with a dropping funnel over a period of 40 min to a mixture of 0.46 g (3.24 mmol) of $BF_3 \cdot OEt_2$ and 52 g (0.6 mol, 6.0 eq.) of γ-butyrolactone under a nitrogen atmosphere and cooling with a water bath. After stirring at room temperature for 1 h, the reaction was quenched by the addition of 0.36 g (3.56 mmol) of NEt_3. The mixture was extracted with CH_2Cl_2 (40 mL) and H_2O (20 mL). The organic layer was dried over Na_2SO_4, and the solvent was evaporated under reduced pressure. For purification, the crude product was distilled under reduced pressure yielding 19.2 g (48 mmol, 48 %) of a colourless liquid (boiling point 115 °C / 0.1 mbar).

^{1}H-NMR (300 MHz, 298 K, CDCl$_3$) δ (ppm) = 1.90-2.06 (m, 2H), 2.11-2.20 (m, 2H), 3.42-3.43 (m, 0.5H), 3.44-3.50 (m, 1H), 3.52-3.64 (m, 0.5H), 3.67-3.75 (m, 1H), 3.85-4.09 (m, 4 H), 4.11- 4.30 (m, 1 H), 4.32-4.43 (m, 0.5 H), 4.43-4.48 (m, 0.5H), 5.17-5.30 (m, 2 H), 5.85-5.91 (m, 1H).

^{13}C-NMR (300 MHz, 298 K, CDCl$_3$) δ (ppm) = 24.1, 24.2, 32.7, 32.9, 66.5, 66.9, 67.2, 70.3, 71.5, 72.4, 72.5, 74.3, 75.3, 117.3, 117.4, 129.5, 129.7, 134.4

IR (ATR) ν (cm^{-1}) = 3081, 2955, 2879, 1776, 1737, 1647, 1458, 1332, 1244, 1195, 1130, 84 1040, 954, 922, 867, 807, 736.

8.7 Preparation of the Test Specimens

Two different polymer systems were used, poly(2-nonyl-2-oxazoline)-*stat*-poly(2-dec-9'-enyl-2-oxazoline) and Nylon 12.

8.7.1 Preparation of the POx samples

Pure POx. For the preparation of the pure POx sample, 5 mol-% of dicumyl peroxide referred to the double bonds of the copolymer was added. The mixture was homogenized by fine grinding.

POx with SOE. For the preparation of the POx samples with SOE, 5 mol-% of dicumyl peroxide referred to the double bonds of the copolymer was added. For the respective test specimen 15 wt.-% or 30 wt.-% of SOE was added. The amount of SOE refers to the amount of POx. The amount of 1-butylpyridin-1-ium hexafluoro phosphate(V) was 5 wt.-% referred to the amount of SOE. The mixture was homogenized by fine grinding.

POx with particles. For the preparation of the POx samples with particles, 5 mol-% of dicumyl peroxide based on to the double bonds of the copolymer and the particle contents (referred to the amount of POx) were added. The mixture was homogenized by fine grinding.

POX with SOE and particles. For the Preparation of the POx samples with SOE and particles, 5 mol-% of dicumyl peroxide referred to the double bonds of the copolymer and the particle contents (referred to the amount of POx) were added. 15 or 30 wt.-% of 2-((allyloxy)methyl)-1,4,6-trioxaspiro[4.4] nonane were added. The SOE amount referred to the amount of POx. The amount of 1-butylpyridin-1-ium hexafluoro phosphate(V) was 5 wt.-% referred to the amount of SOE. The mixture was homogenized by fine grinding.

POx: IR (ATR): ν (cm^{-1}) = 2921, 2852, 1638, 1464, 1420, 1419, 1120, 777, 722.

POx + SOE 15 wt.-%: IR (ATR): ν (cm^{-1}) = 2921, 2852, 1740, 1638, 1464, 1420, 1419, 1120, 777, 722.

POx + SOE 30 wt.-%: IR (ATR): ν (cm^{-1}) = 2921, 2852, 1740, 1638, 1464, 1420, 1419, 1120, 777, 722.

POx + BN 40 wt.-%: IR (ATR): ν (cm^{-1}) = 2921, 2852, 1644, 1362, 781.

POx + AlN/AlN 20/20 wt.-%: IR (ATR): ν (cm^{-1}) = 2921, 2852, 1638, 1464, 1420, 1419, 1120, 683.

POx + BN/AlN/AlN 20/10/10 wt.-%: IR (ATR): ν (cm^{-1}) = 2921, 2852, 1640, 1464, 1430, 1419, 1160, 909, 722, 589.

POx + BN 40 wt.-% + SOE 15 wt.-%: IR (ATR): ν (cm^{-1}) = 2921, 2852, 1644,1740, 1442, 1420, 1419, 1120, 777, 722.

POx + BN 40 wt.-% + SOE 30 wt.-%: IR (ATR): ν (cm^{-1}) = 2921, 2852, 1644,1740, 1442, 1420, 1419, 1120, 777, 722.

POx + AlN/AlN 20/20 wt.-% + SOE 15 wt.-%: IR (ATR): ν (cm^{-1}) = 2921, 2852, 1740, 1638, 1464, 1420, 1419, 1120, 683, 581.

POx + AlN/AlN 20/20 wt.-% + SOE 30 wt.-%: IR (ATR): ν (cm^{-1}) = 2921, 2852, 1740, 1638, 1464, 1420, 1419, 1120, 683, 581.

POx + BN/AlN/AlN 20/10/10 wt.-% + SOE 15 wt.-%: IR (ATR): ν (cm^{-1}) = 2921, 2852, 1740, 1640, 1464, 1430, 1419, 1160, 909, 722, 589.

POx + BN/AlN/AlN 20/10/10 wt.-% + SOE 30 wt.-%: IR (ATR): ν (cm^{-1}) = 2921, 2852, 1740, 1640, 1464, 1430, 1419, 1160, 909, 722, 589.

8.7.2 Preparation of the Nylon 12 samples

Pure Nylon 12. For the preparation of the pure Nylon 12 samples, 2 wt.-% of dicumyl peroxide referred to the amount Nylon 12 was added. The mixture was homogenized by fine grinding.

Nylon 12 with SOE. For the preparation of the Nylon 12 samples with SOE, 2 wt.-% of dicumyl peroxide referred to the amount Nylon 12 was added. For the respective test specimen, 15 or 30 wt.-% of 2-((allyloxy)methyl)-1,4,6-trioxaspiro[4.4] nonane was added. The amount of SOE referred to the amount of Nylon 12. The amount of the 1-butylpyridin-1-ium hexafluoro phosphate(V) was 5 wt.-% referred to the amount of SOE. The mixture was homogenized by fine grinding.

Nylon 12 with particles. For the preparation of the Nylon 12 samples with particles, 2 wt.-% of dicumyl peroxide referred to the amount of Nylon 12 were added. For the respective test specimen, the particles were added referred to the amount of Nylon 12. The mixture was homogenized by fine grinding.

Nylon 12 with SOE and particles. For the preparation of the Nylon 12 samples with SOE and particles, 2 wt.-% of dicumyl peroxide referred to the amount PA were added. For the respective test specimen, the particles were added referred to the amount of Nylon 12. For the respective test specimen 15 or 30 wt.-% of 2-((allyloxy)methyl)-1,4,6-trioxaspiro[4.4] nonane were added. The SOE amount referred to the amount of Nylon 12. The amount of 1-butylpyridin-1-ium hexafluoro phosphate(V) was 5 wt.-% referred to the amount of SOE. The mixture was homogenized by fine grinding.

Nylon 12: IR (ATR): ν (cm^{-1}) = 3300, 3090, 2915, 2848, 1634, 1550, 1466, 1100, 720.

Nylon 12 + SOE 15 wt.-%: IR (ATR): ν (cm^{-1}) = 3300, 3090, 2915, 2848, 1740, 1634, 1550, 1466, 1100, 720.

Nylon 12 + SOE 30 wt.-%: IR (ATR): ν (cm^{-1}) = 3300, 3090, 2915, 2848, 1740, 1634, 1550, 1466, 1100, 720.

Nylon 12 + BN 40 wt.-%: IR (ATR): ν (cm^{-1}) = 3300, 3090, 2915, 2848, 1635, 1375, 775, 752.

Nylon 12 + AlN/AlN 20/20 wt.-%: IR (ATR): ν (cm^{-1}) = 3300, 3090, 2915, 2848, 1635, 1554, 1464, 1364, 695.

Nylon 12 + BN/AlN/AlN 20/10/10 wt.-%: IR (ATR): ν (cm^{-1}) = 3300, 3090, 2915, 2848, 1635, 1554, 1380, 783, 718.

Nylon 12 + BN 40 wt.-% + SOE 15 wt.-%: IR (ATR): ν (cm^{-1}) = 3300, 3090, 2915, 2848, 1740, 1635, 1375, 775, 752.

Nylon 12 + BN 40 wt.-% + SOE 30 wt.-%: IR (ATR): ν (cm^{-1}) = 3300, 3090, 2915, 2848, 1740, 1635, 1375, 775, 752.

Nylon 12 + AlN/AlN 20/20 wt.-% + SOE 15 wt.-%: IR (ATR): ν (cm^{-1}) = 3300, 3090, 2915, 2848, 1740, 1635, 1554, 1464, 1364, 695.

Nylon 12 + AlN/AlN 20/20 wt.-% + SOE 30 wt.-%: IR (ATR): ν (cm^{-1}) = 3300, 3090, 2915, 2848, 1740, 1635, 1554, 1464, 1364, 695.

Nylon 12 + BN/AlN/AlN 20/10/10 wt.-% + SOE 15 wt.-%: IR (ATR): ν (cm^{-1}) = 3300, 3090, 2915, 2848, 1740, 1635, 1554, 1380, 783, 718, 661.

Nylon 12 + BN/AlN/AlN 20/10/10 wt.-% + SOE 30 wt.-%: IR (ATR): ν (cm^{-1}) = 3300, 3090, 2915, 2848, 1740, 1635, 1554, 1380, 783, 718, 661.

9 References

[1] B. Chu *et al.*, "A dielectric polymer with high electric energy density and fast discharge speed," *Science (80-.).*, vol. 313, no. 5785, pp. 334–336, Jul. 2006, doi: 10.1126/science.1127798.

[2] J. Y. Li, L. Zhang, and S. Ducharme, "Electric energy density of dielectric nanocomposites," *Appl. Phys. Lett.*, vol. 90, no. 13, pp. 13–16, 2007, doi: 10.1063/1.2716847.

[3] D. Q. Tan, "Review of Polymer-Based Nanodielectric Exploration and Film Scale-Up for Advanced Capacitors," *Adv. Funct. Mater.*, p. 1808567, Apr. 2019, doi: 10.1002/adfm.201808567.

[4] J. H. Cho *et al.*, "Printable ion-gel gate dielectrics for low-voltage polymer thin-film transistors on plastic," *Nat. Mater.*, vol. 7, no. 11, pp. 900–906, Oct. 2008, doi: 10.1038/nmat2291.

[5] F. Hussain, J. Chen, and M. Hojjati, "Epoxy-silicate nanocomposites: Cure monitoring and characterization," *Mater. Sci. Eng. A*, vol. 445–446, pp. 467–476, Feb. 2007, doi: 10.1016/j.msea.2006.09.071.

[6] D. Tan and P. Irwi, "Polymer Based Nanodielectric Composites," *Adv. Ceram. - Electr. Magn. Ceram. Bioceram. Ceram. Environ.*, 2011, doi: 10.5772/23012.

[7] J. Ho and T. R. Jow, "High field conduction in heat resistant polymers at elevated temperature for metallized film capacitors," in *Proceedings of the 2012 IEEE International Power Modulator and High Voltage Conference, IPMHVC 2012*, 2012, pp. 399–402, doi: 10.1109/IPMHVC.2012.6518764.

[8] Q. Li *et al.*, "Flexible higherature dielectric materials from polymer nanocomposites," *Nature*, vol. 523, no. 7562, pp. 576–579, 2015, doi: 10.1038/nature14647.

[9] M. F. Fréchette, M. L. Trudeau, H. D. Alamdari, and S. Boily, "Introductory remarks on nanodielectrics," *IEEE Trans. Dielectr. Electr. Insul.*, vol. 11, no. 5, pp. 808–818, 2004, doi: 10.1109/TDEI.2004.1349786.

[10] P. Marx *et al.*, "Effect of interfacial polarization and water absorption on the dielectric properties of epoxy-nanocomposites," *Polymers (Basel).*, vol. 9, no. 6, pp. 1–16, 2017, doi: 10.3390/polym9060195.

[11] J. R. Rochester, "Bisphenol A and human health: A review of the literature," *Reproductive Toxicology*, vol. 42. pp. 132–155, Dec. 2013, doi:

10.1016/j.reprotox.2013.08.008.

[12] B. S. Rubin, "Bisphenol A: An endocrine disruptor with widespread exposure and multiple effects," *J. Steroid Biochem. Mol. Biol.*, vol. 127, no. 1–2, pp. 27–34, Oct. 2011, doi: 10.1016/j.jsbmb.2011.05.002.

[13] K. Pivnenko, D. Laner, and T. F. Astrup, "Dynamics of bisphenol A (BPA) and bisphenol S (BPS) in the European paper cycle: Need for concern?," *Resour. Conserv. Recycl.*, 2018, doi: 10.1016/j.resconrec.2018.01.021.

[14] Y. Zhu, C. Romain, and C. K. Williams, "Sustainable polymers from renewable resources," *Nature*, vol. 540, no. 7633. Nature Publishing Group, pp. 354–362, Dec. 14, 2016, doi: 10.1038/nature21001.

[15] M. Glassner, M. Vergaelen, and R. Hoogenboom, "Poly(2-oxazoline)s: A comprehensive overview of polymer structures and their physical properties," *Polym. Int.*, vol. 67, no. 1, pp. 32–45, Jan. 2018, doi: 10.1002/pi.5457.

[16] M. Fimberger, I. A. Tsekmes, R. Kochetov, J. J. Smit, and F. Wiesbrock, "Crosslinked poly(2-oxazoline)s as 'green' materials for electronic applications," *Polymers (Basel).*, vol. 8, no. 1, 2016, doi: 10.3390/polym8010006.

[17] F. Awaja, S. Zhang, M. Tripathi, A. Nikiforov, and N. Pugno, "Cracks, microcracks and fracture in polymer structures: Formation, detection, autonomic repair," *Progress in Materials Science*, vol. 83. Elsevier Ltd, pp. 536–573, Oct. 01, 2016, doi: 10.1016/j.pmatsci.2016.07.007.

[18] W. J. Sarjeant and I. W. Clelland, "Capactive Components for Power Electronics," *Proc. IEEE*, vol. 89, no. 6, pp. 846–855, 2001, doi: 10.1109/5.931475.

[19] T. Zhang, W. Li, Y. Zhao, Y. Yu, and W. Fei, "High Energy Storage Performance of Opposite Double-Heterojunction Ferroelectricity–Insulators," *Adv. Funct. Mater.*, vol. 28, no. 10, pp. 1–9, 2018, doi: 10.1002/adfm.201706211.

[20] M. Mackey *et al.*, "Reduction of dielectric hysteresis in multilayered films via nanoconfinement," *Macromolecules*, vol. 45, no. 4, pp. 1954–1962, 2012, doi: 10.1021/ma202267r.

[21] G. Picci and M. Rabuffi, "Status quo and future prospects for metallized polypropylene energy storage capacitors," *PPPS 2001 - Pulsed Power Plasma Sci. 2001*, vol. 1, no. 5, pp. 417–420, 2015, doi: 10.1109/PPPS.2001.01002122.

[22] M. J. Pan and C. Randall, "A brief introduction to ceramic capacitors," *IEEE Electr. Insul. Mag.*, vol. 26, no. 3, pp. 44–50, May 2010, doi:

10.1109/MEI.2010.5482787.

[23] W. J. Sarjeant, J. Zirnheld, and F. W. Macdougall, "Capacitors," vol. 26, no. 5, pp. 1368–1392, 1998.

[24] N. Dielectrics and T. J. Lewis, "Nanomet ric Dielectrics," vol. 1, no. 5, pp. 812–825, 1994.

[25] T. J. Lewis, "Interfaces are the dominant feature of dielectrics at the nanometric level," *IEEE Trans. Dielectr. Electr. Insul.*, vol. 11, no. 5, pp. 739–753, 2004, doi: 10.1109/TDEI.2004.1349779.

[26] J. K. Nelson, J. C. Fothergill, L. A. Dissado, and W. Peasgood, "Towards an understanding of nanometric dielectrics," in *Conference on Electrical Insulation and Dielectric Phenomena (CEIDP), Annual Report*, 2002, pp. 295–298, doi: 10.1109/ceidp.2002.1048793.

[27] K. Y. Lau *et al.*, "Nanodielectrics : Opportunities and Challenges," vol. 31, no. 4, pp. 45–54, 2015.

[28] T. Tanaka, "Dielectric nanocomposites with insulating properties," *IEEE Trans. Dielectr. Electr. Insul.*, vol. 12, no. 5, pp. 914–928, 2005, doi: 10.1109/TDEI.2005.1522186.

[29] T. Tanaka, M. Kozako, N. Fuse, and Y. Ohki, "Proposal of a multi-core model for polymer nanocomposite dielectrics," *IEEE Trans. Dielectr. Electr. Insul.*, vol. 12, no. 4, pp. 669–681, 2005, doi: 10.1109/TDEI.2005.1511092.

[30] T. Tanaka and T. Imai, "Advances in nanodielectric materials over the past 50 years," *IEEE Electr. Insul. Mag.*, vol. 29, no. 1, pp. 10–23, 2013, doi: 10.1109/MEI.2013.6410535.

[31] T. Imai, Y. Hirano, H. Hirai, S. Kojima, and T. Shimizu, "Preparation and properties of epoxy-organically modified layered silicate nanocomposites," in *Conference Record of IEEE International Symposium on Electrical Insulation*, 2002, pp. 379–383, doi: 10.1109/elinsl.2002.995955.

[32] W. Zhou, S. Qi, Q. An, H. Zhao, and N. Liu, "Thermal conductivity of boron nitride reinforced polyethylene composites," *Mater. Res. Bull.*, vol. 42, no. 10, pp. 1863–1873, Oct. 2007, doi: 10.1016/j.materresbull.2006.11.047.

[33] H. Ishida and S. Rimdusit, "Very high thermal conductivity obtained by boron nitride-filled polybenzoxazine," *Thermochim. Acta*, vol. 320, no. 1–2, pp. 177–186, Nov. 1998, doi: 10.1016/s0040-6031(98)00463-8.

[34] K. Sato *et al.*, "Thermally conductive composite films of hexagonal boron nitride

and polyimide with affinity-enhanced interfaces," *J. Mater. Chem.*, vol. 20, no. 14, pp. 2749–2752, Mar. 2010, doi: 10.1039/b924997d.

[35] S. Choi and J. Kim, "Thermal conductivity of epoxy composites with a binary-particle system of aluminum oxide and aluminum nitride fillers," *Compos. Part B Eng.*, vol. 51, pp. 140–147, Aug. 2013, doi: 10.1016/j.compositesb.2013.03.002.

[36] C. Dervos, C. Paraskevas, P. Skafidas, and P. Vassiliou, "A Complex Permittivity Based Sensor for the Electrical Characterization of High-Voltage Transformer Oils," *Sensors*, vol. 5, no. 4, pp. 302–316, May 2005, doi: 10.3390/s5040302.

[37] Adrianus J. Dekker, "Electrical Engineering Materials," in *Electrical Engineering Materials*, 1st ed., Prentice-Hall, 1959, pp. 23–61.

[38] D. D. L. Chung, "No Title," in *Composite Materials*, 1, Ed. Springer-Verlag London, 2003, pp. 125–133.

[39] Adrianus J. Dekker, "Electrical Engineering Materials," in *Electrical Engineering Materials*, 1st ed., Prentice-Hall, 1959, pp. 73–75.

[40] J. Maitra and V. Kumar Shukla, "Cross-linking in Hydrogels-A Review," *Am. J. Polym. Sci.*, vol. 2014, no. 2, pp. 25–31, 2014, doi: 10.5923/j.ajps.20140402.01.

[41] K. Vanherck, G. Koeckelberghs, and I. F. J. Vankelecom, "Crosslinking polyimides for membrane applications: A review," *Prog. Polym. Sci.*, vol. 38, no. 6, pp. 874–896, 2013, doi: 10.1016/j.progpolymsci.2012.11.001.

[42] S. Mane and S. Ponra, "Effect of Chemical Crosslinking on Properties of Polymer Microbeads: A Review," *Can. Chem. Trans.*, vol. 3, no. 4, pp. 473–485, 2016, doi: 10.13179/canchemtrans.2015.03.04.0245.

[43] A. N. Fraga, E. Frullloni, O. De La Osa, J. M. Kenny, and A. Vázquez, "Relationship between water absorption and dielectric behaviour of natural fibre composite materials," *Polym. Test.*, vol. 25, no. 2, pp. 181–187, Apr. 2006, doi: 10.1016/j.polymertesting.2005.11.002.

[44] C. Lee, Y. Shul, and H. Han, "Dielectric properties of oxydianiline-based polyimide thin films according to the water uptake," *J. Polym. Sci. Part B Polym. Phys.*, vol. 40, no. 19, pp. 2190–2198, Oct. 2002, doi: 10.1002/polb.10277.

[45] L. E. Nielsen, "Journal of Macromolecular Science , Part C : Polymer Reviews Cross-Linking – Effect on Physical Properties of Polymers," *J. Macromol. Sci. Part C Polym. Rev.*, vol. 3, no. 1, pp. 69–103, 2008, doi: 10.1080/15583726908545897.

[46] D. U. Shah and P. J. Schubel, "Evaluation of cure shrinkage measurement

techniques for thermosetting resins," *Polym. Test.*, vol. 29, no. 6, pp. 629–639, Sep. 2010, doi: 10.1016/j.polymertesting.2010.05.001.

[47] "Expanding Monomers: Synthesis, Characterization, and Applications - Rajender Kumar Sadhir, Mr. Russell M. Luck - Google Books." https://books.google.at/books?hl=de&lr=&id=BVgjPRmhnX4C&oi=fnd&pg=PA1 &dq=shrinking+radical+polymerisation+polyamid&ots=u71PefyOsW&sig=tH5h _rT8Fsa7dICK1NvtaU1xVjk#v=onepage&q=shrinking radical polymerisation polyamid&f=false (accessed Apr. 14, 2020).

[48] F. Awaja, S. Zhang, M. Tripathi, A. Nikiforov, and N. Pugno, "Cracks, microcracks and fracture in polymer structures: Formation, detection, autonomic repair," *Prog. Mater. Sci.*, vol. 83, pp. 536–573, 2016, doi: 10.1016/j.pmatsci.2016.07.007.

[49] T. Takata and T. Endo, "Recent advances in the development of expanding monomers: Synthesis, polymerization and volume change," *Progress in Polymer Science*, vol. 18, no. 5. Pergamon, pp. 839–870, Jan. 01, 1993, doi: 10.1016/0079-6700(93)90019-9.

[50] S. Chikaoka, T. Takata, and T. Endo, "New Aspects of Cationic Polymerization of Spiroorthoester: Cationic Single Ring-Opening Polymerization and Equilibrium Polymerization," *Macromolecules*, vol. 24, no. 25, pp. 6557–6562, Dec. 1991, doi: 10.1021/ma00025a001.

[51] M. Hong and E. Y. X. Chen, "Towards Truly Sustainable Polymers: A Metal-Free Recyclable Polyester from Biorenewable Non-Strained γ-Butyrolactone," *Angew. Chemie - Int. Ed.*, vol. 55, no. 13, pp. 4188–4193, 2016, doi: 10.1002/anie.201601092.

[52] P. Marx, A. Romano, R. Fischer, I. Roppolo, M. Sangermano, and F. Wiesbrock, "Dual-Cure Coatings: Spiroorthoesters as Volume-Controlling Additives in Thiol–Ene Reactions," *Macromol. Mater. Eng.*, vol. 304, no. 4, 2019, doi: 10.1002/mame.201800627.

[53] D. A. Tomalia and D. P. Sheetz, "Homopolymerization of 2-alkyl- and 2-aryl-2-oxazolines," *J. Polym. Sci. Part A-1 Polym. Chem.*, vol. 4, no. 9, pp. 2253–2265, Sep. 1966, doi: 10.1002/pol.1966.150040919.

[54] T. Kagiya, S. Narisawa, T. Maeda, and K. Fukui, "Ring-opening polymerization of 2-substituted 2-oxazolines," *J. Polym. Sci. Part B Polym. Lett.*, vol. 4, no. 7, pp. 441–445, Jul. 1966, doi: 10.1002/pol.1966.110040701.

[55] T. G. Bassiri, A. Levy, and M. Litt, "Polymerization of cyclic imino ethers. I. Oxazolines," *J. Polym. Sci. Part B Polym. Lett.*, vol. 5, no. 9, pp. 871–879, Sep. 1967, doi: 10.1002/pol.1967.110050927.

[56] W. Seeliger *et al.*, "Recent Syntheses and Reactions of Cyclic Imidic Esters," *Angew. Chemie Int. Ed. English*, vol. 5, no. 10, pp. 875–888, Oct. 1966, doi: 10.1002/anie.196608751.

[57] F. Wiesbrock, R. Hoogenboom, C. H. Abeln, and U. S. Schubert, "Single-Mode Microwave Ovens as New Reaction Devices: Accelerating the Living Polymerization of 2-Ethyl-2-Oxazoline," *Macromol. Rapid Commun.*, vol. 25, no. 22, pp. 1895–1899, Nov. 2004, doi: 10.1002/marc.200400369.

[58] B. Guillerm, S. Monge, V. Lapinte, and J.-J. Robin, "How to Modulate the Chemical Structure of Polyoxazolines by Appropriate Functionalization," *Macromol. Rapid Commun.*, vol. 33, no. 19, pp. 1600–1612, Oct. 2012, doi: 10.1002/marc.201200266.

[59] T. X. Viegas *et al.*, "Polyoxazoline: Chemistry, properties, and applications in drug delivery," *Bioconjug. Chem.*, vol. 22, no. 5, pp. 976–986, May 2011, doi: 10.1021/bc200049d.

[60] C. O. Kappe, "Controlled Microwave Heating in Modern Organic Synthesis," *Angew. Chemie Int. Ed.*, vol. 43, no. 46, pp. 6250–6284, Nov. 2004, doi: 10.1002/anie.200400655.

[61] D. R. Baghurst and D. M. P. Mingos, "Superheating effects associated with microwave dielectric heating," *J. Chem. Soc. Chem. Commun.*, no. 9, pp. 674–677, Jan. 1992, doi: 10.1039/C39920000674.

[62] R. Hoogenboom, M. A. M. Leenen, F. Wiesbrock, and U. S. Schubert, "Microwave Accelerated Polymerization of 2-Phenyl-2-oxazoline: Microwave or Temperature Effects?," *Macromol. Rapid Commun.*, vol. 26, no. 22, pp. 1773–1778, Nov. 2005, doi: 10.1002/marc.200500370.

[63] F. Wiesbrock, R. Hoogenboom, M. A. M. Leenen, M. A. R. Meier, and U. S. Schubert, "Investigation of the living cationic ring-opening polymerization of 2-methyl-, 2-ethyl-, 2-nonyl-, and 2-phenyl-2-oxazoline in a single-mode microwave reactor," *Macromolecules*, vol. 38, no. 12, pp. 5025–5034, Jun. 2005, doi: 10.1021/ma0474170.

[64] B. Verbraeken, B. D. Monnery, K. Lava, and R. Hoogenboom, "The Chemistry of Poly(2-oxazoline)s," in *Encyclopedia of Polymer Science and Technology*,

Hoboken, NJ, USA: John Wiley & Sons, Inc., 2018, pp. 1–59.

[65] R. Hoogenboom, "Poly(2-oxazoline)s: A Polymer Class with Numerous Potential Applications," *Angew. Chemie Int. Ed.*, vol. 48, no. 43, pp. 7978–7994, Oct. 2009, doi: 10.1002/anie.200901607.

[66] E. Rossegger, V. Schenk, and F. Wiesbrock, "Design Strategies for Functionalized Poly(2-oxazoline)s and Derived Materials," *Polymers (Basel).*, vol. 5, no. 3, pp. 956–1011, Jul. 2013, doi: 10.3390/polym5030956.

[67] J. A. Frump, "Oxazolines. Their preparation, reactions, and applications," *Chem. Rev.*, vol. 71, no. 5, pp. 483–505, 1971, doi: 10.1021/cr60273a003.

[68] S. Gabriel, "Zur Kenntniss des Bromäthylamins," *Berichte der Dtsch. Chem. Gesellschaft*, vol. 22, no. 1, pp. 1139–1154, Jan. 1889, doi: 10.1002/cber.188902201248.

[69] K. Kempe, M. Lobert, R. Hoogenboom, and U. S. Schubert, "Screening the synthesis of 2-substituted-2-oxazolines," *J. Comb. Chem.*, vol. 11, no. 2, pp. 274–280, Mar. 2009, doi: 10.1021/cc800174d.

[70] R. V. Jagadeesh, H. Junge, and M. Beller, "Green synthesis of nitriles using non-noble metal oxides-based nanocatalysts," *Nat. Commun.*, vol. 5, no. 1, pp. 1–8, Jul. 2014, doi: 10.1038/ncomms5123.

[71] H. Witte and W. Seeliger, "Cyclische Imidsäureester aus Nitrilen und Aminoalkoholen," *Justus Liebigs Ann. Chem.*, vol. 1974, no. 6, pp. 996–1009, Jul. 1974, doi: 10.1002/jlac.197419740615.

[72] H. Wenker, "Syntheses from Ethanolamine. V. Synthesis of Δ2-Oxazoline and of 2,2′-Δ2-Di-oxazoline," *J. Am. Chem. Soc.*, vol. 60, no. 9, pp. 2152–2153, Sep. 1938, doi: 10.1021/ja01276a036.

[73] H. Wenker, "The Synthesis of Δ2-Oxazolines and Δ2-Thiazolines from N-Acyl-2-aminoethanols," *J. Am. Chem. Soc.*, vol. 57, no. 6, pp. 1079–1080, Jun. 1935, doi: 10.1021/ja01309a034.

[74] A. Gress, A. Völkel, and H. Schlaad, "Thio-click modification of poly[2-(3-butenyl)-2-oxazoline]," *Macromolecules*, vol. 40, no. 22, pp. 7928–7933, Oct. 2007, doi: 10.1021/ma071357r.

[75] S. S. Y. Wang, S. Kiang, and W. Merkl, "Investigation of a thermal runaway hazard-drum storage of thionyl chloride/ethyl acetate mixture," *Process Saf. Prog.*, vol. 13, no. 3, pp. 153–158, Jul. 1994, doi: 10.1002/prs.680130308.

[76] T. R. Dargaville, K. Lava, B. Verbraeken, and R. Hoogenboom, "Unexpected

Switching of the Photogelation Chemistry When Cross-Linking Poly(2-oxazoline) Copolymers," *Macromolecules*, vol. 49, no. 13, pp. 4774–4783, Jul. 2016, doi: 10.1021/acs.macromol.6b00167.

[77] M. Beck *et al.*, "Polyoxazoline auf fettchemischer Basis," *Angew. Makromol. Chemie*, vol. 223, no. 1, pp. 217–233, Dec. 1994, doi: 10.1002/apmc.1994.052230116.

[78] L. Mat??jka, P. Chabanne, L. Tighzert, and J. P. Pascault, "Cationic polymerization of diglycidyl ether of bisphenol A," *J. Polym. Sci. Part A Polym. Chem.*, vol. 32, no. 8, pp. 1447–1458, Jun. 1994, doi: 10.1002/pola.1994.080320806.

[79] Hermann Diesen, "DE3938552A1 - Crosslinking polyethylene and polyamide by organic peroxide - esp. re-use of composite packaging material - Google Patents." https://patents.google.com/patent/DE3938552A1/en (accessed Apr. 18, 2020).

[80] J. Kruželák, R. Sýkora, and I. Hudec, "Peroxide vulcanization of natural rubber. Part I: Effect of temperature and peroxide concentration," *J. Polym. Eng.*, vol. 34, no. 7, pp. 617–624, Sep. 2014, doi: 10.1515/polyeng-2014-0034.

[81] "EPO - European publication server." https://data.epo.org/publication-server/rest/v1.0/publication-dates/19821208/patents/EP0066543NWA2/document.html (accessed Apr. 18, 2020).

[82] "1-Butylpyridinium Hexafluorophosphate 186088-50-6 | TCI America." https://www.tcichemicals.com/eshop/en/ca/commodity/B2196/ (accessed Apr. 18, 2020).

[83] E. A. Cherney, "Nanodielectrics applications-today and tomorrow," *IEEE Electrical Insulation Magazine*, vol. 29, no. 6. pp. 59–65, 2013, doi: 10.1109/MEI.2013.6648754.

[84] M. Geoghegan and G. Krausch, "Wetting at polymer surfaces and interfaces," *Progress in Polymer Science (Oxford)*, vol. 28, no. 2. Pergamon, pp. 261–302, Feb. 01, 2003, doi: 10.1016/S0079-6700(02)00080-1.

[85] W. Y. Chou *et al.*, "Effect of surface free energy in gate dielectric in pentacene thin-film transistors," *Appl. Phys. Lett.*, vol. 89, no. 11, p. 112126, Sep. 2006, doi: 10.1063/1.2354426.

[86] M. Stamm, *Polymer surfaces and interfaces: Characterization, modification and*

applications. Springer Berlin Heidelberg, 2008.

[87] C. C. Ku and R. Liepins, *Electrical Properties of Polymers*. Munich, Germany: Hanser Publishers, 1987.

10 Appendix

10.1 List of Abbreviations

[(R)Φ2I]$^+$[SbF6]$^-$	(4-(octyloxy)phenyl)(phenyl)iodonium-hexafluoro antimonate(V)
AC	alternating current
ACN	Acetonitrile
AIN	Aluminium nitride
BAPO	Phenylbis(2,4,6-trimethylbenzoyl)phosphine oxide
BN	Boron nitride
BOPP	biaxially oriented polypropylene
CROP	cationic ring-opening polymerization
DC	direct current
DCM	Dichloromethane
DCP	Dicumyl peroxide
Dec=Ox	2-dec-9'-enyl-oxazoline
EDAC	1-(3-dimethylpropyl)-3-ethylcarbodiimide hydrochloride
HV	High Voltage
IEP	Isoelectric point
LDA	Lithium diisopropylamide
LFA	Laser flash analysis
MeOTs	methyl tosylate
MLC	multilayer ceramic capacitor
NEt$_3$	Triethylamine
NHS	N-hydroxy succinimide
NonOx	2-nonyl-oxazoline
PA	Polyamide
pNonOx$_{80}$-*stat*-pDec=Ox$_{20}$	Poly(2-nonyl-2-oxazoline)-*stat*-poly(2-dec-9'-enyl-2-oxazoline)
POx	Poly(2-oxazoline)
SOE	Spiro-orthoester
T$_g$	Glass transition temperature
THF	Tetrahydrofuran
TMS	Tetramethylsilane
wt.-%	weight percent

10.2 List of Figures

10.3 List of Schemes

10.4 List of Tables